



Supplementary Materials for

Selective targeting of BD1 and BD2 of the BET proteins in cancer and immuno-inflammation

Authors: Omer Gilan^{1,2†}, Inmaculada Rioja^{3†}, Kathy Knezevic¹, Matthew J Bell³, Miriam M. Yeung¹, Nicola R Harker³, Enid Y.N. Lam^{1,2}, Chun-wa Chung³, Paul Bamborough³, Massimo Petretich⁴, Marjeta Urh⁵, Stephen J Atkinson³, Anna K Bassil³, Emma J Roberts³, Dane Vassiliadis^{1,2}, Marian L. Burr^{1,2}, Alex G.S Preston³, Christopher Wellaway³, Thilo Werner⁴, James R Gray³, Anne-Marie Michon⁴, Thomas Gobetti³, Vinod Kumar⁶, Peter E Soden³, Andrea Haynes³, Johanna Vappiani⁴, David F Tough³, Simon Taylor³, Sarah-Jane Dawson^{1,2,7}, Marcus Bantscheff⁴, Matthew Lindon³, Gerard Drewes⁴, Emmanuel H Demont³, Danette L. Daniels⁵, Paola Grandi⁴, Rab K Prinjha^{3*}, Mark A. Dawson^{1,2,7*}

Corresponding Author(s):

Professor Mark A. Dawson

Cancer Epigenetics Laboratory and Department of Haematology,

Peter MacCallum Cancer Centre, 305 Grattan Street, Melbourne, Australia, 3000

Email – mark.dawson@petermac.org

Phone: +61 3 8559 7131; Fax: +61 3 8559 8054

Rab Prinjha PhD, FRSB, FMedSci

VP Head of Epigenetics Research Unit

GSK Gunnels Wood Road, Stevenage, Herts, SG1 2NY UK

Email – Rabinder.Prinjha@gsk.com

Phone: +44 (0)7920 568929

This PDF file includes:

Materials and Methods

Figs. S1 to S18

Tables S1 to S5

Captions for Data S1 to S18

Supplementary methods - Chemistry

Materials and Methods

Compounds

GSK1210151A (I-BET151(19)), iBET-BD1 (GSK778), iBET-BD2 (GSK046) and GSK620 were developed at GlaxoSmithKline (GSK) and synthesised as described in the **Supplementary Chemistry synthesis** section. Apremilast, a PDE4 inhibitor was purchased from AMATEK Chemical. Telmisartan, an angiotensin II receptor antagonist (QW32M-GS), was purchased from Tokyo chemical industry CO. LTD.

BET BD1 and BD2 time-resolved fluorescence energy transfer (TR-FRET) Assays

Tandem bromodomains of 6His-Thr-BRD4 (1–477) were expressed with a mutation in BD2 (Y390A) to monitor compound binding to BD1 or a mutation in BD1 (Y97A) to monitor compound binding to BD2. Analogous Y→A mutants were used to measure binding to the other BET bromodomains: 6His-Thr-BRD2 (1–473 Y386A or Y113A), 6His-Thr-BRD3 (1–435 Y348A or Y73A), 6His-FLAG-Tev-BRDT (1–397 Y309A or Y66A). AlexaFluor 647 labeled BET bromodomain ligand was prepared by addition of 1.8-fold excess of N-(5-aminopentyl)-2-((4S)-6-(4-chlorophenyl)-8-methoxy-1-methyl-4H-benzo[f][1,2,4]triazolo[4,3-a][1,4]-diazepin-4-yl)acetamide in DMF to a solution of AlexaFluor 647 hydroxysuccinimide ester in DMF. The solution was basified by addition of 3-fold excess of diisopropylethylamine. Reaction progress was followed by electrospray LC/MS, and when complete the product was isolated and purified by reversed-phase C18 HPLC. The final compound was characterized by MS and analytical reversed-phase HPLC. Compounds were titrated from 10 mM in 100% DMSO and 50nL transferred to a low volume black 384 well micro titre plate using a Labcyte Echo 555. 5μL of 20 nM protein was dispensed in an assay buffer of 50mM HEPES, 150 mM NaCl, 5% glycerol, 1 mM DTT and 1 mM CHAPS, pH 7.4 (Thermo Scientific Multidrop Combi) in the presence of 100nM fluorescent ligand (~K_D concentration for the interaction between BRD4 BD1 and ligand). After 30 mins equilibration 5μL 3 nM europium chelate labelled anti-6His antibody was added and bromodomain protein:fluorescent ligand interaction was detected using TR-FRET (Perkin Elmer, W1024, AD0111). Time resolved fluorescence (TRF) was then detected on a TRF laser equipped Perkin Elmer Envision multimode plate reader (excitation = 337 nm; emission 1 = 615 nm; emission 2 = 665 nm; dual wavelength bias dichroic = 400 nm, 630 nm). TR-FRET ratio was calculated using the following equation: Ratio = ((Acceptor fluorescence at 665 nm) / (Donor fluorescence at 615 nm)) * 1000. TR-FRET ratio data was normalised to high (DMSO) and low (compound control derivative of I-BET762) controls and LogIC₅₀ values determined for each of the compounds tested by fitting the fluorescence ratio data to a four parameter model in GraphPad Prism v5.04: $y = a + (d - a) / (1 + 10^{((\text{Log}c - x) * b)})$ where 'a' is the minimum, 'b' is the Hill slope, 'c' is the IC₅₀, 'd' is the maximum, 'x' is the log of the concentration and 'y' is the response.

BROMOscan® Bromodomain Profiling

BROMOscan® bromodomain profiling was provided by Eurofins DiscoverX Corp. (Fremont, CA, USA, <http://www.discoverx.com>). Determination of the K_D between test compounds and DNA tagged bromodomains was achieved through binding competition against a proprietary reference immobilized ligand.

Surface plasmon resonance (SPR)

SPR-based ligand binding assays were performed using a Biacore S200 instrument (GE Healthcare) on CM5 chips (GE Healthcare) at 25 °C. Proteins were immobilised using standard

amine coupling chemistry (7 minutes activation with EDC/NHS, protein injection, then quenching with 1 M ethanolamine pH 8.5 for 7 min), with a running buffer of 0.01 M HEPES pH 7.4, 0.15 M NaCl, 3 mM EDTA, 0.005% v/v Tween 20. Two proteins 1. 6His-Thr-Brd4(1-477)Y390A, which tests for binding to the N-terminal bromodomain of BRD4, BRD4BD1 and 2. His-tagged cleaved BRD4 (347-463), which tests for the binding to the C-terminal bromodomain of BRD4, BRD4-BD2, were immobilised for 7 min at 50-60 $\mu\text{g}/\text{mL}$, immediately after a 20-fold dilution into 10mM Na acetate pH 5.5 and 5.0 respectively in the presence of 50 μM of a nanomolar inhibitor. These two proteins were always immobilised onto the same CM5 chip to allow affinity data for BRD4-BD1 and BRD4-BD2 binding to be obtained simultaneously. Binding assays were performed in 10 mM HEPES, 500 mM NaCl, 3 mM EDTA, 0.005% Tween 20, 1% DMSO, pH 7.4, with a 30 $\mu\text{g}/\text{min}$ flow-rate. Ligands were injected in a concentration-response series (11-point, 3-fold serial dilutions), with solvent correction and positive/negative control cycles being used throughout assays to control for differences in response to bulk refractive index changes and loss of binding activity from the surface respectively (positive control 5 μM I-BET151 negative control 1.5% DMSO. An injection time of 90 s was used with dissociation time of 360 s. Concentration-response data (from reference- subtracted curves) were fitted to a steady-state 1:1 binding model to determine K_D with the BIAevaluation software. The top concentration used for concentration-response titrations was 10 μM for iBET-BD1 (GSK778) and for iBET-BD2 (GSK046) and 5 μM for I-BET151.

Chemoproteomic profiling on BD1/BD2 matrix

Competition binding assays on BET BD1 and BET BD2 resins were performed as described previously(4). Briefly, sepharose beads were derivatized with a 0.1mM of a proprietary linkable BD1-selective BET inhibitor (pIC_{50} BRD4 BD1/BD2 = 5.3/<4.3) (BD1 resin) and 0.02 mM of a proprietary linkable BD2-selective BET inhibitor (pIC_{50} BRD4 BD1/BD2 =4.9/7) (BD2 resin). Benzonase assisted total lysates from HL60 cells was performed as described(4). Lysates were pre-incubated with increasing concentration of GSK778 and GSK046 for 45 min at 4°C followed by addition of BD1 or BD2 resin for 1 hour at 4 °C. The beads were washed, eluted with 2 \times SDS sample buffer and subjected to SDS gel electrophoresis. Samples were further processed for LC-MS analysis. Sample preparation, labelling with TMT isobaric mass tags, peptide fractionation, and mass spectrometric analyses were performed as previously described (4). Apparent dissociation constants (K_{Dapp}) were derived from the EC_{50} values accounting for the amount of protein sequestered by the affinity-matrix using the Cheng-Prusoff relationship.

Crystallisation Methods

All the statistics for the data collection and refined co-ordinates are given in **supplementary Table 3**. The final crystal structures are deposited in the Protein Data Bank under the accession codes shown in **supplementary Table 3**.

BRD2 BD2/ iBET-BD1 (GSK778) soaks and structure determination

iBET-BD1 (GSK778) was soaked overnight into crystals of BRD2 BD2. These crystals were grown by streak seeding into hanging drops of 500 μl protein solution at 14.3 mg/mL and 500 μL well solution of 30% PEG 300, 0.1 M MES buffer pH6.5 at 20°C. Crystals appeared within 24 hrs and were transferred into a fresh solution of the same well solution with 2% DMSO and compound at nominally > 4 mM. Soaked crystals were briefly transferred into a solution consisting of 30%w/v PEG300, 0.1 M MES buffer, pH6.5 supplemented with 10% ethylene glycol prior to flash freezing

in liquid nitrogen. Data from a single crystal was collected 100K on an in-house RIGAKU FR-E⁺ SUPERBRIGHT/Saturn A200 detector/ACTOR robotic system and processed to 1.60 Å using XDS and AIMLESS. The P₂₁₂₁ cell ($\alpha=\beta=\gamma=90^\circ$, a=71.97 Å, b=52.71 Å, c=32.04 Å) has a single molecule in the ASU. Manual model building was performed using COOT and refined using REFMAC within the CCP4 software suite. Clear difference in density for the ligand in the acetylated lysine binding site was observed and the ligand was unambiguously modelled.

BRD4 BD1/ iBET-BD1 (GSK778) co-crystallisation and structure determination

BRD4 BD1/ iBET-BD1 (GSK778) was co-crystallised with at least 3:1 excess of compound over protein at 8.1 mg/ml in 120 nL+120 nL sitting drops using a 96 well MRC plate. Crystals grown with a well solution of 20% w/v PEG3350, 0.2 M NaI, 0.1 M bis-tris-propane, pH 7.5 at 20°C were cryoprotected using well solution with 20% ethylene glycol prior to flash freezing in liquid nitrogen. Data from a single crystal was collected 100K on ID29 at the European Synchrotron Facility (ESRF) at Genoble and processed to 1.28 Å using XDS and AIMLESS. A molecular replacement solution was determined using Phaser and a previously determined in house structure as a starting model. The P₂₁₂₁ cell ($\alpha=\beta=\gamma=90^\circ$, a=38.28 Å, b=42.32 Å, c=90.82 Å) has a single molecule in the ASU. Manual model building was performed using COOT and refined using REFMAC within the CCP4 software suite (44). There was a clear difference in density for the ligand in the acetylated lysine binding site, allowing the ligand to be unambiguously modelled.

BRD2 BD2/ iBET-BD2 (GSK046) soaks and structure determination

iBET-BD2 (GSK046) was soaked overnight into crystals of BRD2 BD2. These crystals were grown by streak seeding into hanging drops of 500 µL protein solution at 11.5 mg/mL and 500 µL well solution of 30% PEG 300, 0.1 M MES buffer pH6.5 at 20°C. Crystals appeared within 24 hrs and were transferred into a fresh solution of the same well solution with 2% DMSO and compound at nominally > 4 mM. Soaked crystals were briefly transferred into a solution consisting of 30% w/v PEG300, 0.1M MES buffer, pH 6.5 supplemented with 10% ethylene glycol prior to flash freezing in liquid nitrogen. Data from a single crystal was collected 100K on an in-house RIGAKU FR-E⁺ SUPERBRIGHT/Saturn A200 detector/ACTOR robotic system and processed to 1.60 Å using XDS and AIMLESS. The P₂₁₂₁ cell ($\alpha=\beta=\gamma=90^\circ$, a=72.20 Å, b=52.39 Å, c=32.02 Å) has a single molecule in the ASU. Manual model building was performed using COOT and refined using REFMAC within the CCP4 software suite (44). Clear difference in density for the ligand in the acetylated lysine binding site was observed and the ligand was unambiguously modelled.

BRD4 BD1/ iBET-BD2 (GSK046) co-crystallisation and structure determination

BRD4 BD1/ iBET-BD2 (GSK046) was co-crystallised with at least 3:1 excess of compound over protein at 8.1 mg/mL in 100 nL+100 nL sitting drops using a 96 well MRC plate at 20°C. Crystals grown with a well solution of 25%w/v PEG1500, 0.1 M SPG buffer, pH6 were cryoprotected using well solution with 33% ethylene glycol prior to flash freezing in liquid nitrogen. Data from a single crystal was collected 100K on an in-house RIGAKU FR-E⁺ SUPERBRIGHT/Saturn A200 detector/ACTOR robotic system and processed to 1.60 Å using autoPROC and AIMLESS (45). A molecular replacement solution was determined with a previously collected in house structure. The P₂₁₂₁ cell ($\alpha=\beta=\gamma=90^\circ$, a=37.13 Å b=44.06 Å, c=78.88 Å) has a single molecule in the ASU. Manual model building was performed using COOT and refined using REFMAC within the CCP4 software suite (44). There was clear difference in density for the ligand in the acetylated lysine binding site, allowing the ligand to be unambiguously modelled.

BioMAP® Diversity Plus System™

The BioMAP® Diversity Plus System™ was utilised to determine patterns of biological responses across compounds (<https://www.discoverx.com/services/drug-discovery-development-services/primary-cell-phenotypic-profiling>). Adherent cells were incubated to confluence at 37°C. Cells were pre-incubated with compound for 1 hour prior to appropriate stimulation. Assay plates were incubated for 24 hours for standard readouts. MyoF system was stimulated for 48 hours and BT was stimulated for either 72 hours (soluble readouts) or 6 days (secreted IgG). Cell proliferation was determined using either sulforhodamine B (SRB) assay for adherent cell types or Alamar Blue for PBMC cells. For proliferation assays, individual cell types were cultured at subconfluence and were read at specific times for different primary cell types (48, 72, or 96 hours). After stimulation, plates and supernatants were harvested and biomarkers quantified by ELISA. The grey envelope displayed on the graph represents the 95% confidence interval for vehicle control. Values with 2 concentrations that are outside of the 95% confidence interval are considered statistically different and those analytes are annotated in the graphical representation.

Cell line cultures

HEK293T cells were cultured in DMEM with 10% FCS with streptomycin (100µg/mL) and penicillin (100 units/mL) in 10% CO₂, 37 °C. Human AML cell lines (MV4;11, THP-1, MOLM13, K562) were grown in RPMI-1640 supplemented with 20% FCS, streptomycin (100µg/mL), penicillin (100 units/mL) and glutamax, under standard culture conditions (5% CO₂, 37 °C). MDA-MB-231 or MDA-453 were cultured in DMEM with 10% FCS with Streptomycin (100ug/ml) and penicillin (100units/mL).

All cell lines were subjected to regular mycoplasma testing and underwent authentication short tandem repeat (STR) profiling through the Australian Genome research facility (Melbourne, Victoria).

In vitro drug treatment

DMSO, I-BET151, iBET-BD1, iBET-BD2, and IAA (Auxin) were dosed by direct addition to the culture media at 0.1%. Drugs were refreshed every three days to ensure maximal activity. I-BET151, iBET-BD1, and iBET-BD2 were used at a final concentration of 1000 nM unless indicated otherwise. IAA was used at a concentration of 500µM. IFN γ was used at 10ng/ml and treatment for 48hrs for FACS analysis and 6hrs for SLAM-seq/ChIP-seq analysis.

Cancer cell line proliferation and concentration-response assays

For concentration-response assays, serial dilutions of compounds were prepared in media before addition to 96-well plates containing cells, to obtain a 0.1% DMSO final concentration. After 72 h incubation, resazurin was added to each well and plates were further incubated for 3 h. Fluorescence was then read at 560 nm/590 nm on a Cytation 3 Imaging Reader (BioTek). For proliferation assays, cells were seeded at a consistent density prior to treatment in triplicate and treated with DMSO, iBET-BD1, iBET-BD2 or I-BET151 over the indicated time period. Drug was refreshed at least every three days where needed. Cell number was calculated each day using the BD FACsVerse (BD Biosciences).

Flow Cytometry, Apoptosis and Cell Cycle

Apoptosis assays performed at 72 hrs post treatment with compounds, cells were washed once with PBS and assessed using FITC conjugated Annexin V (640906, Biolegend) and DAPI (D9542, Sigma) staining according to manufacturer's instructions. For cell cycle analysis performed 72 hrs post treatment with compounds, cells were washed with PBS and fixed for at least 2 hours at -20°C in 70% ethanol. Fixed cells were PBS washed and incubated at 4°C in 4',6-diamidino-2-phenylindole (DAPI) staining solution (1 mg/ mL DAPI, 0.05% (v/v) Triton X-100 in PBS) for 30 min. For surface expression of MHC-I, cells were washed in PBS and stained for HLA/B/C on ice for 30 min in PBS plus 5% FCS. All flow cytometry analyses were performed on a LSR Fortessa X-20 flow cytometer (BD Biosciences) and all data analysed with FlowJo. Cell sorting was performed on a FACSAria Fusion 5 (BD Biosciences).

Human primary CD4⁺ T cell culture assay

Human whole blood was obtained from three healthy volunteers from Clinical Trials Laboratory Service (for RNAseq and CHIPseq, London, UK) or GSK blood donation unit (Stevenage). Human biological samples were sourced ethically, and their research use was in accord with the terms of the informed consents under an IRB/EC approved protocol. PBMCs were isolated by Ficoll density-gradient centrifugation and total CD4⁺ T cells were purified using MACS CD4⁺ T cell isolation negative selection microbeads (Miltenyi Biotech).

CD4⁺ T cells were stained using Cell Trace Violet™ dye for subsequent proliferative analysis as per manufacturer's instructions, before being plated at 2×10^5 cells/ well in RPMI- 1640 medium supplemented with 10% heat-inactivated FBS, penicillin (100 units/mL), streptomycin (100 µg/mL) and 2 mM L-Glutamine over 72 hours in the presence of serial dilution of compound or 0.1% DMSO control. The supernatants were analysed by MesoScaleDiscovery (MSD). The cells were assessed for proliferative and viability end points by flow cytometry. Cell pellets were stained with Annexin V FITC (BD Pharmingen) and TOPRO-3 iodide (Invitrogen) as per manufacturers' protocol. Flow cytometry analyses were performed using a Becton Dickinson FACSCantoII™ and all data analysed by FlowJo version 7.6.5 (Becton-Dickinson). In all instances, data were analysed in GraphPad Prism v5.0.4 using the log(inhibitor) vs response – variable slope (four parameters) fit to determine IC50 and 95 % confidence intervals for each compound and to plot graphs.

THP-1 differentiation assay

THP-1 monocytic cells obtained from ATCC (TIB-202) were differentiated in RPMI 1640 culture medium supplemented with 10 % heat-inactivated FBS, penicillin (100 units/mL), streptomycin (100 µg/mL), L-Glutamine (2mM) and Phorbol 12-Myristate 13-Acetate (PMA; 20 ng/mL; EMD Millipore Corp) over 48 h in the presence of a serial dilution of compound or 0.5 % DMSO. Cell supernatants were harvested and analysed by MSD electrochemoluminescence assay. Cell pellets were assessed for ATP content using Cell Titre Glo (Promega) according to the manufacturer's protocol as a measure of metabolic activity and viability. Plates were read using a Perkin Elmer Envision 2104 Multilabel Reader.

2- dimensional thermal proteome profiling (2D-TPP)

Experiments were performed as described(42). In brief, THP1 cells (HepG2 cells for RVX 208) were treated with vehicle (DMSO) or compound (10, 1, 0.1 , 0.01 µM for GSK778 and GSK046; 20, 4, 0.57 , 0.082 µM for RVX 208) for 90 min at 37 °C and 5% CO₂, and collected by centrifugation. Cells were resuspended in PBS and transferred to 96-well PCR plates and heated

for 3 min to one of the 12 tested temperatures covering the range from 42°C to 64 °C. After cell lysis (in presence of Igepal CA-630 (I3021) 0.8%, MgCl₂ (M1028) 1.5 mM and benzonase 1 kU ml⁻¹) the aggregated proteins were separated by ultracentrifugation (20 min, 100,000g). Soluble proteins were digested following a modified solid-phase-enhanced sample preparation (SP3) protocol. In brief, proteins in 2% SDS were bound to paramagnetic beads (SeraMag Speed beads, GE Healthcare, 45152105050250, 651521050502) in filter plates (Multiscreen, Merck-Millipore, 10675743) and the plates were filled with 50% ethanol. Following washing of beads with four times 200 µl of 70% ethanol, beads were resuspended in trypsin and LysC in 0.1 mM HEPES, pH 8.5 containing TCEP and chloracetamide and incubated at room temperature overnight and subjected to TMT labeling. Labeled peptide extracts at 2 consecutive temperatures were combined in one TMT10 experiment. (in total 6 TMT 10 experiments per compound) and analyzed by LC-MS. The data analysis was performed as in (42). The stabilization score as a measure of monotonously increasing or decreasing protein thermal stability in response to increasing treatment concentrations across different temperatures was calculated as in (Perrin *et al.*2020)

MesoScaleDiscovery (MSD) electrochemiluminescence assays

CD4⁺ T cell supernatants were analysed by MSD electrochemiluminescence assay using a custom human 5-plex kit to measure IL-10, IL-13, IL-17, IFN γ and TNF α according to the manufacturer's protocol, or bespoke electrochemiluminescence assay using standard bind plates (MSD) and IL-22 antibody pairing (MabTech), using standard manufacturer's methodologies. THP-1 supernatants were analysed using a human MMP-9 ultrasensitive kit (MesoScaleDiscovery) according to the manufacturer's protocol. Plates were read using an MSD Sector Imager 6000 and analysed with Discovery workbench software v4.0.11, cytokine data were back-fitted to the MSD standard curve. Data were analysed in GraphPad Prism v5.0.5 using the log(inhibitor) vs response – variable slope (four parameters) fit to determine IC₅₀ and 95 % confidence intervals for each compound.

NanoBRET assays

HEK293 cells cultured in DMEM and 10% FBS, were plated in a 6-well plate at a density of 8x10⁵ cells/well and bulk co-transfected using Fugene HD (Promega) with 0.02µg of one of the following N-terminal NanoLuc fusion donor vectors: Full-length BRD4 (1362 AA, NM_058243), Full-length BRD4 N140F BD1 mutant, Full-length BRD4 N433F BD2 mutant, BRD4 BD1 alone domain (AA 44-168) or BRD4 BD2 alone domain (AA 333-460) in combination with 2µg of the C-terminal HaloTag fusion vector of Histone H4 (NP_003533). An additional control experiment was performed with NanoLuc-BRD4: HaloTag alone control vector (Promega G6591) with the same 0.02:2µg donor:acceptor ratio respectively. Eighteen hours post-transfection, cells were collected, washed with PBS, and exchanged into media containing phenol red-free OptiMEM and 4% FBS. Cells were then re-plated into Corning Costar plates (#3917) at a density of at 2x10⁴ cells/well in either the presence of 100nM NanoBRET 618 fluorescent ligand (Promega G9801) or the absence of the 618 ligand (no ligand control). Cells were then treated with a final concentration of 1µM of each indicated GSK compound, ABBV-744 (MedChemExpress #HY-112090), or DMSO and incubated for 24 hrs at 37°C in the presence of 5% CO₂. A 10-point dose response curve from 0-10µM was performed similarly on the NanoLuc-BRD4WT:HistoneH4 pair. NanoBRET Nano-Glo live cell substrate (Promega N1661) was added to all samples at a final concentration of 10µM. Readings were performed within immediately using the GloMax Discover Microplate Reader (Promega) equipped with 450/8 nm bandpass and 600 nm longpass filters.

Corrected BRET ratios were calculated to account for background and are defined as the ratio of the emission at 600 nm/450 nm for experimental samples (+ NanoBRET 618 ligand) subtracted by and the emission at 600 nm/450 nm for control samples (no 618 ligand). BRET ratios are expressed as milliBRET units (mBU), where 1 mBU corresponds to the corrected BRET ratio multiplied by 1000. To express the level of displacement from or increase of histone binding achieved after treatment with each compound for the different NanoBRET pairings, the % Occupancy was determined. For this calculation, the starting NanoBRET ratio of the DMSO control for each pair was set as 100% and the fractional loss or increase of NanoBRET ratio relative to this starting point was determined for each compound treatment.

Competitive Degradation Binding experiments

HEK293 cells stably expressing the LgBiT fusion protein (Promega) were edited using CRISPR/Cas9 to introduce HiBiT, an 11AA peptide tag, to the endogenous N-terminal genomic loci of BRD4 as described previously(43). The HiBiT-BRD4 CRISPR cell line was plated in white 96-well tissue culture plates at a density of 2×10^4 cells/well in 100 μ L DMEM + 10% FBS, and incubated for 18 hrs at 37°C in the presence of 5% CO₂. Medium was replaced with CO₂-independent medium (Gibco) including 20 μ M Endurazine (Promega N2570), an extended NanoGlo live cell substrate. The cells were incubated at 37°C in 5% CO₂ for 2.5 hours and then treated with a final concentration of 0.1 μ M MZ1 (Tocris #6154) or DMSO control. Plates were then read every 5 minutes on a GloMax Discover Microplate Reader (Promega) with a heated lid set to 37°C. Five hours post-addition of MZ1, the various inhibitors or a DMSO control were added directly to cells to a final concentration of 1 μ M and kinetic luminescent reading continued for a further 22 hours. The reported RLU signal of the DMSO control without any compound addition (no MZ1, no inhibitor) at each timepoint measured in kinetic analysis was set as the normalized baseline with a value of 1. The resultant loss of signal in samples treated with compounds were then calculated as a fractional RLU relative to the DMSO control, demonstrating both degradation and recovery.

Sample preparation for RNAseq and ChIPseq

Total CD4⁺ T cells were incubated at 1×10^6 cells/ ml with 0.1% DMSO, 0.5 μ M I-BET151, 0.5 μ M iBET-BD1 and 1 μ M iBET-BD2 for 30 minutes and activated with human T-activator CD3/CD28 dynabeads (Life Technologies) for 4 hours, with an additional unstimulated 0.1% DMSO control sample for RNAseq. For RNAseq: 1×10^6 cells / condition (prepared in triplicate) were harvested in RLT buffer and snap frozen at -80°C. For ChIPseq: Cells were crosslinked in 1% formaldehyde (Sigma) for 15 minutes, quenched with 125 mM glycine (Sigma) and washed in ice cold PBS (Invitrogen). Cell pellets were snap frozen at -80°C.

Chromatin immunoprecipitation sequencing (ChIP-seq)

Chromatin immunoprecipitation was performed as described previously(13). Briefly, for each ChIP, 20 million cells were crosslinked for 15 mins with 1% formaldehyde. Crosslinked material was sonicated to ~200–1000 bp using the Covaris Ultrasonicator e220. Sonicated material was incubated overnight with each antibody, then incubated for 3 h with Protein A magnetic beads. Beads were washed with low and high salt wash buffers, LiCl buffer and TE, before being eluted and decrosslinked overnight. DNA was purified using Qiagen Minelute columns. All ChIP

antibodies were used at ~10 μ g per IP and are listed under the antibodies section. Sequencing libraries were prepared from eluted DNA using Rubicon ThruPLEX DNA-seq kit. Libraries were size selected between 200–500 bps and sequenced on the NextSeq500 using the 75 bp single-end chemistry.

ChIP-seq analysis

Reads were aligned to the human genome (GRCh37.73) with BWA-mem. Duplicate reads and reads mapping to blacklist regions or the mitochondria were removed. Peak calling was performed with MACS2 with default parameters. Genome-browser images of ChIP-seq data was generated by converting the bam files from BWA to TDF files with igvtools and viewing in IGV. ChIP-seq coverage across selected genomic regions was calculated with BEDtools. Average profile plots were generated using the NGSplot software.

RNA-seq

RNA was extracted using the Qiagen RNeasy kit. RNA concentration was quantified with a NanoDrop spectrophotometer (Thermo Scientific). Libraries were prepared using QuantSeq 3' mRNA-seq Library Prep kit (Lexigen). Libraries were sequenced on the NextSeq500 using the 75 bp single end chemistry.

RNA-seq analysis

Reads were aligned to the human genome (GRCh37.73) using HiSAT and reads were assigned to genes using htseq-count. Differential expression was calculated using edgeR. Genes with a false discovery rate corrected for multiple testing using the method of Benjamini and Hochberg below 0.05 and an absolute log fold-change greater than 1 were considered significantly differentially expressed. Principal component analysis was performed on the RNA-Seq data. Heatmaps were generated using heatmap.2 function from the gplots package in R.

SLAM-seq

All SLAM-seq assays were performed at 60% of the maximum cell density counted on a hemocytometer for suspension cells. 5-7h prior to each assay, growth medium was aspirated and replaced. Unless stated otherwise, cells were pretreated with indicated small molecule inhibitors. Newly synthesized RNA was labeled for the last 60 minutes at the end of the treatment with the inhibitors at a final concentration of 100 μ M 4-Thiouridine (4sU, Carbosynth). Suspension cells were spun down and immediately snap-frozen, before RNA extraction using the RNeasy Plus Mini Kit (Qiagen). Total RNA was subjected to alkylation by iodoacetamide (Sigma, 10mM) for 15 minutes and RNA was re-purified by ethanol precipitation. 500ng alkylated RNA were used as input for generating 3' UTR mRNA sequencing libraries using a commercially available kit (QuantSeq 3' mRNA-Seq Library Prep Kit FWD for Illumina and PCR Add-on Kit for Illumina, Lexigen). Deep sequencing was performed using the Nextseq platform (Illumina).

SLAM-seq analysis

Reads were trimmed to remove adapters using cutadapt 1.14 . The SlamDunk pipeline v0.2.4 was used to align reads to the human genome (GRCh37.73) and the 3' UTR of genes. The coordinates of the 3' UTR were obtained from ensembl with the biomaRt package in R . The 3' UTR for each ensembl gene was merged using bedtools . The parameters used for running the SlamDunk pipeline were as described in Muhar et al. (28). The DESeq2 package in R was used to normalise the T to

C converted read counts using the size factors calculated from the total read counts. Differential expression was calculated using the NOISeq package in R. The false discovery rate from the NOISeq BIO algorithm of 0.05 and a fold change of greater than 2 was used to determine statistically significant differential expression. Principal component analysis was performed using the DESeq2 package in R, and heatmaps were drawn with the pheatmap package. Scatterplots of log fold change, average expression or FDR, and boxplots of log fold change were drawn using the ggplot2 and cowplot packages. Venn diagrams were drawn using the eulerr package.

New enhancer analysis

New enhancers were identified by H3K27ac peaks with > 2-fold higher read coverage after PMA or IFN γ or anti-CD3/CD28 treatment in THP-1 or K562 cells within 50 kb of genes. Average profiles and heatmaps of ChIP-seq in the 5 kb around the new enhancers were generated with ngs.plot.

Generation of CRISPR mediated HDR Knock-in

K562 cells were nucleofected using Amaxa Nucleofector (Lonza) with plasmids containing Cas9 and guideRNAs targeting BRD4 (1 μ g) along with plasmid template (1 μ g) containing 400bp long homology arms flanking Blast^R-T2A-mAID cassette. Modified cells were selected with blasticidin and individual clones were picked and checked for homozygous knock-in by western blot and genotyping PCR.

qRT-PCR

RNA was extracted using the Qiagen RNeasy kit. cDNA was prepared using SuperScript Vilo (Thermo Fisher) according to the manufacturers' instructions. Quantitative real-time PCR was performed on the Applied Biosystems StepOnePlus System using Fast SYBR green reagents (Thermo Fisher). Expression levels were determined using the $\Delta\Delta$ Ct method normalised to Gapdh or β 2 microglobulin.

Primer sequences for qRT-PCR

Primers	Sequence	Species	5`-3`
MYC	CTGGTGCTCCATGAGGAGA	human	forward
MYC	CCTGCCTCTTTCCACAGAA	human	reverse
GAPDH	GGAGCGAGATCCCTCCAAAAT	human	forward
GAPDH	GGCTGTTGTCATACTTCTCATGG	human	reverse
B2M	TGACTTTGTCACAGCCCAAG	human	forward
B2M	AGCAAGCAAGCAGAATTTGG	human	reverse
TAP1	CCTGTGGCACAACTCGGG	human	forward
TAP1	ATCTCCCAAGAGAGGAGAGGA	human	reverse

Immunoblotting

Cells were lysed using RIPA whole cell lysis buffer and solubilized by brief sonication. Whole cell lysates were then mixed with Laemmli buffer and separated via SDS-PAGE. SDS-PAGE gels were then transferred to PVDF membranes (Millipore) and incubated with primary antibodies (described below) at 1:1000 of the supplied concentration and secondary antibody conjugated with horseradish peroxidase at 1:10000 of the supplied concentration. Membranes were then incubated with ECL (GE Healthcare) and detected on X-ray film (Kodak).

Antibodies

Antibody		Clone	Lot No.	Cat	Company
BRD4	rabbit monoclonal	E2A7X	6	13440S	Cell Signalling
BRD4	rabbit monoclonal	EPR5150(2)	GR3251918-3	ab128874	Abcam
BRD3	rabbit polyclonal			A302-368A	Bethyl
BRD2	rabbit monoclonal	D89B4	3	5848S	Cell Signalling
Anti-Histone H3 (acetyl K27)	rabbit polyclonal		GR3231937-1	ab4729	Abcam
c-MYC	rabbit polyclonal		11	9402S	cell Signalling
Hsp60		C-10	G0119	sc-376240	Santa Cruz
Pol II		CTD4H8	3018777	05-623	Millipore
APC Annexin V			3186884	550475	BD Pharmingen
APC anti-human HLA-A,B,C		W6/32	B270596	311410	Biolegend

Clonogenic Assays in Methylcellulose

Clonogenic potential was assessed through colony growth of AML patient bone marrow plated in cytokine-supplemented methylcellulose (MethoCult H4434, Stemcell Technologies). Bone marrow was plated in duplicate at a cell dose of 2×10^4 cells per plate in the presence of vehicle (0.1% DMSO) or 1 μ M I-BET151, iBET-BD1 or iBET-BD2. Cells were incubated at 37°C and 5% CO₂ for 12 days at which time colonies were counted.

Patient Material

Patient samples used for analysis were collected as part of a study approved by the Peter MacCallum Cancer Centre human research ethics committee (10/78). Bone marrow containing >80% blasts was obtained from patients following consent and under full ethical approval by the Peter MacCallum Cancer Centre Research Ethics Committee.

Animal studies

All animal studies were ethically reviewed and carried out in accordance with Animals (Scientific Procedures) Act 1986 and the GSK Policy on the Care, Welfare and Treatment of Animals. The

studies here presented were reviewed and approved by the Institutional Animal Care and Use Committee at GSK and the Animal Experimentation Ethics Committee (AEEC) at Peter MacCallum Cancer Centre. All mice were randomized before the commencement of experiment.

Syngeneic mouse models of leukemia

Survival studies were performed with intravenous injection of 2×10^6 MLL-AF9 cells, into C57BL/6 female mice. The cells were obtained from bone marrow or spleen of mice that were injected with cells subjected to serial passaging (3°) *in vivo* as described previously(13). All mice were inspected daily and sacrificed upon signs of distress and disease. All mice were 6–8 weeks old at the time of sublethal irradiation at a dose of 3.5 Gy. Treatment with vehicle, I-BET151, iBET-BD1 or iBET-BD2 began at day 9 with daily BID. All compounds were administered at 15 mg/kg/BID. All mice were kept in a pathogen-free animal facility, inspected daily and sacrificed upon signs of distress and disease. Differences in Kaplan–Meier survival curves were analysed using the log-rank statistic.

Mouse Keyhole Limpet Hemocyanin (KLH) immunisation

Male C57bl/6 mice (8/10-weeks-old) were obtained from Charles River Laboratories UK. Mice were single housed for at least 7 days for acclimatisation to the laboratory environment. Animals received food and water *ad libitum*. On day 0 mice (n=10 per group) were intravenously injected via the tail vein with keyhole limpet hemocyanin (KLH)-saline solution (Imject Mariculture (mc) KLH, ThermoFisher Scientific, UK) delivering 1.2 mg/kg at 5 mL/kg solution. Animals were treated subcutaneously from day 0 until the end of the study with iBET-BD1 (15 mg/kg, BID), iBET-BD2 (40 mg/kg, QD), I-BET151 (15 mg/kg, QD) or vehicle control (2% DMSO with 98% - 10 % w/v - Kleptose in saline, BID or QD). On day 7 and 14 blood samples were collected via tail nick sampling from each mouse using EDTA coated microcapillary tubes and centrifuged to isolate plasma for T cell dependent antibody response (TDAR) assay. KLH specific antibodies were detected using mouse anti-KLH IgM (RB-14-006: Ray Biotech, UK) and anti-IgM HRP (Abcam, UK). The assay was read via colorimetric change, initiated by the substrate TMB (Cambridge Bioscience, UK), quenched by a dilute acid stop reagent (Cambridge Bioscience, UK) and quantified by spectrophotometry at a wavelength of 450 nm (Molecular Devices, Spectramax 250).

Rat collagen-induced arthritis (CIA)

Female Lewis rats (5-6 weeks age) were obtained from Charles River Laboratories UK, housed in groups of 4 according to treatment (n=8 per group) and acclimatised for 14 days to the laboratory environment. Animals received food and water *ad libitum*. On day 0, arthritis was induced by intradermal injection at the base of the tail of 100 μ L containing 200 μ g bovine type II collagen (MD Bioproducts, Switzerland) and Incomplete Freund's Adjuvant (IFA; Sigma-Aldrich, UK) emulsion. On day 7 a booster injection containing 200 μ g collagen, 3 μ g MDP and IFA was given. Rats were dosed orally once daily with 1% methylcellulose (vehicle), GSK620 (3, 10 or 30 mg/kg) or I-BET151 (3 mg/kg) from day 0 until termination on day 21 at a volume of 5 mL/kg body weight. Body weights were measured daily for the entire duration of the study. Arthritis was assessed blinded by clinical score of hind limbs. Clinical score was recorded on a 0-4 scale per paw according to the following criteria: 0 = no signs of arthritis; 1 = slight oedema and erythema on the foot or ankle; 2 = slight oedema and erythema to the entire paw; 3 = moderate oedema and

erythema to the entire paw; 4 = severe oedema and ankylosis (the maximum clinical score attainable per animal being 8). Paw swelling was measured using a plethysmometer (Linton Instrumentation, UK) on day 6, 12, 13, 14, 15, 18, 19 and 21 and recorded as the mean paw volume of both hind paws. On day 21, blood was collected via cardiac puncture under terminal anaesthesia. Blood was assessed for anti-rat collagen IgG1 antibodies by ELISA (Chondrex; AMS Biotechnology, UK).

Rats were culled by cervical dislocation and both hind limbs were removed, skinned and fixed in 4% paraformaldehyde, prior to obtaining Micro Computed Tomography (CT) scans processing for histological analysis. After a minimum of 24 h of fixation, the hind limbs were removed from fixative and analysed (Skyscan 1176 microCT scanner, Bruker). Projection images were acquired through 180° with source voltages and current of 50 kV and 500 mA respectively. Individual 3D reconstructions were generated with individual voxel dimensions of 35 x 35 x 35 µm. A subjective scoring technique examining new bone growth, erosion/uneven bone surface and apparent reduction in joint space was applied to determine the degree of arthritic changes seen in the ankle joints. All scoring was blinded to treatment group. The number of affected bones per hind limb (maximum of 14 per hind limb: 5 metatarsals, 5 main tarsals, calcaneus, talus, tibia and fibula), and an overall severity between 0 and 4 (none, minimal, mild, moderate, marked) were determined. The severity for each hind limb was calculated as the total number of affected bones multiplied by the severity with a maximum possible score per animal of 112 (sum of both hind limbs).

Following 7 days fixation the hind paws and knees were decalcified in 10% EDTA for 14 days at 4°C, then embedded in paraffin. Serial paraffin sections (4 µm) were stained with hematoxylin and eosin (H&E). All sections were evaluated histologically by two independent observers, and the gradation of arthritis was scored as described. H&E-stained hind limb sections were examined by light microscopy. Each section was assigned a qualitative score for the severity of arthritic changes; 0 = normal joint architecture, 1 = inflammation virtually absent, minimal synovial thickening, no bone remodelling or fibrosis, 2 = minimal mononuclear cell inflammation, some bone remodelling with rare new bone formation and fibrosis, synovial thickening present, 3 = moderate inflammatory changes and fibrosis with bone remodelling; lesion usually focal, 4 = marked remodelling of the bones, with degeneration/necrosis and new bone formation, chronic active inflammation and fibrosis, extensive lesions, involving all the joints/bones and 5 = severe remodelling of the bones, with degeneration/necrosis and new bone formation, chronic active inflammation, fibrosis and cyst formation, extensive lesions, involving all the joints/bones. Statistical analysis was performed using GraphPad Prism v5.0.4, with an ANOVA test followed by a Dunnet's multiple comparisons test.

Mouse imiquimod (IMQ)-induced psoriasis

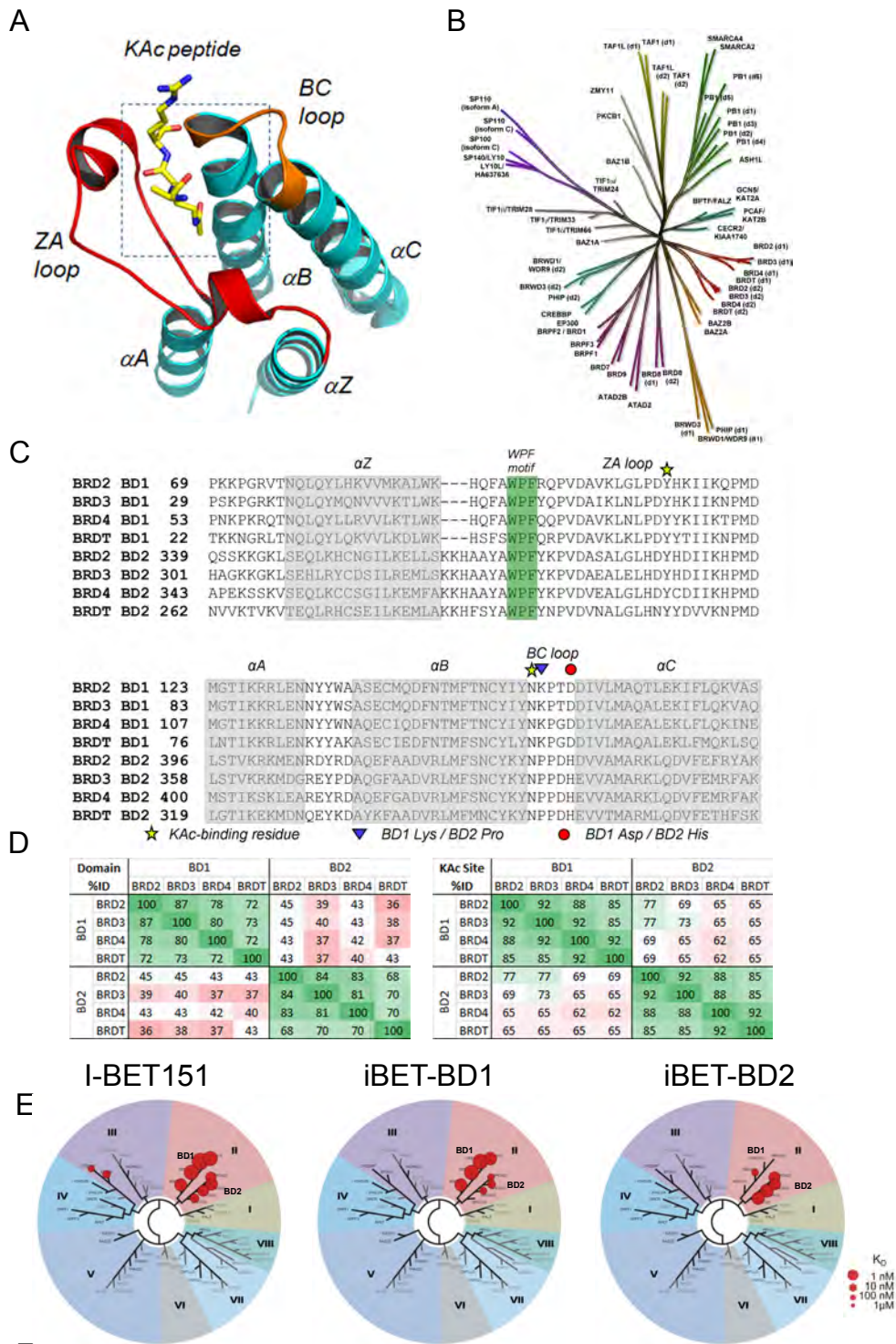
Female BALB/c mice (BALB/cByJRj) were obtained from Janvier (France). Mice (8-week-old at study initiation) were orally treated with 10 mL/kg of GSK620 (20 mg/kg QD), Apremilast (20 mg/kg BID) or vehicle (1% Methylcellulose in water) from Day -1 until the end of the study (Day 3). Starting on day 0, mice were challenged with imiquimod (IMQ) cream (5%) on their shaved back skin to induce psoriatic lesions. Vanicream was used as non-inflammatory inert cream control. Mice were monitored for changes in body weight and clinical symptoms over the course of the study. The psoriasis clinical score was established by daily visual observation from day 0, according to a 0-4 scale in ascending order of severity as follows: 0 = normal, 1 = slight erythema, 2 = moderate to severe erythema and some plaques, 3 = marked erythema and plaques, 4 = very marked erythema and plaques. On day 3 mice were sacrificed and blood and skin samples were

taken for subsequent processing. Skin samples were embedded in paraffin and 5µm serial sections were stained with hematoxylin and phloxin (H&P) to visualize histopathological changes and evaluate the severity of psoriasis. Epidermis thickness (10 measures per animal) was quantified with NanoZoomer Digital Pathology System C9600-02 (Hamamatsu). Gene expression the skin biopsies was measured by qPCR using Taqman probes (Life Technologies), ΔCt computed relative to β -actin and data shown as Mean \pm SEM relative gene expression to the vehicle + vanicream-treated group ($2^{-\Delta\Delta\text{Ct}}$). For histological analysis of the skin, the % reduction in epidermal thickening following compound treatment was calculated after subtraction of the mean value of the Vehicle treated group to all other Imiquimod-treated groups. Statistical analysis was performed using GraphPad Prism v5.0.4, with an ANOVA test followed by a Dunnet's multiple comparisons test.

nSTZ-HFD induced STAM NASH mouse model

The STAM mouse model of NASH was used to evaluate the *in vivo* efficacy of the BD2-selective BET inhibitor GSK620 against NASH and hepatic fibrosis. The overall design of the study is shown in **fig. S18A** (NASH phase **and fig. S18E** (fibrosis phase). The study was carried out at Wuxi AppTec (90 Delin Rd, Shanghai, China) on behalf of GlaxoSmithKline (GSK). 2-day old male C57BL/6 mice were injected by a single subcutaneous injection of 200 µg of streptozotocin to cause islet destruction and fed a high fat diet (60% energy from fat, D12492; Research Diets, Inc) from 4 weeks of age and continuing for the entire duration of each study. GSK620 (20 mg/kg), positive control Telmisartan (10 mg/kg)- an angiotensin II receptor antagonist (QW32M-GS; Tokyo chemical industry Co. Ltd)- or vehicle (1% (w/v) Methylcellulose in water) were administered orally QD for the periods of time indicated in the study design. Changes in body weight were monitored throughout the study duration. At study termination animals were sacrificed by exsanguination through direct cardiac puncture under terminal ether anaesthesia. Liver biopsies were collected for gene expression and histopathological analysis. Formalin-Fixed Paraffin-Embedded (FFPE) Liver blocks were stained with H&E or Sirius Red to assess NAFLD score and liver fibrosis respectively. Total RNA was extracted from each liver sample using RNeasy Mini Kit (Qiagen). cDNA was prepared using a High Capacity cDNA Reverse Transcription Kit (AB). Real-time PCR for each gene was performed using Faststart Universal Probe Master (ROX) (Roche). ΔCt was computed relative to the 18S rRNA and data shown as Mean \pm SEM relative gene expression to the healthy group ($2^{-\Delta\Delta\text{Ct}}$). NAFLD Activity score (NAS) and Fibrosis score: For H&E staining, 4 µm) thick serial sections were cut from FFPE blocks of liver tissue obtained from the left lateral lobe and stained with Lillie-Mayer's H&E solution. Oil-red staining was performed on 15 µm thick sections obtained from snap frozen tissue samples embedded in OCT blocks. To visualize collagen deposition, fixed liver sections were stained using picro-Sirius red solution. NAS was calculated according to Kleiner's criteria. Scoring using NAS was performed by two certified pathologists blinded to treatment group using the three criteria of steatosis, hepatocyte ballooning, and lobular inflammation, and a third in-house pathologist was included in the final assessment of NAS scores. Steatosis in hepatocytes was scored as 0, 1, 2, or 3 if there were less than 5%, 5–33%, 33–66%, and greater than 66% hepatocytes with fat, respectively. Hepatocyte ballooning was scored as 0 if there was none, 1 if there were few ballooned cells, and 2 if there were many cells with prominent ballooning. Lobular inflammation was scored as 0, 1, 2, or 3 if there were none, less than 2, 2–4, or greater than 4 inflammatory foci per 200x field, respectively. These individual scores were summed to give the NAS for each animal. Statistical analysis of the histological scoring was determined using Kruskal-Wallis

followed by Dunnett's multiple comparison test and One-way ANOVA followed by Dunnett's multiple comparison test for gene expression data.



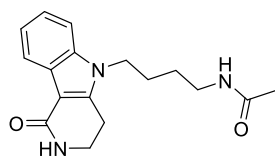
F

Compound	BRD4 (nM)		Fold selectivity
	BD1 (TR-FRET IC ₅₀)	BD2 (TR-FRET IC ₅₀)	
I-BET151	36	329	9 ^a
iBET-BD1	41	5843	143 ^a
iBET-BD2	> 50119	49	>1023 ^b

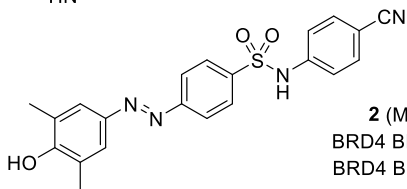
^a BD1 vs BD2; ^b BD2 vs BD1

Fig. S1. (A) Prototypical bromodomain architecture with Kac peptide bound. **(B)** Bromodomain phylogenetic tree **(C)** Sequence alignment of BET bromodomains. **(D)** Amino acid sequence homology (percent identity, green=high red=low) between BET family bromodomains, calculated at the domain level (left panel) and over the 26 residues surrounding the acetyl-lysine site (right panel, BRD4 BD1 residues 81-89,91-94,97-98,132,135-136,139-141,144-147,149). **(E)** Phylogenetic tree of bromodomains demonstrating preferential compound binding for the BD1 and/or BD2 domains using the BROMOscan bromodomain competition binding assay (Eurofins DiscoverX Corporation). Red dots represent K_D values. **(F)** Comparison of TR-FRET and surface plasmon resonance (SPR) potency and selectivity of compounds for BRD4 BD1 and BD2.

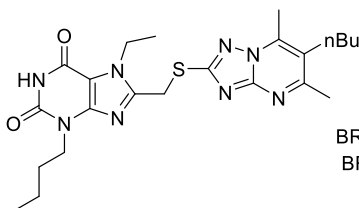
BD1-Biased Inhibitors



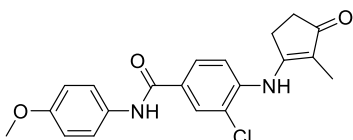
1 (Olinone): ITC
BRD4 BD1 $K_d = 3.4 \mu\text{M}$
BRD4 BD2 $K_d > 300 \mu\text{M}$



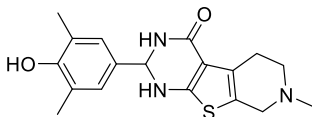
2 (MS611): FAB
BRD4 BD1 $K_i = 0.41 \mu\text{M}$
BRD4 BD2 $K_i = 41.3 \mu\text{M}$



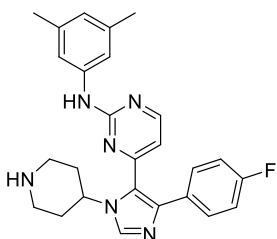
3: HTRF
BRD4 BD1 $\text{IC}_{50} = 5.0 \mu\text{M}$
BRD4 BD2 $\text{IC}_{50} > 50 \mu\text{M}$



4 (MS402): FAB
BRD4 BD1 = 77 nM
BRD4 BD2 = 718 nM

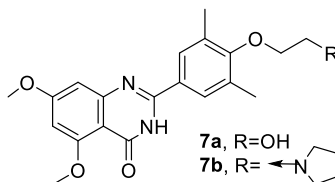


5 (FL-411): TR-FRET
BRD4 BD1 = 0.47 μM
BRD4 BD2 = 0.93 μM
BRD2 BD1 = 25 μM
BRD2 BD2 > 100 μM



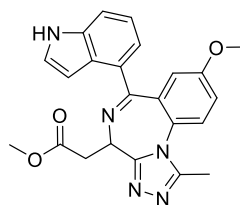
6: ALPHAscreen
Brd4 BD1 $\text{IC}_{50} = 1.8 \mu\text{M}$
Brd4 BD2 $\text{IC}_{50} > 100 \mu\text{M}$

BD2-Biased Inhibitors

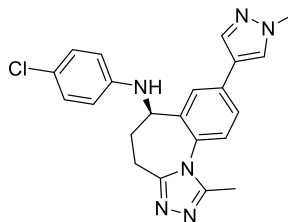


9 (RVX-208): ITC
BRD4 BD1 $K_d = 8.9 \mu\text{M}$
BRD4 BD2 $K_d = 0.3 \mu\text{M}$

10 (RVX-297): ITC
BRD4 BD1 $K_d = 1.4 \mu\text{M}$
BRD4 BD2 $K_d = 0.18 \mu\text{M}$

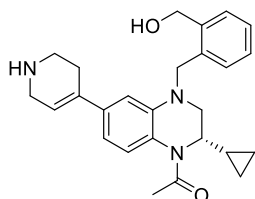


11: ITC
BRD4 BD1 $K_d = 520 \text{ nM}$
BRD4 BD2 $K_d = 50 \text{ nM}$



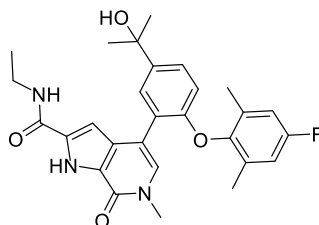
12 (BY27): FP
BRD4 BD1 $K_d = 80 \text{ nM}$
BRD4 BD2 $K_d = 7.3 \text{ nM}$

DiscoverX BROMOscan
BRD4 BD1 $K_d = 26 \text{ nM}$
BRD4 BD2 $K_d = 3.5 \text{ nM}$



13 (GSK340): FRET
BRD4 BD1 $\text{IC}_{50} = 3.0 \mu\text{M}$
BRD4 BD2 $\text{IC}_{50} = 60 \text{ nM}$

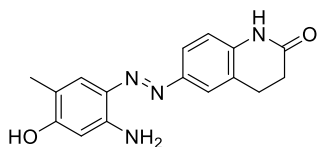
DiscoverX BROMOscan
BRD4 BD1 $K_d = 1.6 \mu\text{M}$
BRD4 BD2 $K_d = 6 \text{ nM}$



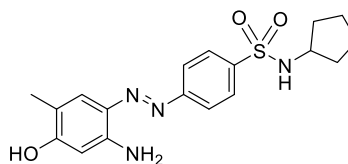
14 (ABBV-744): SPR
BRD4 BD1 $K_d = 3.3 \mu\text{M}$
BRD4 BD2 $K_d = 2.1 \text{ nM}$

NanoBRET
BRD4 BD1 $\text{IC}_{50} = 20.7 \mu\text{M}$
BRD4 BD2 $\text{IC}_{50} = 27.5 \text{ nM}$

Inhibitors reported to show BRD4 selectivity



7 (ZL0420): FRET
BRD4 BD1 $\text{IC}_{50} = 27 \text{ nM}$
BRD4 BD2 $\text{IC}_{50} = 32 \text{ nM}$
BRD3 BD1 $\text{IC}_{50} = 2.3 \mu\text{M}$
BRD3 BD2 $\text{IC}_{50} = 2.2 \mu\text{M}$



8 (ZL0454): FRET
BRD4 BD1 $\text{IC}_{50} = 49 \text{ nM}$
BRD4 BD2 $\text{IC}_{50} = 32 \text{ nM}$
BRD3 BD1 $\text{IC}_{50} = 2.5 \mu\text{M}$
BRD3 BD2 $\text{IC}_{50} = 2.2 \mu\text{M}$

Fig. S2. Structures of selected literature compounds with reported BET domain bias and their reported affinities.

A

Cpd	Name	TR-FRET BRD4 BD1 pIC ₅₀	TR-FRET BRD4 BD2 pIC ₅₀	TR-FRET selectivity (Δ pIC ₅₀)	BRD4 BD1 pK _d BROMOscan	BRD4 BD2 pK _d BROMOscan
2	MS611	6.2 ± 0.06 (4)	5.1 ± 0.17 (4)	1.1	ND	ND
3	-	4.5 ± 0.01 (2/3)	< 4.3 (3)	ND	ND	ND
4	MS402	6.1 ± 0.06 (3)	5.1 ± 0.07 (3)	1.0	ND	ND
5	FL-411	5.5 (1)	< 4.3 (1)	ND	ND	ND
7	ZL0420 †	5.8 ± 0.12 (4)	5.2 ± 0.08 (4)	0.6	ND	ND
8	ZL0454 †	6.1 ± 0.06 (6)	5.7 ± 0.16 (6)	0.4	ND	ND
9	RVX-208	5.2 ± 0.03 (5)	5.8 ± 0.06 (5)	0.6	ND	ND
10	RVX-297	5.5 ± 0.04 (3)	6.1 ± 0.05 (3)	0.6	ND	ND
13	GSK340	5.5 ± 0.13 (6)	7.2 ± 0.07 (6)	1.7	5.8 (1)	8.2 (1)
14	ABBV-744	6.4 ± 0.05 (8)	8.3 ± 0.1 (8) ‡	1.9	6.6 ± 0.09 (2)	9.3 ± 0.03 (2)
15	I-BET151	7.6 ± 0.03 (15)	6.5 ± 0.03 (16)	1.1	8.2 ± 0.02 (2)	7.5 ± 0.02 (2)
16	GSK778	7.4 ± 0.15 (16)	5.2 ± 0.09 (16)	2.2	8.2 (1)	6.2 (1)
17	GSK046	4.3 ± 0.44 (3/11)	7.3 ± 0.17 (12)	≥ 3.0	6.1 ± 0.02 (2)	8.0 ± 0.01 (2)
18	GSK620	4.8 ± 0.16 (14)	7.1 ± 0.19 (16)	2.3	5.6 (1)	8.2 (1)

† ZL0420 and ZL0454 show similar micromolar inhibition in all eight BRD2/3/4/T TR-FRET assays, e.g.

ZL0420 TR-FRET pIC₅₀ BRD3 BD1 5.8 (2), BRD3 BD2 5.5 ± 0.01 (2)

ZL0454 TR-FRET pIC₅₀ BRD3 BD1 6.1 ± 0.01 (2), BRD3 BD2 6.0 ± 0.01 (2)

‡ Possible underestimate: theoretical tight-binding limit of BRD4 BD2 TR-FRET assay is estimated to be ~ 5nM

B

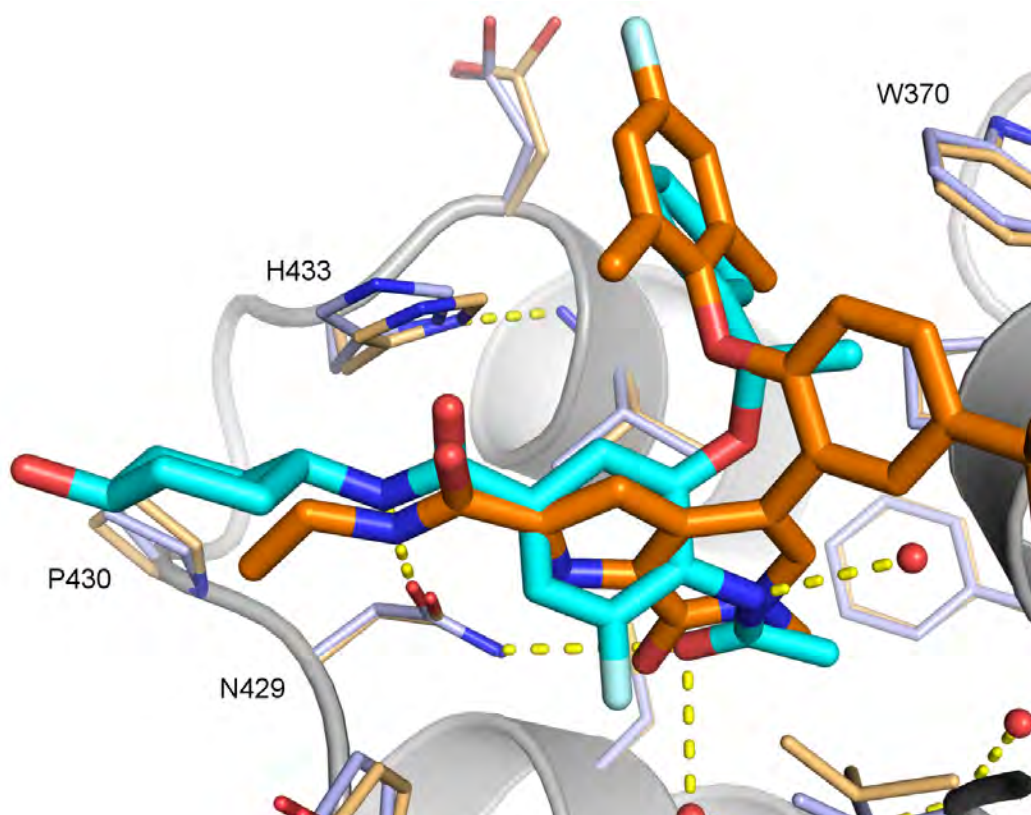
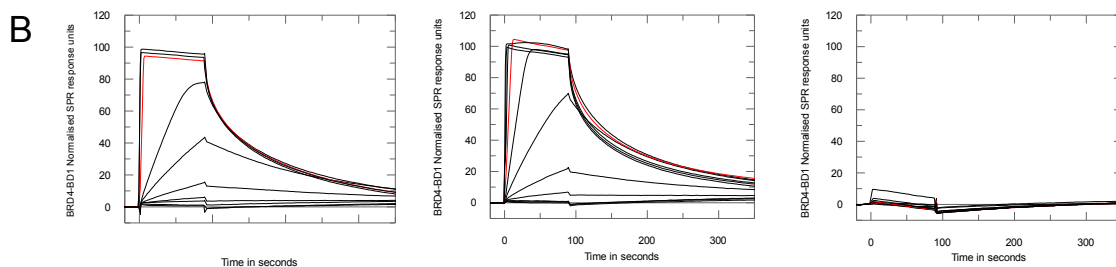
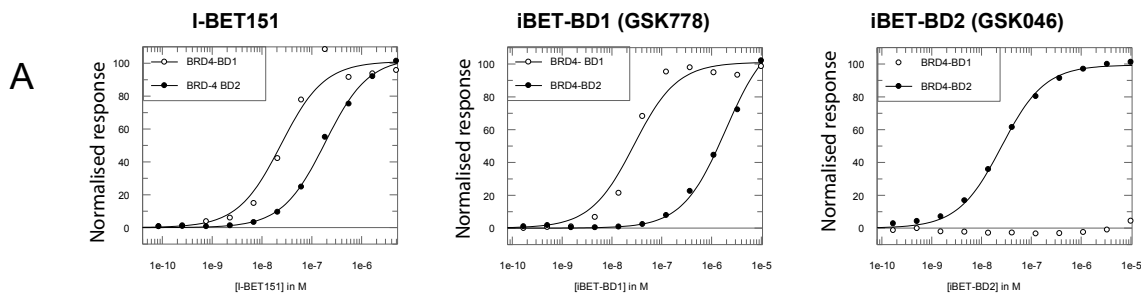


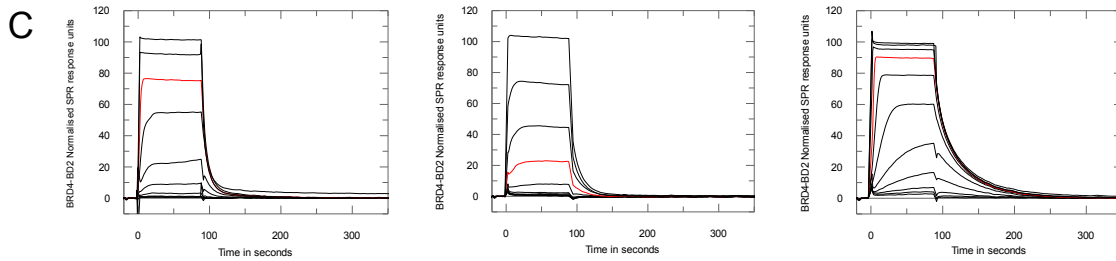
Fig. S3. (A) Affinity of compounds measured in a TR-FRET assay at GlaxoSmithKline and in the BROMOscan assay at DiscoverX.^{13,14} The TR-FRET assay uses 6H-Thr-BRD4(1-477) tandem bromodomain with Y390A or Y97A mutations to monitor BD1 and BD2 fluoroligand binding respectively. Data represents the mean $pIC_{50} \pm SD$ (number of test occasions). Some pIC_{50} results below the curve-fitting threshold ($pIC_{50} < 4.3$) cannot be included in mean and SD and in these cases the (number included in mean / number of times tested) are shown. For each assay technology, the greater of the BD1 and BD2 results is color-coded (green = higher affinity). The selectivity column shows the absolute difference between BD1 and BD2 pIC_{50} (green = greater selectivity). ND = not determined. We systematically find lower K_d values in the BROMOscan assays than IC_{50} values in TR-FRET. **(B)** Superimposed crystal structures of BRD2 BD2 bound to iBET-BD2 (cyan, PDB 6SWP) and ABBV-744 (orange, PDB 6E6J¹⁵).



(red = 0.56 μ M)

(red = 0.37 μ M)

(red = 0.37 μ M)



(red = 0.56 μ M)

(red = 0.37 μ M)

(red = 0.37 μ M)

D

Compound	BRD4-BD1			BRD4-BD2		
	Mean	SEM	n	Mean	SEM	n#
I-BET151	19	6	3	172	24	4
iBET-BD1	19	4	4	2480	525	5
iBET-BD2	>10000	N/A	3	30	4	4

No of independent measurements

Fig. S4. Exemplar data of SPR data for the three compounds **(A)** Normalised dose response curves for binding to BRD4 BD1 and BRD4 BD2. Normalised sensorgrams at the same concentrations as used for **(B)** showing binding of BRD4 BD1 **(C)** and BRD4 BD2. The sensorgram from a single concentration, where the highest affinity domain is saturated, is highlighted in red to illustrate degree of selectivity displayed by the compound. **(D)** Summary table of SPR potency for binding to BRD4 BD1 and BRD4 BD2.

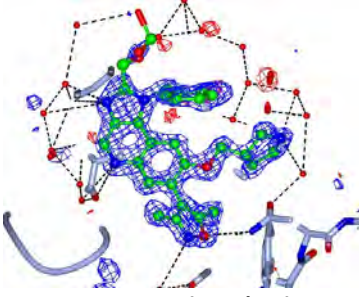
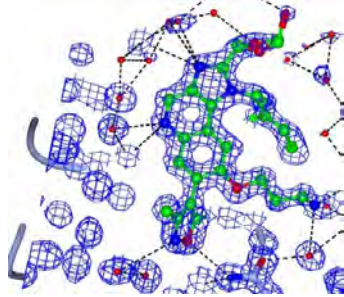
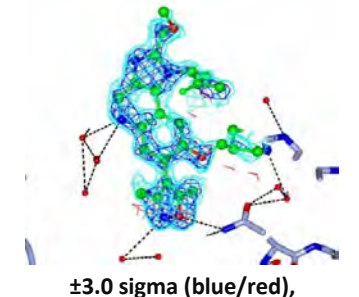
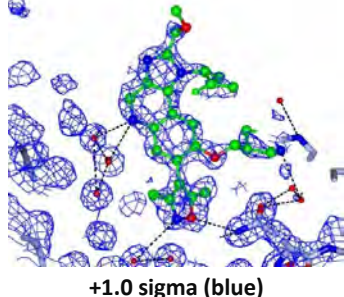
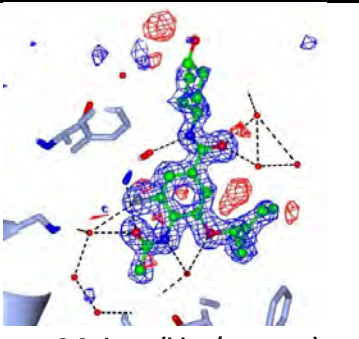
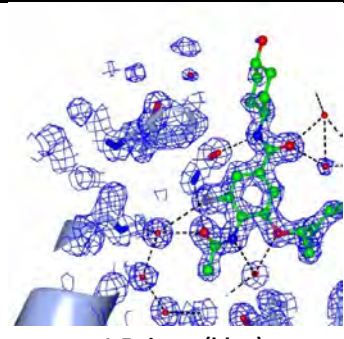
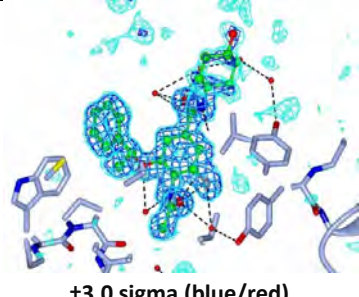
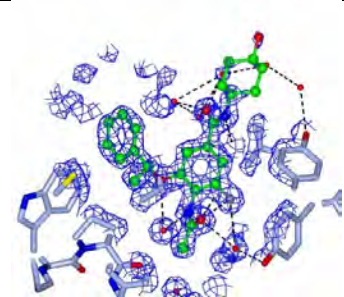
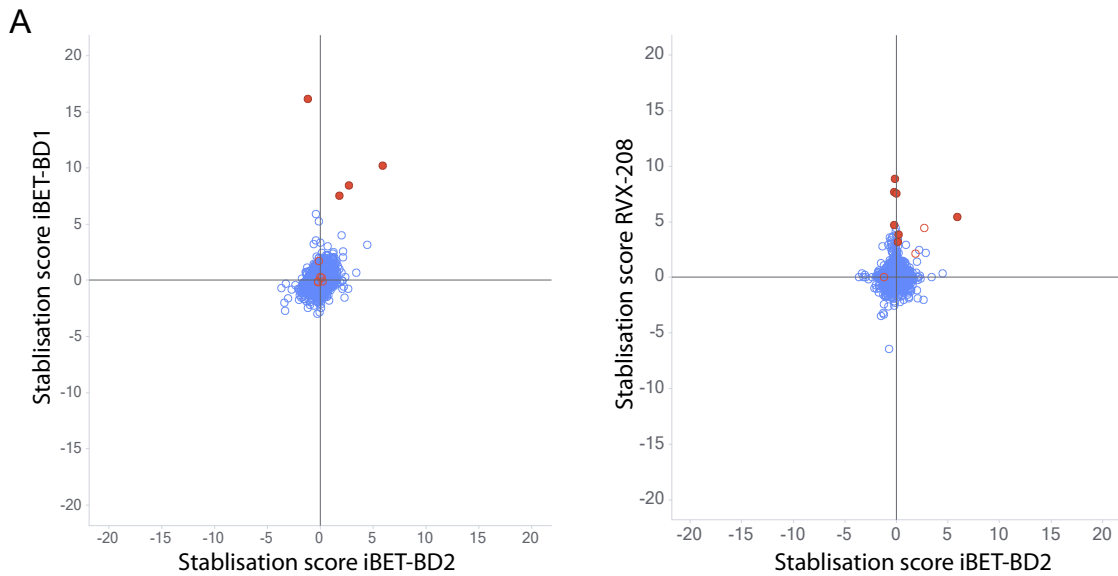
Protein/compound	Fo-Fc OMIT map	2Fo-Fc OMIT map
BRD4 BD1 / iBET-BD1 (GSK778) PDB 6SWN	 <p data-bbox="581 598 807 632">±3.0 sigma (blue/red)</p>	 <p data-bbox="976 598 1154 632">+1.5 sigma (blue)</p>
BRD2 BD2 / iBET-BD1 (GSK778) PDB 6SWO	 <p data-bbox="581 913 807 968">±3.0 sigma (blue/red), +2.0 sigma (cyan)</p>	 <p data-bbox="976 913 1154 947">+1.0 sigma (blue)</p>
BRD2 BD2 / iBET-BD2 (GSK046) PDB 6SWP	 <p data-bbox="553 1312 834 1335">±3.0 sigma (blue/magenta)</p>	 <p data-bbox="976 1312 1154 1335">+1.5 sigma (blue)</p>
BRD4 BD1 / iBET-BD2 (GSK046) PDB 6SWQ	 <p data-bbox="581 1617 807 1684">±3.0 sigma (blue/red), +2.0 sigma (cyan)</p>	 <p data-bbox="976 1638 1154 1671">+1.5 sigma (blue)</p>

Fig. S5. Electron density maps showing ligand density for BRD4 BD1 and BRD2 BD2 X-ray structures.



B

compound	GSK778	GSK046	RVX 208
cells system	THP1 cells	THP1 cells	HepG2 cells
Top concentration	10 μ M	10 μ M	20 μ M
#	protein	Stabilization score	Stabilization score
1	BRD2	7.6	1.8
2	BRD3	10.2	5.9
3	BRD4	8.5	2.7
4	CYP4F12	n.d.	6.1
5	FECH	1.7	-0.1
6	HEBP1	-0.2	-0.2
7	NMRAL1	-0.1	0.2
8	NSDHL	-0.1	-0.2
9	NUDT1	16.1	-1.2
10	OSBP1	0.2	0.2
11	SDR39U1	-0.1	n.d.
12	TXNIP*	0.3	0

* Temperature independent expression or extraction effect

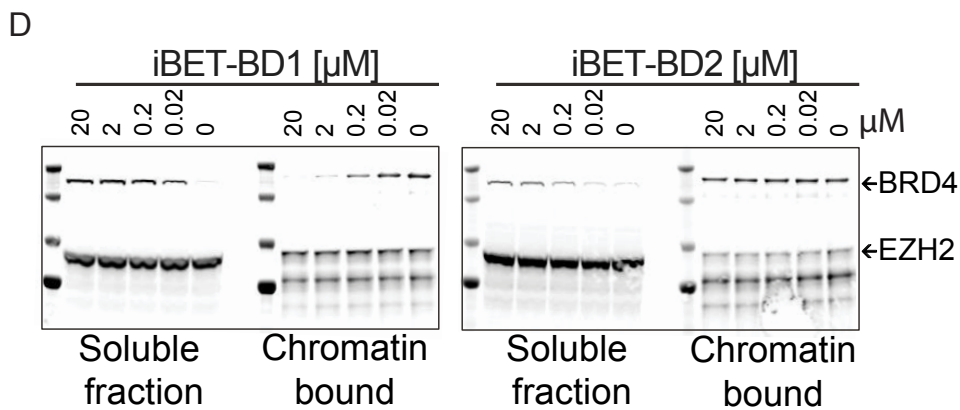
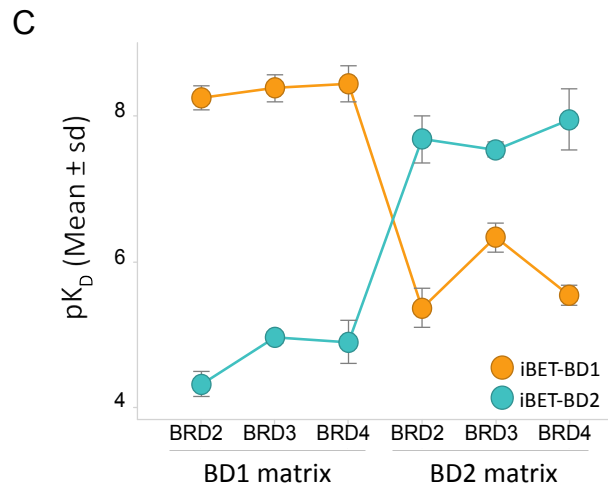


Fig. S6. (A) Scattered plot illustrating proteome-wide selectivity of BET inhibitors as determined by 2- dimensional thermal proteome profiling. Dose-dependent stabilization was aggregated to stabilization scores representing a measure of monotonously increasing or decreasing protein thermal stability in response to increasing treatment concentrations (10, 1, 0.1, 0.01 μM for THP1 cells and 20, 4, 0.57, 0.082 μM for HepG2 cells) across different temperatures. Highlighted proteins (red) were identified as hits (see table **(B)**) with at least one compound requiring dose-dependent stabilization at least two adjacent temperatures, quantification based on at least 2 unique peptides and 2-fold stabilization in one of the experiments. Red circles indicate proteins that qualified as hit by one of the compounds. Blue circles indicate proteins not affected in any of the compounds. **(C)** Potency and domain selectivity of iBET-BD1 and iBET-BD2 for endogenous BET proteins. The affinity (pK_D) of compounds for the BD1 and BD2 domains is measured in a concentration response competition experiment in cell lysates on BD1 and BD2 selective matrices. pK_D 's were calculated after assessment of matrix depletion factors. Data are the mean \pm SD (n = 3). **(D)** Soluble and chromatin fractions were separated from HL-60 cells treated for 90 mins with a combination of vorinostat and BET inhibitors at different concentrations as indicated. Immunoblotting using antibodies specific for BRD4 and EZH2 (negative control) are shown. Soluble fraction represents the proteins that are eluted from the chromatin fraction after drug treatment.

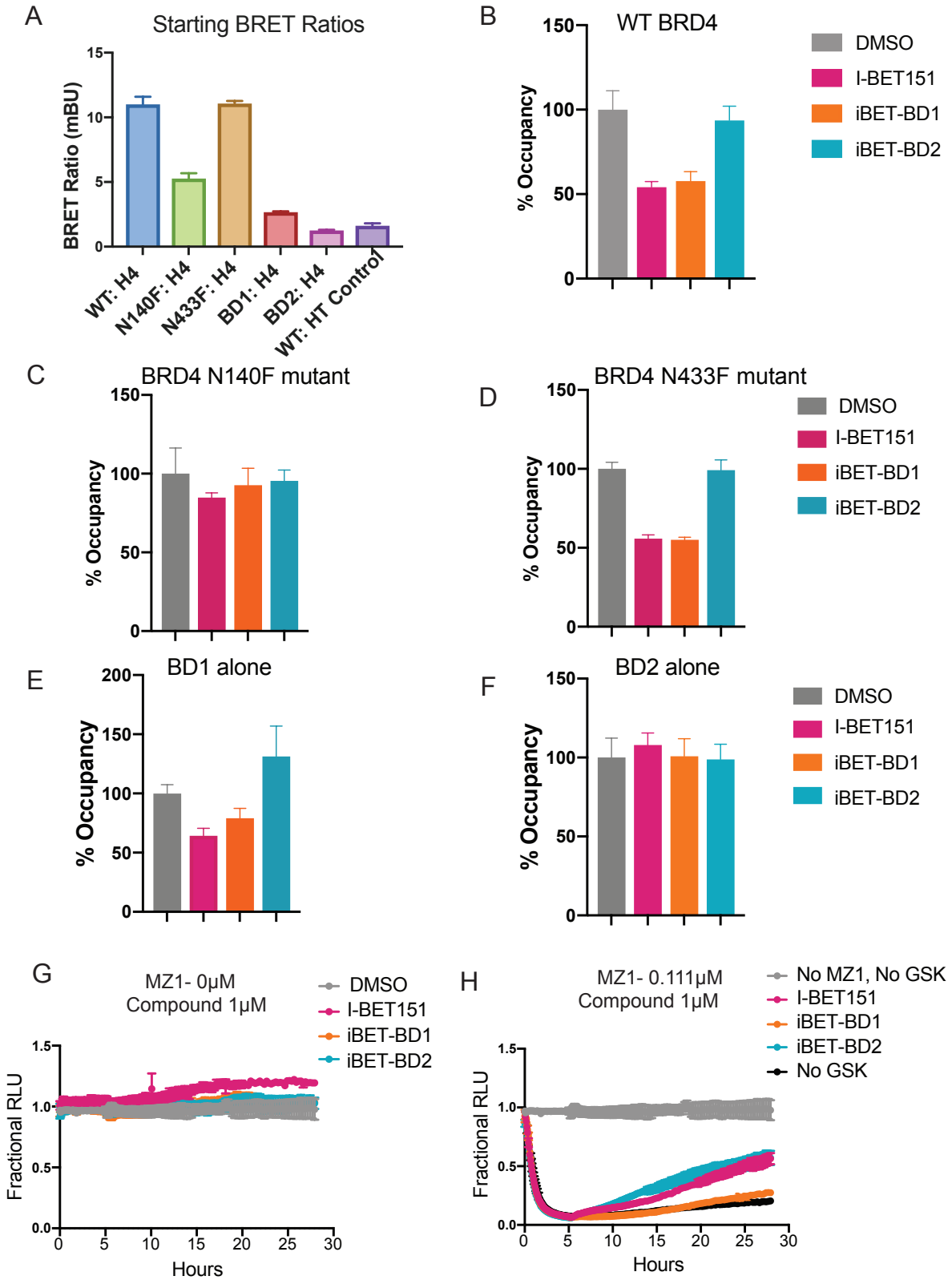


Fig. S7. (A-F) NanoBRET cellular interaction assays of BRD4 with Histone H4. **(A)** Initial NanoBRET ratios were calculated as described in Methods for HEK293 cells co-transfected with Histone H4-HaloTag and one of the following NanoLuc-BRD4 fusions; WT, N140F, N433F, BD1, or BD2. Difference of initial ratios reflect differences in chromatin binding of the BRD4 variants. A NanoBRET negative control of BRD4 WT with HaloTag alone vector is also shown. Error bars are expressed as SEM from n=4 experiments. This assay further illustrates the critical role of BD1 in chromatin binding. **(B-F)** NanoBRET assays in HEK293 cells of the indicated BRD4:H4 pairs showing resulting % Occupancy of global cellular chromatin binding after a twenty-four hour treatment with 1 μ M of I-BET151, iBET-BD1, iBET-BD2, or DMSO control. Chromatin displacement patterns of I-BET151 and iBET-BD1 are similar, with significant displacement only of BRD4 variants that contain a functional BD1 domain. iBET-BD2 does not show chromatin displacement of any of the BRD4 constructs. The % Occupancy is expressed as the fractional loss or increase in NanoBRET ratio relative to the DMSO control. Error bars are expressed as SEM from n=4 experiments. **(G-H)** HEK293 cells containing endogenously tagged HiBiT- BRD4 **(G)** and co-expressing LgBiT (Riching et al., ACS Chem Bio 2018), were treated with DMSO for 5 hours, followed by 1 μ M of I-BET151, i-BET-BD1, iBET-BD2, or DMSO control. Luminescence (RLU) was continuously monitored for the time indicated on graphs and any changes in endogenous BET family proteins levels post-treatment of inhibitors are directly correlated with changes in measured luminescence. Profiles are plotted as mean fractional RLU values by normalizing each time point to DMSO control and error bars are expressed as SEM from n=4 experiments. **(H)** Competitive cellular binding experiments with BET family PROTAC, MZ1 (Zengerle, et. al., ACS Chem Biol 2015). HEK293 cells containing endogenously tagged HiBiT-BRD4 (N) were treated with 0.1 μ M MZ1 for 5 hours to initiate degradation, followed by 1 μ M treatment of I-BET151, i-BET-BD1, iBET-BD2, or DMSO control. Luminescence (RLU) was continuously monitored in live cells for the time indicated on graphs. All compounds, with the exception of iBET-BD1, showed the ability to compete degradation driven by the MZ1 PROTAC, which has shown to have BD2 binding preference over BD1 (Gadd, et. al, Nature Chem Biol 2017). Fractional RLU was plotted similar to graphs shown in I-K and error bars are expressed as SEM from n=4 experiments. These data provide an orthogonal approach to confirm the BD2 specificity for iBET-BD2 and illustrate that iBET-BD1 is incapable of efficiently engaging the BD2 domain in a cellular context.

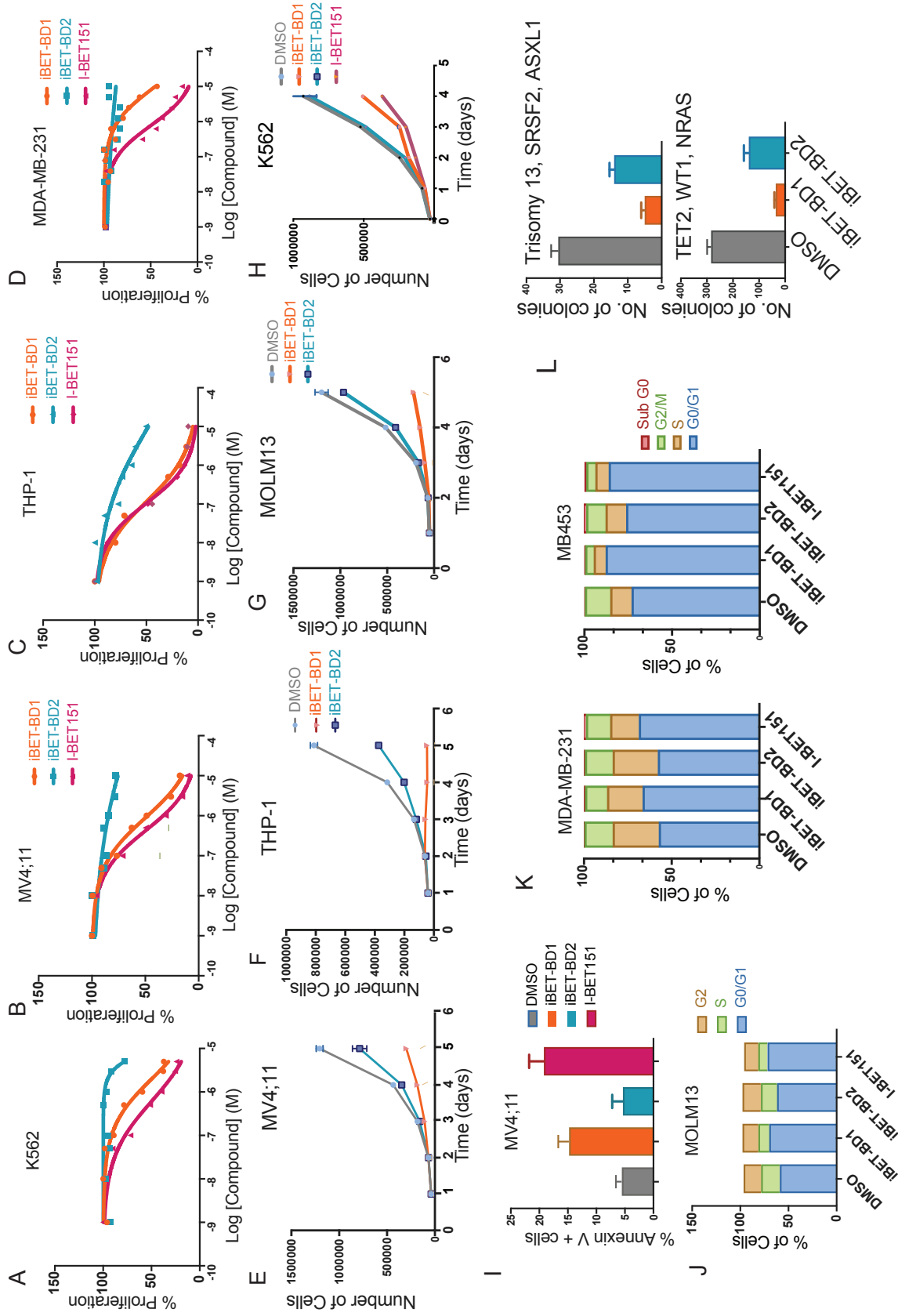


Fig. S8. (A-D) IC50 assays performed at 72hrs in K562, MV411, THP-1, and MDA-231 following incubation with increasing doses of iBET-BD1, iBET-BD2, or IBET151 **(E-H)** Proliferation assays performed with human MV4;11, THP-1, MOLM13 and K562 cells treated with DMSO, iBET-BD1 or iBET-BD2 at 1000nM. Mean \pm s.d. (n = 3 cell culture replicates) are plotted in a representative from three independent experiments. **(I)** Apoptosis assay performed on MV4;11. Cells treated with DMSO, I-BET151 (1000nM), iBET-BD1 (1000nM), or iBET-BD2 (1000nM), cells were stained with Annexin V and analysed by flow cytometry. **(J-K)** Cell cycle analysis of MOLM13, MDA-MB-231 and MB453 cells treated with DMSO, I-BET151 (1000nM), iBET-BD1 (1000nM) or iBET-BD2 (1000nM). Cells were fixed, permeabilized, stained with DAPI and analysed by Flow cytometry. **(L)** Colony assays with two relapsed/refractory AML patient samples treated with either Vehicle (DMSO), iBET-BD1 or iBET-BD2 (1000nM). Assay was done in duplicates for each patient.

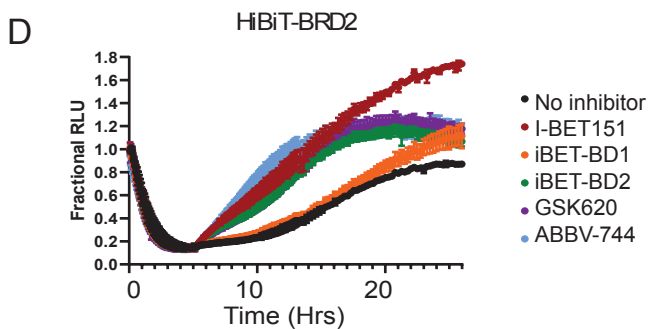
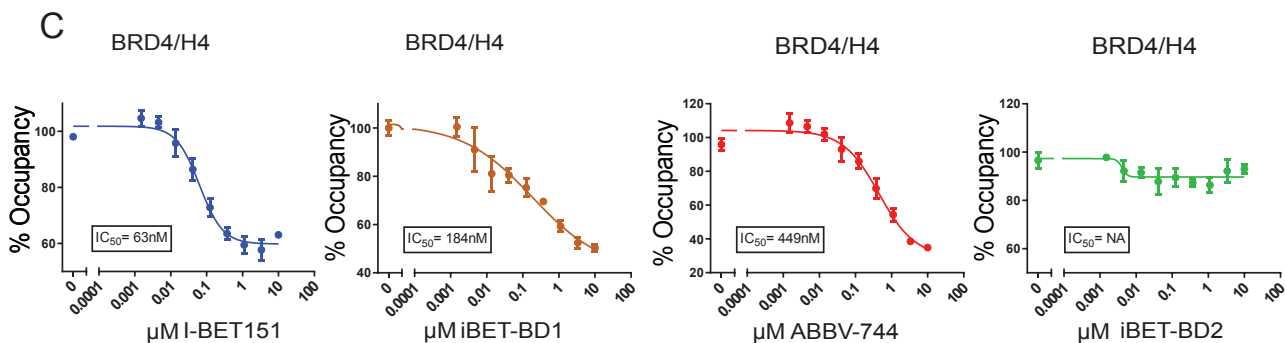
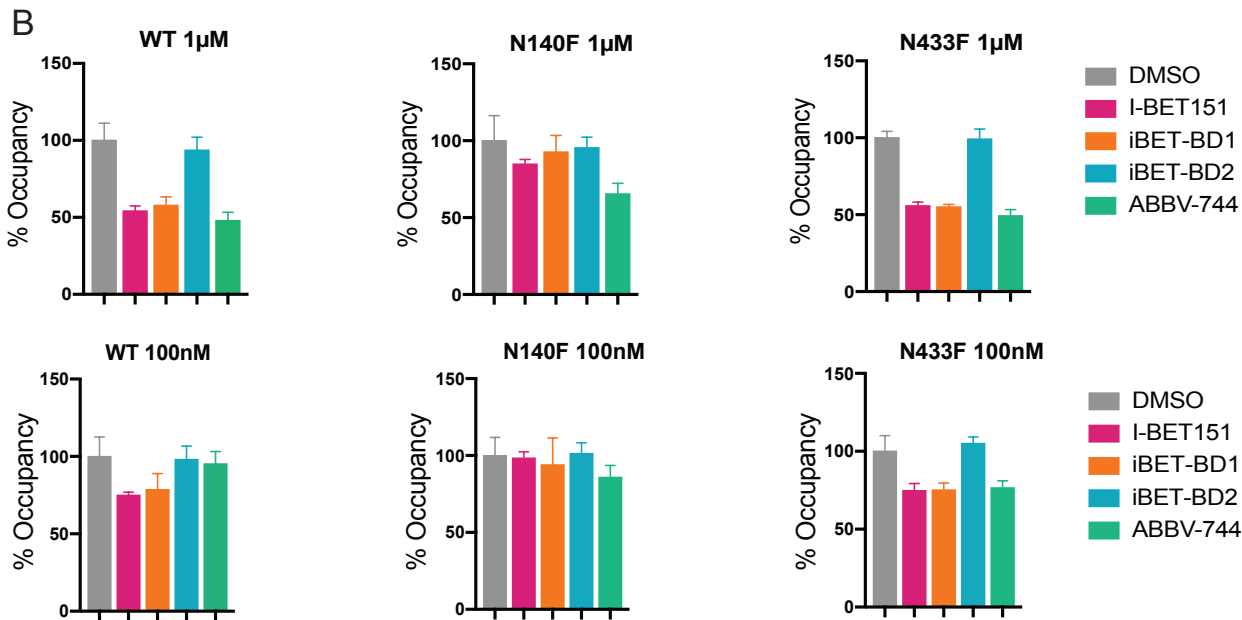
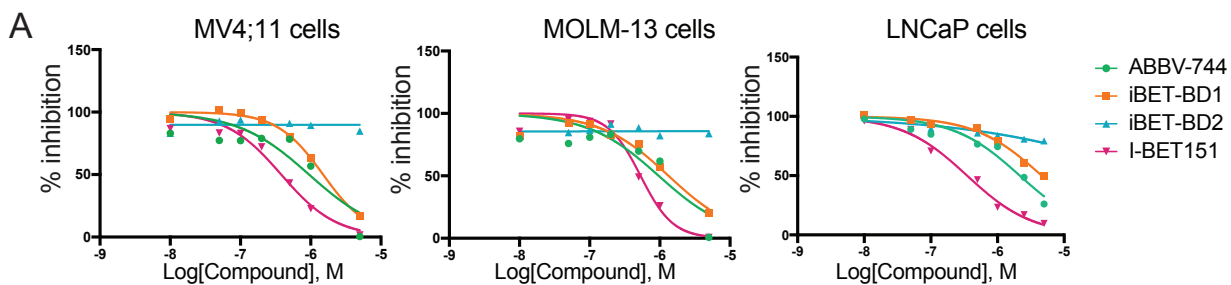


Fig. S9. (A) IC₅₀ assays performed at 72hrs in MV411, MOLM-13, and LNCaP cells following incubation with increasing doses of iBET-BD1, iBET-BD2, IBET151 or ABBV-744. These data show that the cellular activity of ABV-744 more closely parallels iBET-BD1 rather than iBET-BD2. **(B)** NanoBRET cellular interaction assays of BRD4 with Histone H4. NanoBRET assays in HEK293 cells of the indicated BRD4:H4 pairs showing resulting % Occupancy of global cellular chromatin binding after a 24hr treatment with 1 μ M or 100nM of I-BET151, iBET-BD1, iBET-BD2, ABBV-774, or DMSO control. Chromatin displacement patterns of I-BET151 and iBET-BD1 are similar, with significant displacement only of BRD4 variants that contain a functional BD1 domain. ABBV-744 shows chromatin displacement of all BRD4 constructs. iBET-BD2 does not show chromatin displacement of any of the BRD4 constructs. The % Occupancy is expressed as the fractional loss or increase in NanoBRET ratio relative to the DMSO control. Error bars are expressed as SEM from n=4 experiments. **(C)** Dose response curves and IC₅₀ determination of cellular chromatin displacement after 24-hour treatment with indicated concentrations of each compound in a NanoBRET WT BRD4:H4 assay in HEK293 cells. % Occupancy is plotted and calculated as in (B) and error bars are expressed as SEM from n=4 experiments. **(D)** Competitive cellular binding experiments with BET family PROTAC, MZ1. HEK293 cells containing endogenously tagged HiBiT-BRD2 were treated with 0.1 μ M MZ1 for 5 hours to initiate degradation, followed by 1 μ M treatment of I-BET151, i-BET-BD1, iBET-BD2, ABBV-774, or DMSO control. Luminescence (RLU) was continuously monitored in live cells for the time indicated on graphs. All compounds, with the exception of iBET-BD1, showed the ability to compete degradation driven by the MZ1 PROTAC, which has shown to have BD2 binding preference over BD1 Fractional RLU was plotted similar to graphs shown in (S7G-H) and error bars are expressed as SEM from n=4 experiments. Together, these data demonstrate that while ABV-744 potentially inhibits BD2, it retains significant activity against BD1, explaining why the phenotypes observed in cancer cells most closely resemble those of a less potent pan-BET inhibitor.

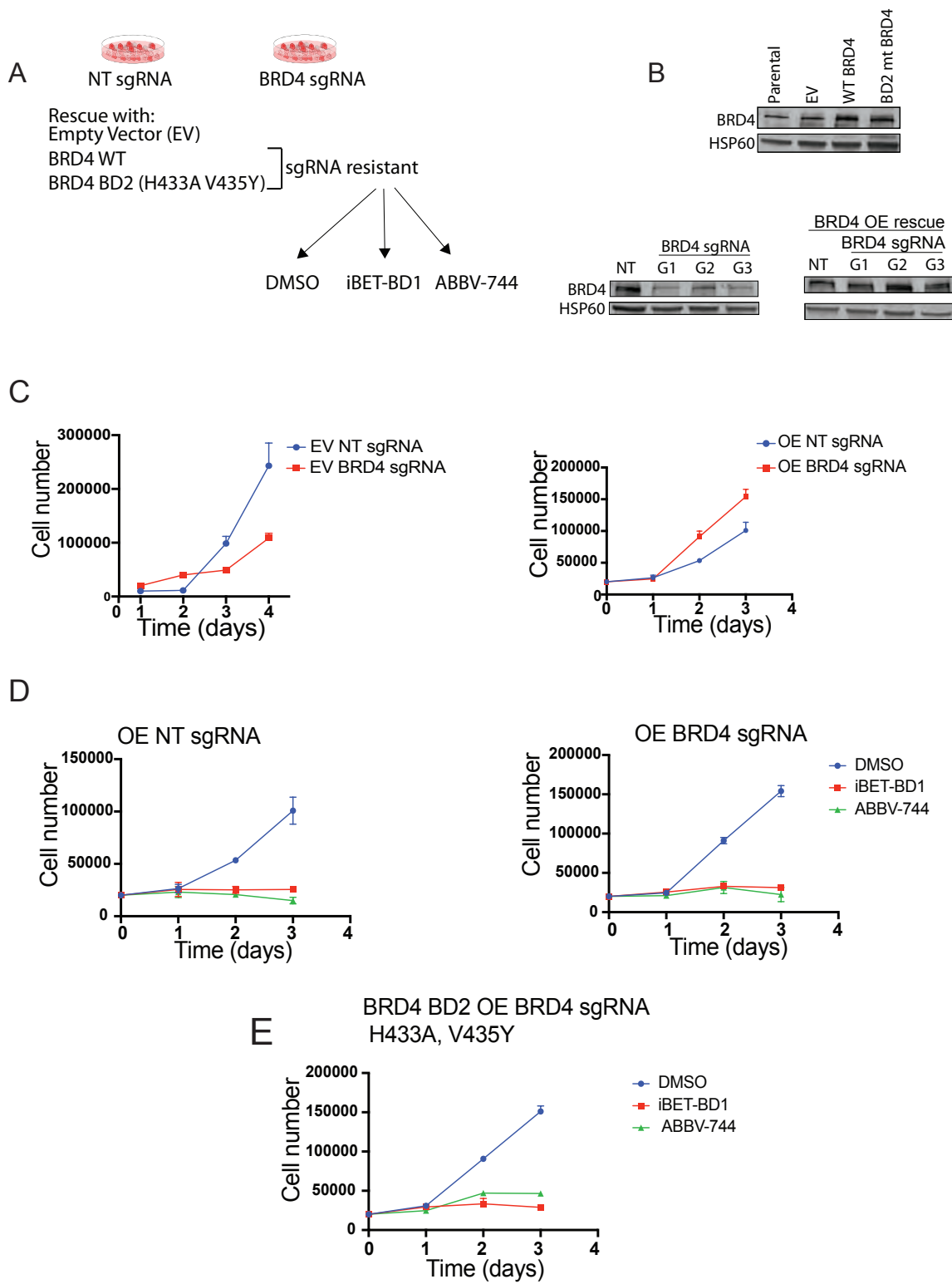


Fig. S10. (A) Schematic of strategy to model BD2 mutations. Endogenous BRD4 was deleted from AML cells (MV4;11) using a pool of BRD4 targeting sgRNA, Non-targeting (NT) sgRNA used as a control. Loss of BRD4 expression was rescued by lenti-viral over-expression of either Empty vector (EV), wild-type BRD4 (OE), or BRD4 BD2 mutant containing mutations in H433A and V435Y. These residues were recently reported to make critical contact with the BD2-inhibitor ABBV-744. Therefore, using these engineered cell lines, we tested the effect of these BRD4 BD2 mutations on the reported anti-proliferative activity of ABBV-744 in comparison with our selective BD1 inhibitor, iBET-BD1. **(B)** Western blot analysis of the various BRD4 constructs over expressed in MV4;11 cells. Three independent guides targeting BRD4 were compared to a non-targeting control in the empty vector control and the guide resistant BRD4 over-expression cell lines. These data show the efficacy of the individual guides in the empty vector control and the resistance mediated by silent guide mutations introduced into BRD4 cDNA, when the over-expression constructs are co-expressed with the guides targeting BRD4, they no longer deplete BRD4. **(C)** Proliferation assay over 72 hours using the EV or wild-type BRD4 cell lines transduced with either NT or a pool of 4 BRD4 guides targeting the 5' region of BRD4. These results confirm the functional rescue of the guide resistant BRD4 construct. **(D)** Proliferation assay over 72 hours using the wild-type BRD4 rescued cell line transduced with either NT or a pool of BRD4 sgRNA and treated with either DMSO, iBET-BD1 or ABBV-744 at a dose of 1 μ M. These data show that as a result of the rescue, deletion of endogenous BRD4 does not impede the growth of these cells and that they respond equally to treatment with either iBET-BD1 or ABBV-744 compared with DMSO. **(E)** Proliferation assay over 72 hours using the BD2 mutant BRD4 rescued cell line transduced with a pool of BRD4 sgRNA and treated with either DMSO, iBET-BD1 or ABBV-744 at a dose of 1 μ M. These data show that over-expression of the BD2 mutant BRD4 is able to rescue these cells from deletion of endogenous BRD4 as their growth rate is equivalent to WT BRD4 cells. Interestingly, despite genetic disruption of the BD2 specificity conferring amino acids, the cellular activity and anti-proliferative effects of this compound are unaltered and remain similar to iBET-BD1. Taken together, these results further confirm that the anti-proliferative effects of ABBV-744 are mediated in large part by inhibition of BD1.

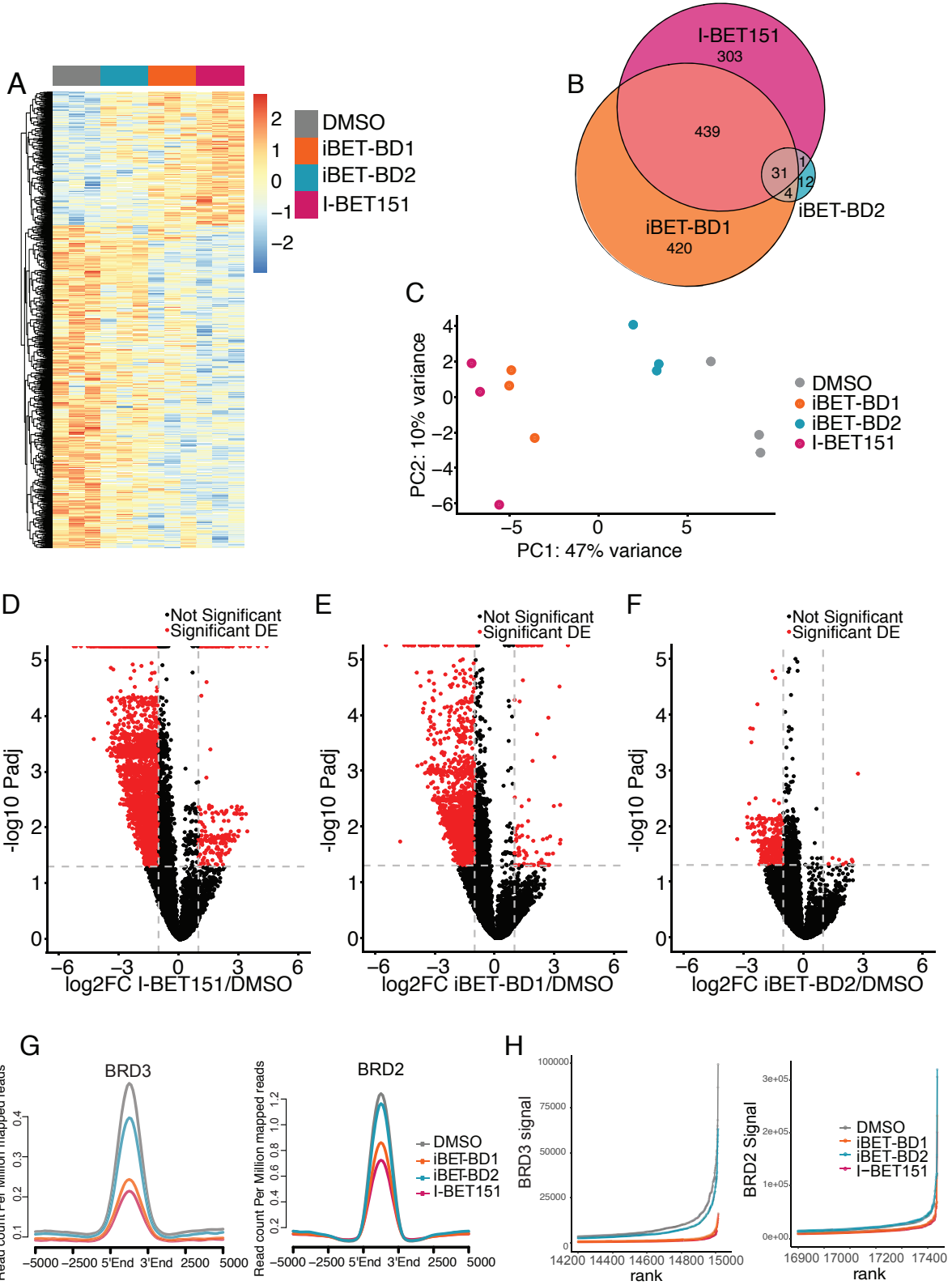


Fig. S11. (A) Hierarchical clustering heatmap of differential gene expression from SLAM-seq in MV4;11 cells. **(B)** Venn diagram of overlap in statistically significant differentially expressed genes in MV4;11 cells. **(C)** Principal component analysis of SLAM-seq data from MV4;11 cells. **(D-F)** Volcano plots of differentially expressed genes (shown in red) from SLAM-seq experiment performed on THP-1 cells treated with iBET-BD1, iBET-5 BD2 or I-BET151 for 6 hrs. dotted line represents p value and logFC cutoff of 0.05 and 1, respectively. **(G)** Average profile plot of BRD2 and BRD3 ChIP-seq signal at Typical enhancers (TE) following treatment with various compounds. **(H)** Superenhancer plot based on ranking of H3K27ac and BRD2 or BRD3 levels in THP-1 cells.

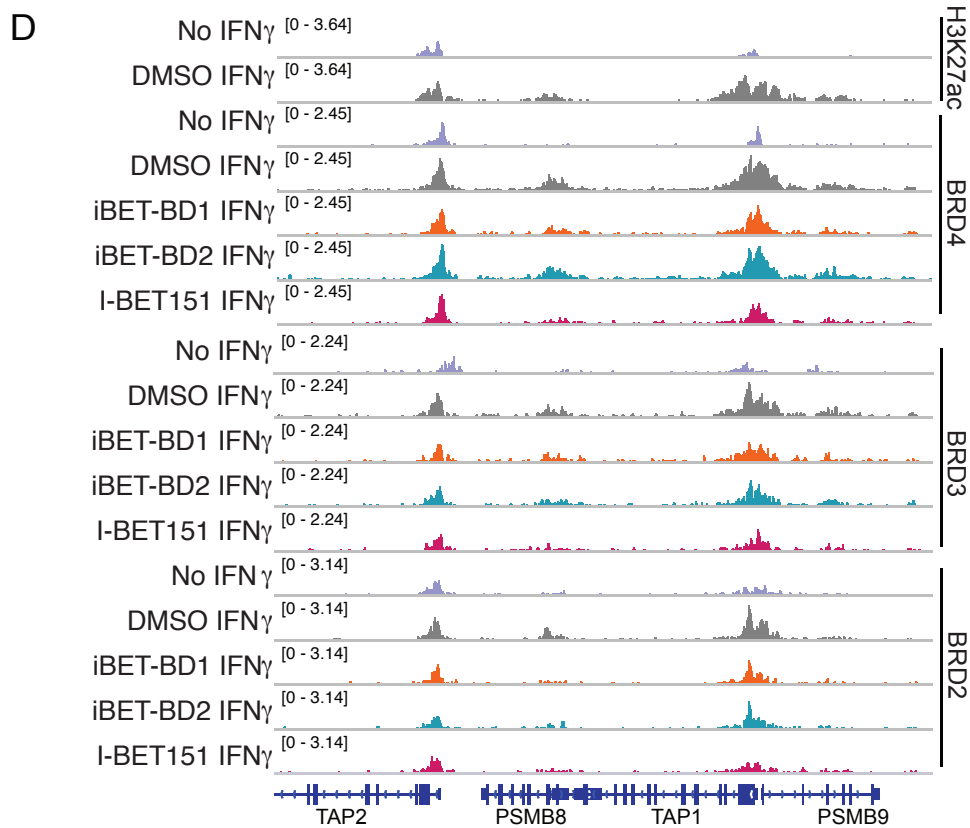
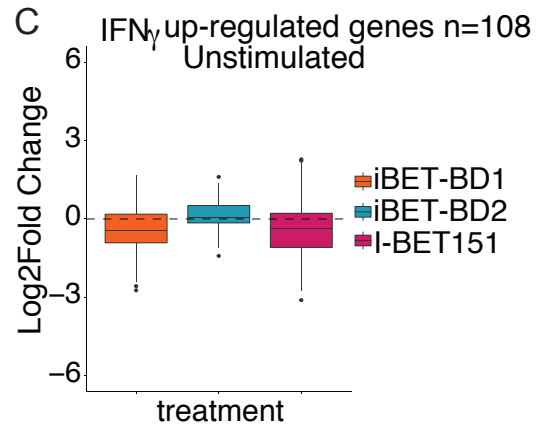
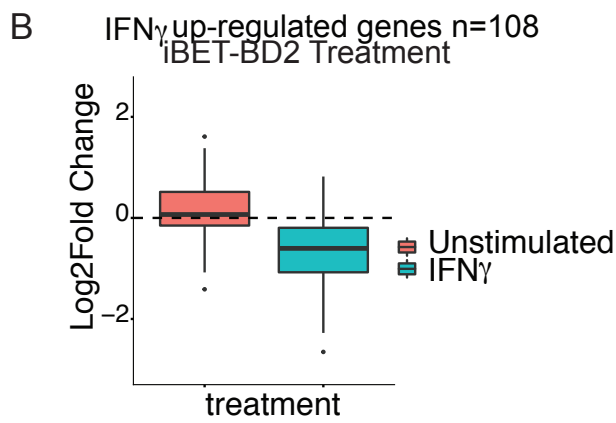
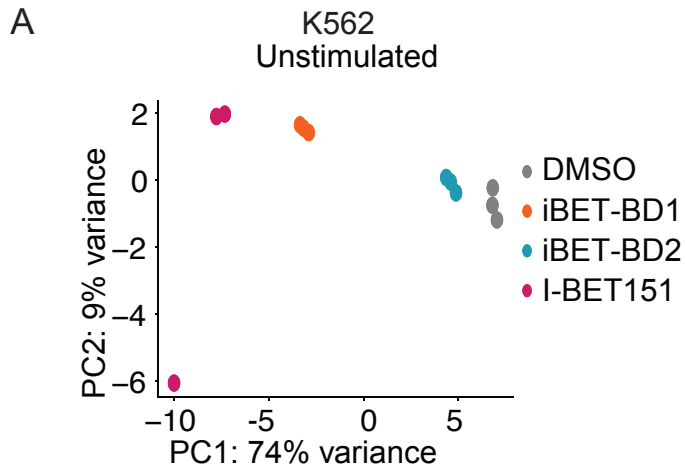


Fig. S12. (A) Principal component analysis of SLAM-seq data from K562 cells under unstimulated conditions treated with the various domain inhibitors for 6 hrs. (B) Boxplot of LogFC following iBET-BD2 treatment of IFN γ target genes from SLAM-seq experiments in K562 cells with and without IFN γ stimulation. (C) Boxplot of LogFC, following treatment with the various domain inhibitors, of IFN γ target genes from SLAM-seq experiment in K562 cells under unstimulated conditions. (D) Genome browser view of IFN γ target genes *TAP1* and *TAP2* in K562 cells showing occupancy of BRD4, BRD3 and BRD2 as well as H3K27ac levels with and without IFN γ and treatments.

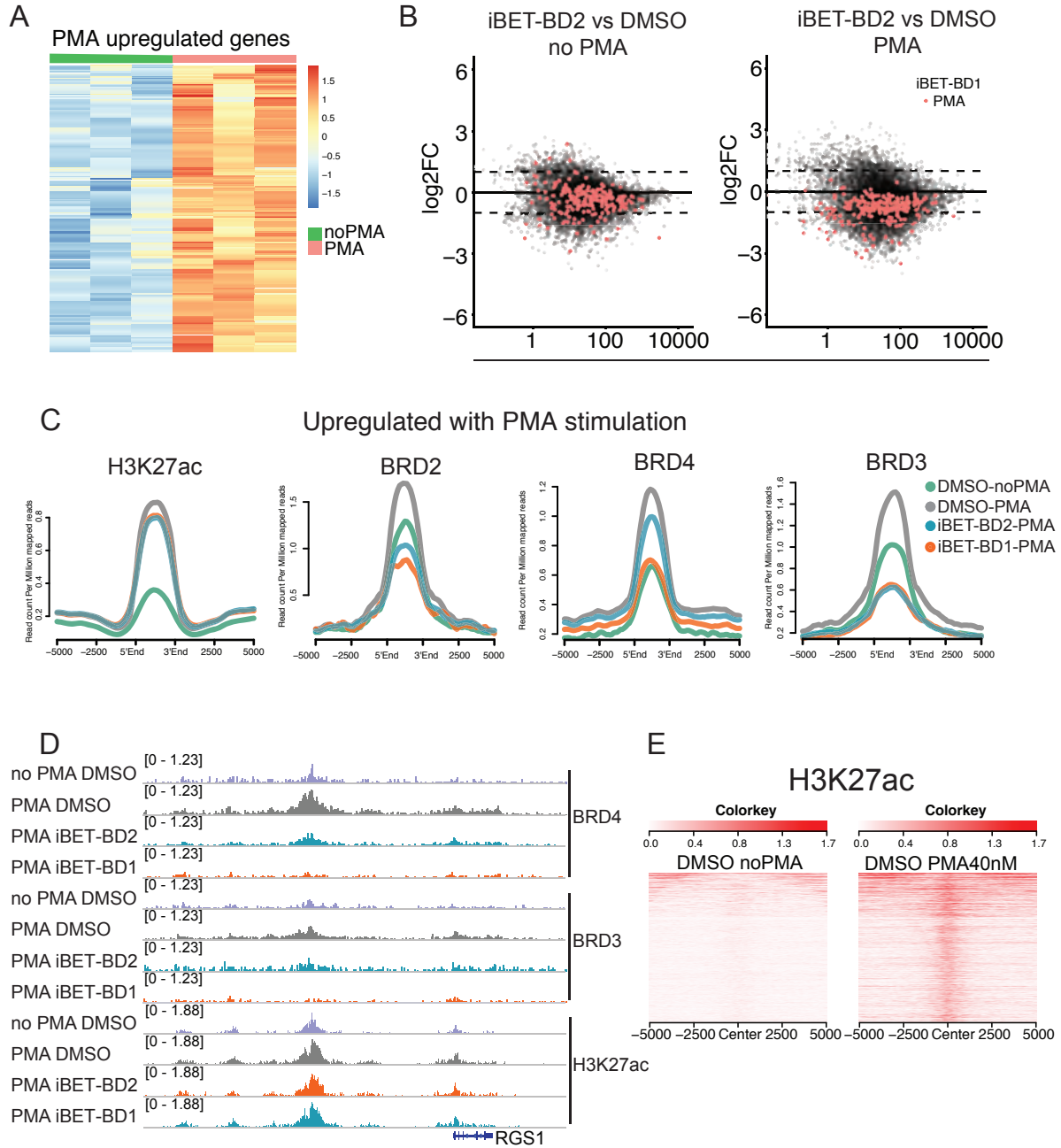


Fig. S13. (A) Heatmap of genes upregulated from SLAM-seq performed in THP-1 cells treated with PMA (40nM) for 2 hours. **(B)** Scatter plot of differential expression of all genes (grey) and genes significantly upregulated by PMA and downregulated by iBET-BD1 (red) in THP-1 cells, data shown for iBET-BD2 vs DMSO in the presence and absence of PMA. **(C)** Average profile plot of increased H3K27ac, BRD4, BRD3 and BRD2 occupancy overlapping loci with increased H3K27ac within 50kb of up regulated genes by SLAM-seq in THP-1 cells following PMA stimulation for 2hrs and 30mins pre-treatment with DMSO, iBET-BD1, iBET-BD2 or I-BET151. **(D)** Genome browser view of a PMA target gene, *RGS1*, in THP-1 cells showing the binding of BRD4, BRD3 and H3K27ac levels prior to and after the addition of PMA for 2 hours and 30 mins pretreatment with DMSO, iBET-BD1, or iBET-BD2. **(E)** Heatmap of increased H3K27ac (LFC>2) peaks in THP-1 cells following PMA treatment for 2 hrs.

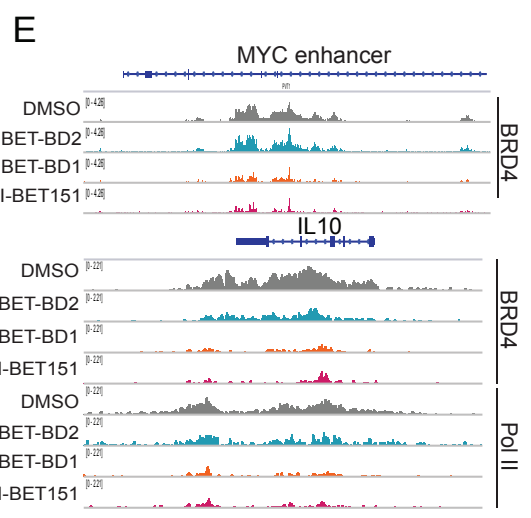
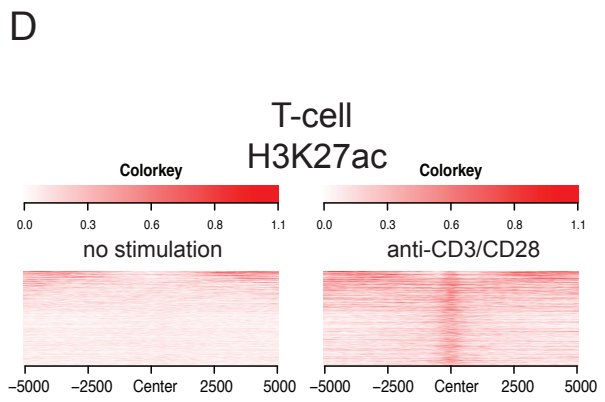
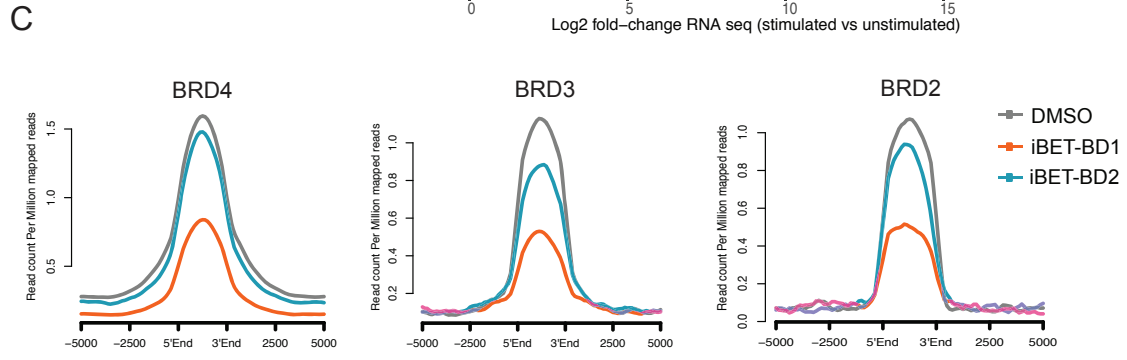
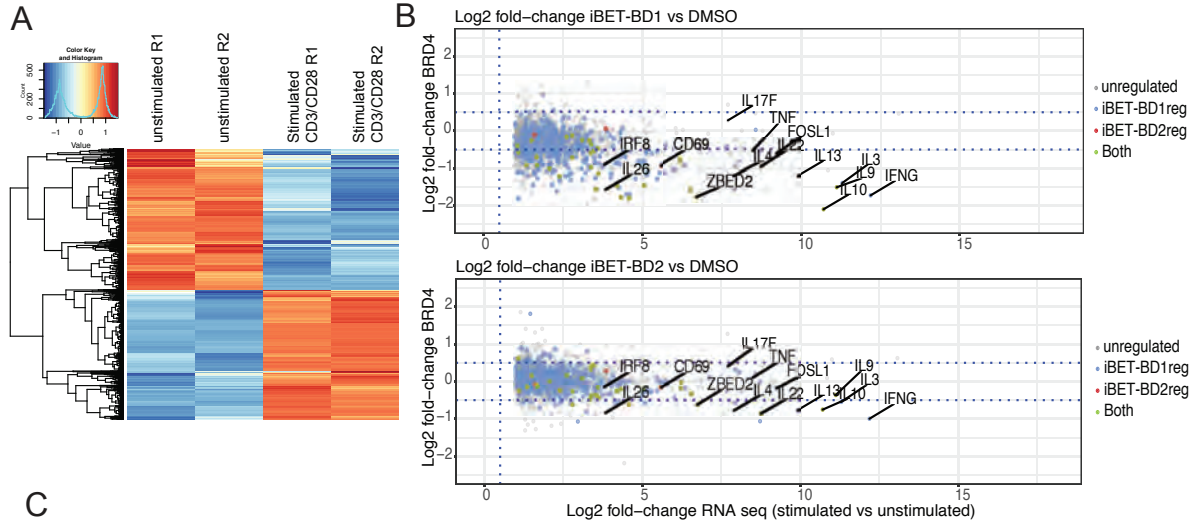


Fig. S14. (A) Heatmap of differential gene expression from RNA-seq of human T cells stimulated with CD3/CD28 for 6 hrs. Performed in experimental duplicates. (B) Scatter plot of genes upregulated in human T cells following activation with CD3/CD28 for 6 hours on the x-axis. Log₂fold change in BRD4 binding after treatment with iBET-BD1 (top) or iBET-BD2 (bottom) on the y-axis. (C) Average profile plot of BRD4, BRD3 and BRD2 binding 50kb +/- around the TSS of genes that show increased binding after stimulation by CD3/CD28 in human T cells for 6 hours and decreased when treated with I-BET151. (D) Heatmap of increased H3K27ac (LFC>2) peaks in T-cells following CD3/CD28 stimulation for 6 hrs. (E) Genome browser view of the MYC enhancer and IL10 locus in human T cells following stimulation with anti-CD3/CD28 antibodies and treatment with either DMSO, iBET-BD2, iBET-BD1 or I-BET151 for 6 hrs.

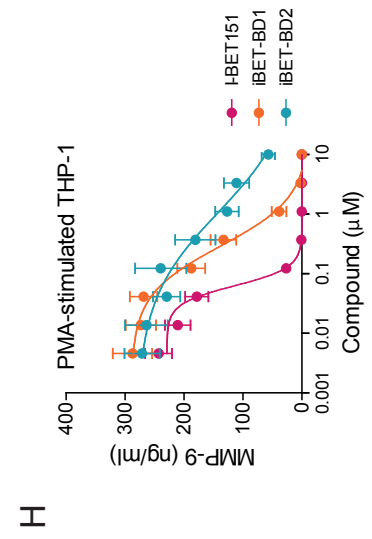
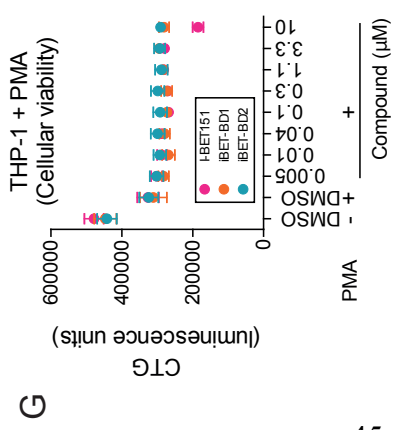
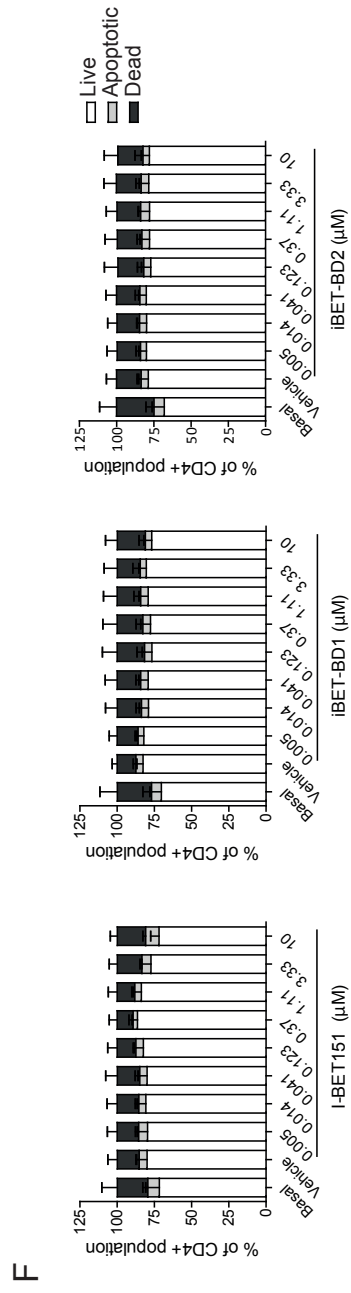
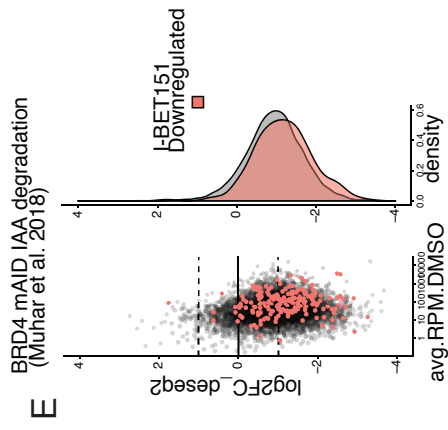
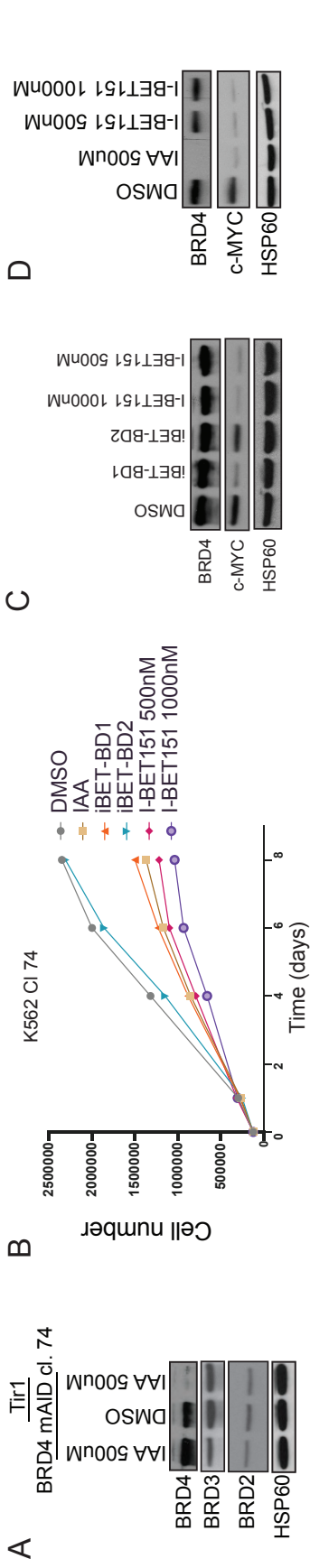


Fig. S15. (A) Immunoblot analysis of K562 mAID-BRD4 knock-in clone expressing Empty vector or osTir1 and treated with either DMSO or Auxin (IAA, 4 hours) as indicated. (B) Proliferation assay of K562 mAID-BRD4 knock-in clone treated with Auxin (500 μ M), iBET-BD1 (1000nM), iBET-5 BD2 (1000nM), I-BET151 (500nM or 1000nM) or DMSO (Vehicle control) for 8 days. (C) Immunoblot analysis of BRD4 and c-MYC in K562 cells following treatment with DMSO, iBET-BD1, iBET-BD2 or I-BET151 at two different doses (500nM or 1000nM). (D) Immunoblot analysis of BRD4 and c-MYC levels in K562 mAID-BRD4 cells treated with DMSO, Auxin (IAA), or I-BET151 at indicated doses. (E) Analysis of I-BET151 regulated genes (highlighted in red) against the set of genes regulated by BRD4 degradation from Muhar et al. 2018. (F) Effect of I-BET151, iBET-BD1 and iBET-BD2 treatment on the viability, assessed by flow cytometry. (G) Effect of I-BET151 (magenta), iBET-BD1 (orange) and iBETBD2 (cyan) treatment on cellular viability, determined by ATP content (Cell Titre Glo, CTG), in 48 hours PMA-stimulated THP-1 cells. (H) Compound effects on MMP-9 production by PMA-activated THP-1 cells. Data represent the mean \pm SEM (n = 6).

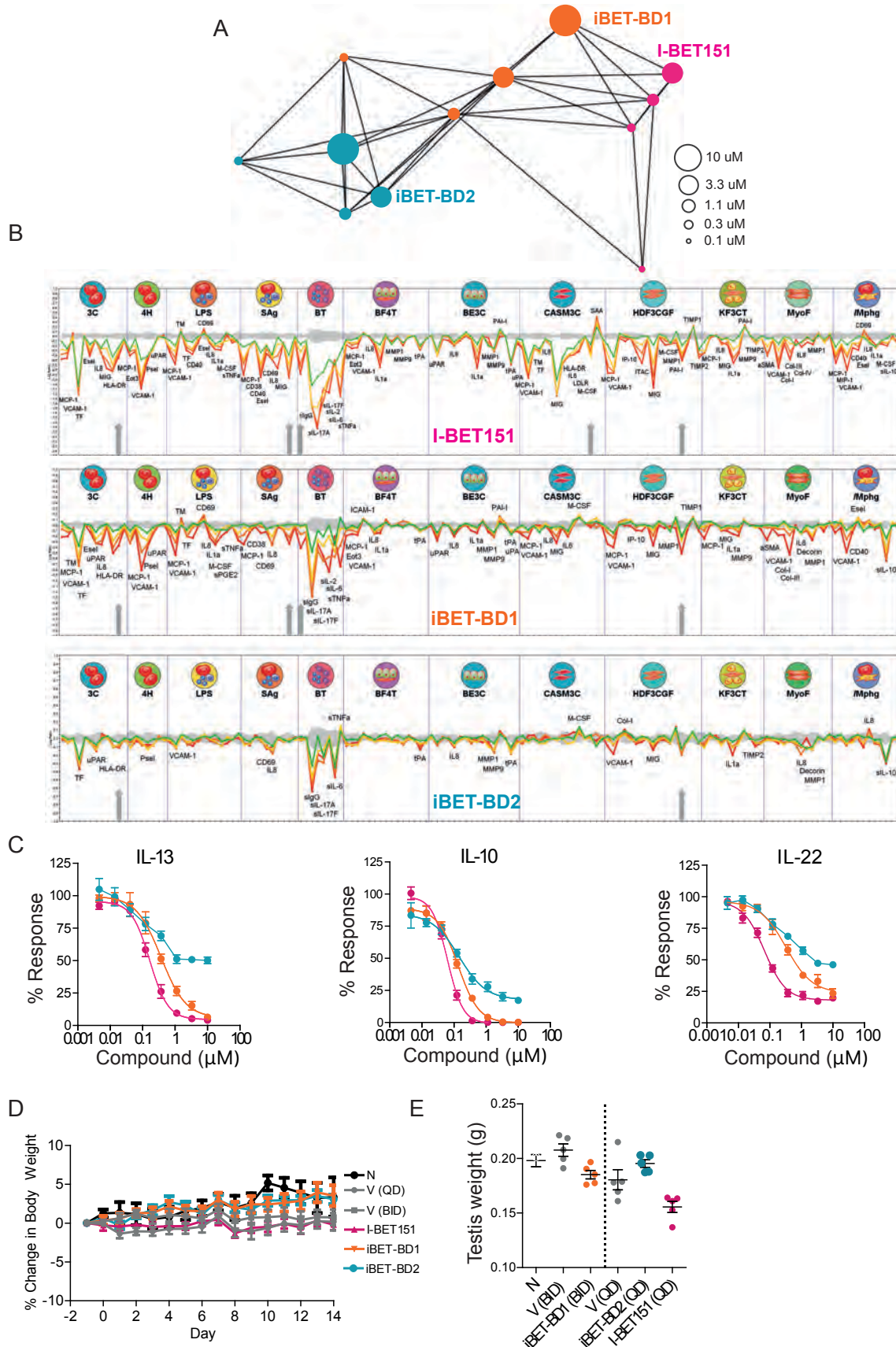


Fig. S16. (A) Functional clustering of BioMAP profiles of I-BET151 (magenta), iBET-BD1 (orange) and iBET-BD2 (cyan) in the Diversity PLUS Panel using Pearson's correlation coefficient (r) for pairwise comparisons of the compound profiles at each concentration. Each circle represents the BioMAP profile of a compound at a specific concentration, with larger circles representing higher concentrations as annotated. Profiles that are similar with $r \geq 0.7$ are connected by lines. (B) BioMAP compound profiles in the Diversity PLUS Panel. Lines in red, orange, yellow and green from higher to lower compound concentrations respectively. Annotated biomarkers are outside of the significance envelope (grey) with an effect size $> 20\%$ ($|\log_{10} \text{ratio}| > 0.1$). Grey arrows indicate inhibition of cell proliferation. (C) cytokine production of human primary CD4⁺ T cells 72 hours post-activation with anti-CD3/anti-CD28. Data represent the mean \pm SEM ($n = 4$ donors). (D) Effect of compounds on body weight in the mouse KLH T cell dependent immunisation model. V, vehicle; iBET-BD1 (15 mg/kg, s.c., BID), iBET-BD2 (40 mg/kg, s.c., QD), I-BET151 (15 mg/kg, s.c., QD). Data represents the mean \pm SEM ($n = 4$ (na.ve) – 10 (treated)). (E) Testis weight of mice from the KLH T cell dependent immunisation model after treatment with iBET-BD1, iBET-BD2 or I-BET151. V, vehicle; iBET-BD1 (15 mg/kg, s.c., BID), iBET-BD2 (40 mg/kg, s.c., QD), I-BET151 (15 mg/kg, s.c., QD). Data represents the mean \pm SEM ($n = 4$ (na.ve) – 10 (treated))

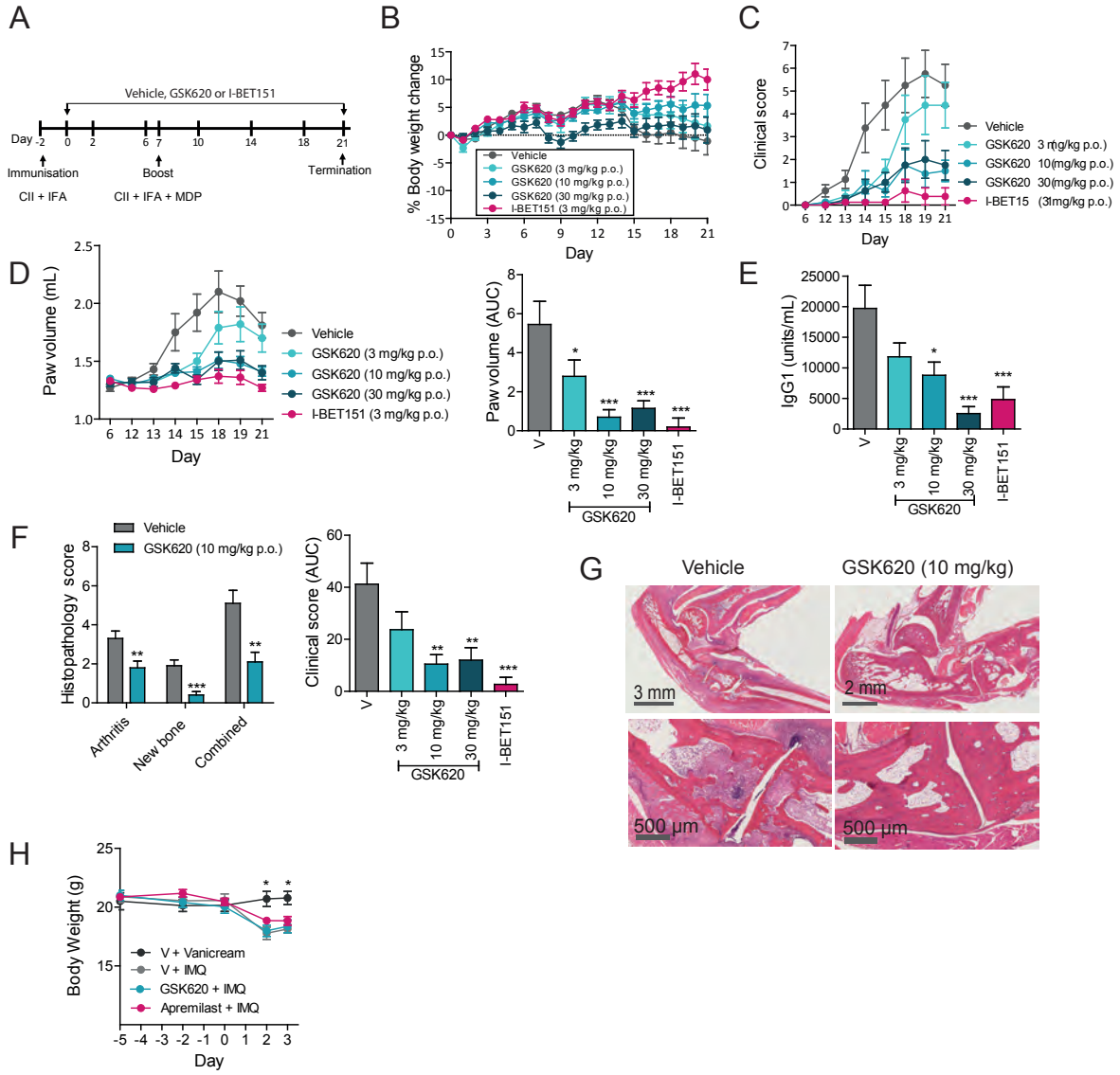


Fig. S17. (A) Rat collagen-induced arthritis (CIA) study design. **(B)** Effect of GSK620 and I-BET151 on body weight after 21 days of oral administration in the rat CIA model. **(C)** Compound effects on clinical score and **(D)** paw volume. Data are the mean \pm SEM (n = 8 animals/ group). One-way ANOVA followed by Dunnett's multiple comparison test was used to determine statistical significance compared with respective vehicle controls (***P<0.001, **P<0.01, *P<0.05). **(E)** circulating immunoglobulin levels in rat CIA. I-BET151 (3mg/kg, p.o., QD) used as comparator. Data represent the mean \pm SEM (n = 8). One-way ANOVA followed by Dunnett's multiple comparison test. (***P<0.0001 vs V, vehicle). **(F)** Effect of GSK620 on histopathology score. **(G)** Representative H&E and Toluidine blue stained sections of rat joints are shown. GSK620 treatment is well tolerated in the imiquimod (IMQ)-induced psoriasis in mice. **(H)** Compound effects on body weight are shown. Data represent the mean \pm SEM (n = 10). One-way ANOVA followed by Dunnett's multiple comparison test (*P<0.05 vs V + IMQ).

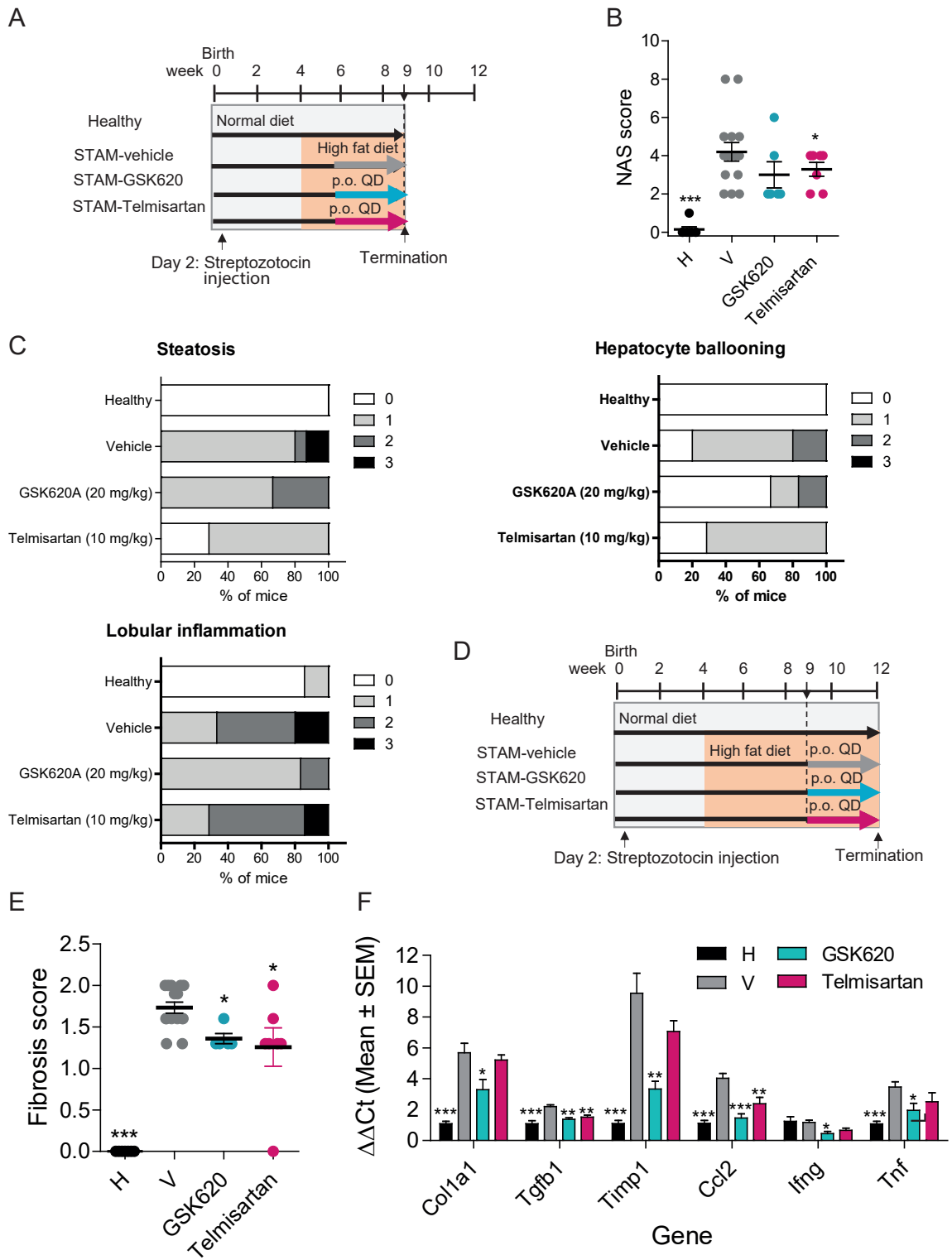


Fig. S18. Reduction of NAS in STAM mice following GSK620 treatment from week 6 to week 9. **(A)** Study design (NASH phase). **(B)** NAS score. Scoring and interpretation was performed by a pathologist blinded to treatment group using the scoring criteria defined in the material and methods section. Telmisartan (10 mg/kg, p.o., QD), n = 7; GSK620 (20 mg/kg, p.o., QD), n = 7; Vehicle (V), n = 16; Healthy (H), n = 7. ***P = 0.001 vs Vehicle Control (Kruskal-Wallis followed by Dunnett's multiple comparison test). **(C)** Individual components of the NAS, which include steatosis, lobular inflammation, and hepatocellular ballooning degeneration, are shown for each of the cohorts. **(D)** Mouse STAM NASH model (fibrosis phase) study design. **(E)** GSK620 reduces fibrosis in STAM mice. The histological scoring was determined based on the NASH Clinical Research Network (CRN) scoring criteria. Data are expressed as mean \pm SEM (n= 6 -14). Asterisks denote significant changes compared to vehicle control (*=p<0.05, Kruskal-Wallis followed by Dunnett's multiple comparison test). **(F)** Gene expression of inflammatory and fibrosis markers from qPCR in liver biopsies from Healthy (H), STAM-Vehicle (V), STAMGSK620 and STAM-Telmisartan groups. Δ Ct was computed relative to 18S rRNA. Asterisks denote significant changes compared to vehicle (***=p<0.001, One-way ANOVA followed by Dunnett's multiple comparison test).

Table S1. Selectivity profile of I-BET151, iBET-BD1, iBET-BD2 and GSK620 determined by TR-FRET assay.

	FRET IC₅₀ (nM)			
	Mean ± SEM (n)			
	I-BET151	iBET-BD1	iBET-BD2	GSK620
BRD2 BD1	7 ± 31(16)	75 ± 4 (6)	10965 (1) ^a	25420 ± 2591 (13) ^d
BRD3 BD1	37 ± 13 (15)	41 ± 5 (6)	36317 ± 1182 (2) ^b	25802 ± 6171 (6) ^e
BRD4 BD1	36 ± 6 (16)	41 ± 3 (16)	70558 ± 51783 (3) ^c	17442 ± 1857 (14)
BRDT BD1	119 ± 4 (16)	143 ± 14 (6)	> 50119 (8)	22634 ± 2353 (9) ^f
BRD2 BD2	274 ± 36 (16)	3950 ± 290 (8)	264 ± 53 (9)	285 ± 20 (20)
BRD3 BD2	87 ± 8 (16)	1210 ± 65 (6)	98 ± 6 (8)	72 ± 4 (16)
BRD4 BD2	329 ± 22 (16)	5843 ± 304 (16)	49 ± 4 (12)	81 ± 9 (16)
BRDT BD2	1680 ± 169 (16)	17451 ± 1938 (6)	214 ± 53 (8)	184 ± 19 (18)

^aalso tested >50119 (n=10); ^balso tested >50119 (n=6); ^calso tested >50119 (n=8); ^dalso tested >50119 (n=8); ^ealso tested >50119 (n=10); ^falso tested >50119 (n=7) plus >16596 (n=2).

Table S2. BROMOscan bromodomain selectivity profile of I-BET151, iBET-BD1, iBET-BD2 and GSK620.

Bromodomain	K_D (nM)			
	I-BET151	iBET-BD1	iBET-BD2	GSK620
ATAD2A	>30000	>30000	>30000	>30000
ATAD2B	>30000	25000	>30000	>30000
BAZ2A	>30000	>30000	>30000	>30000
BAZ2B	>30000	>30000	>30000	>30000
BRD1	>24275	>30000	>30000	28000
BRD2 BD1	6	13	1621	13000
BRD2 BD1 & BD2	20	<i>ND</i>	100	<i>ND</i>
BRD2 BD2	46	840	35	18
BRD3 BD1	2	5	2082	7800
BRD3 BD1 & BD2	14	<i>ND</i>	47	<i>ND</i>
BRD3 BD2	17	310	33	14
BRD4 BD1	6	6	769	2700
BRD4 BD1 & BD2	44	100	9	<i>ND</i>
BRD4 BD2	33	670	9	6
BRD4 (FL, short isoform)	9	11	727	<i>ND</i>
BRD7	>30000	>30000	>30000	>30000
BRD8(1)	>30000	<i>ND</i>	>30000	>30000
BRD8(2)	>30000	<i>ND</i>	>30000	>30000
BRD9	25852	>30000	>30000	>30000
BRDT BD1	18	18	2454	4800
BRDT BD1 & BD2	44	<i>ND</i>	36	<i>ND</i>
BRDT BD2	135	5400	15	16
BRPF1	25894	15000	>30000	>30000
BRPF3	>30000	>30000	>30000	>30000
CECR2	>30000	>30000	>30000	>30000
CREBBP	982	3800	>30000	10000
EP300	353	5700	>30000	8300
FALZ	>30000	>30000	>30000	24000
GCN5L2	>30000	>30000	>30000	>30000
PBRM1(2)	>30000	29000	>30000	>30000
PBRM1(5)	>30000	>30000	>30000	>30000
PCAF	>30000	33000	>30000	>30000
SMARCA2	>30000	>30000	>30000	>30000
SMARCA4	>30000	<i>ND</i>	>30000	>30000
TAF1(2)	>30000	>30000	>30000	3900

TAF1L(2)	>30000	>30000	>30000	26000
TRIM24 (BRD)	>30000	>30000	>30000	<i>ND</i>
TRIM24 (BRD & PHD)	25891	>30000	>30000	>30000
TRIM33 (BRD & PHD)	>30000	>30000	>30000	>30000
WDR9(2)	>30000	>30000	>30000	>30000

FL: Full length; BRD: Bromodomain; ND: not determined. K_D values for I-BET151 and iBET-BD2 (n = 2), iBET-BD1 (n = 1) and GSK620 (n = 1).

Table S3. Data collection and refinement statistics for BRD4-BD1 and BRD4-BD2 X-ray structures

(collection on a single crystal)	BRD4-BD1 / iBET-BD1 (GSK778)	BRD2-BD2 / iBET-BD2 (GSK778)	BRD2-BD2/ iBET-BD2 (GSK046)	BRD4-BD1 / iBET-BD2 (GSK046)
PDB code	6SWN	6SWO	6SWP	6SWQ
Data collection				
Space group	P2 ₁ 2 ₁ 2 ₁	P2 ₁ 2 ₁ 2	P2 ₁ 2 ₁ 2	P2 ₁ 2 ₁ 2 ₁
Cell dimensions				
<i>a, b, c</i> (Å)	38.28, 42.32, 90.82	71.97, 52.71, 32.04	72.20, 52.39, 32.02	37.13, 44.06, 78.88
α, β, γ (°)	90, 90, 90	90, 90, 90	90, 90, 90	90, 90, 90
Resolution (Å)	45.41-1.28 (1.33-1.28)	26.26-1.60 (1.69-1.60)	27.32-1.60 (1.69-1.60)	44.06-1.60 (1.69-1.60)
No. reflections	191,568 (4791)	41,221 (3147)	43,687 (3299)	66,845 (3399)
No. uniq reflections	36,156 (2233)	15,926 (1752)	15,434 (1590)	15,247 (1228)
<i>R</i> _{merge}	0.07 (0.19)	0.03 (0.26)	0.02 (0.06)	0.03 (0.11)
<i>R</i> _{pim}	0.04 (0.18)	0.03 (0.25)	0.01 (0.05)	0.02 (0.10)
<i>CC</i> (1/2)	0.99 (0.90)	0.99 (0.60)	1.00 (0.98)	1.00 (0.70)
<i>I</i> / σ <i>I</i>	17.0 (3.5)	21.3 (3.7)	43.3 (15.7)	28.6 (8.5)
Completeness (%)	93.3 (60.2)	95.6 (73.9)	93.4 (67.6)	87.3 (49.1)
Redundancy	5.3 (2.1)	2.6 (1.8)	2.8 (2.1)	4.4 (2.8)
Refinement				
Resolution (Å)	45.41-1.28	26.26-1.60	27.32-1.60	39.44-1.60
No. uniq reflections	34,292 (1492)	14,986 (746)	14,607 (657)	14,491 (506)
<i>R</i> _{work} / <i>R</i> _{free}	0.19 / 0.21	0.17 / 0.19	0.15 / 0.19	0.16 / 0.18
No. atoms	1488	1138	1251	1393
Protein	1136	920	997	1109
Ligand/ion	76 / 4	38 / 8	30 / 8	30 / 12
Water	272	172	216	242
B-factors (Å ²)				
Wilson Bfactor	12.4	12.4		12.3
Protein	16	19	15	15
Ligand/ion	16 / 15	28 / 34	17 / 41	17 / 20
Water	19	35	35	32
R.m.s deviations				
Bond lengths (Å)	0.0043	0.0065	0.0045	0.0032
Bond angles (°)	1.18	1.19	1.22	1.15
Ramachandran				
Favoured regions (%)	99	99	100	99
Allowed regions(%)	1	1	0	1
Outliers	0	0	0	0

*Highest resolution shell is shown in parenthesis.

Table S4. Mouse PO Pharmacokinetic (PK) profile of iBET-BD1 (GSK778), iBET-BD2 (GSK046) and the in vivo iBET-BD2 tool GSK620.

	iBET-BD1 (GSK778)	iBET-BD2 (GSK046)		GSK620	
Mouse strain	CD1 (n=3)	C57BL6 (n=3)	C57 B16 (n=3)	C57BL6 (n=3)	C57BL6 (n=3)
Gender	M	F	M	M	M
Dose (mg/kg)	10	10	40	3	30
C _{max} (ng/mL)	85 ±56	1589 ±1084	2993 ±1455	746 ±21	3564 ±853
T _{max} * (h)	1.48 (1 – 1.52)	0.73 (0.73 – 1)	0.52 (0.5 – 1)	1.75 (1.5 – 2)	1.98 (1.5 – 3)
t _{1/2} (h)	ND	1.8 ±0.4	1.9 ±0.1	3.5 ±0.4	3.2 ±0.3
AUC _∞ (ng.h/mL)	132 ±22	2877 ±494	6977 ±3342	3753 ±246	32030 ±4869
AUC _∞ /D (min.kg/L)	0.8 ±0.1	16 ±2.9	9.7 ±4.8	73 ±5	59 ±10

*T_{max} expressed as median and range.

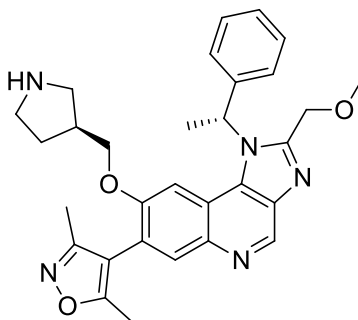
Table S5. Comparison of mouse and rat oral pharmacokinetic (PK) profiles of the BET-BD2 selective molecules iBET-BD2 (GSK046) and GSK620.

	GSK046		GSK620	
	Mouse C57BL6 (n=3)	Rat Lewis (n=3)	Mouse C57BL6 (n=3)	Rat Lewis (n=3)
Gender	F	F	M	F
Dose (mg/kg)	10	10	3	3
C _{max} (ng/mL)	1589 ±1084	202 ±28	746**	488 ±204
T _{max} * (h)	0.73 (0.73 – 1)	0.50 (0.25 – 1)	1.75 (1.5 – 2)	2.02 (1 – 2.98)
t _{1/2} (h)	1.8 ±0.4	1.4 ±0.6	3.5**	3.2**
AUC _∞ (ng.h/mL)	2877 ±494	437 ±27	3753**	2324**
AUC _∞ /D (min.kg/L)	16 ±2.9	2.5 ±0.2	73**	52**

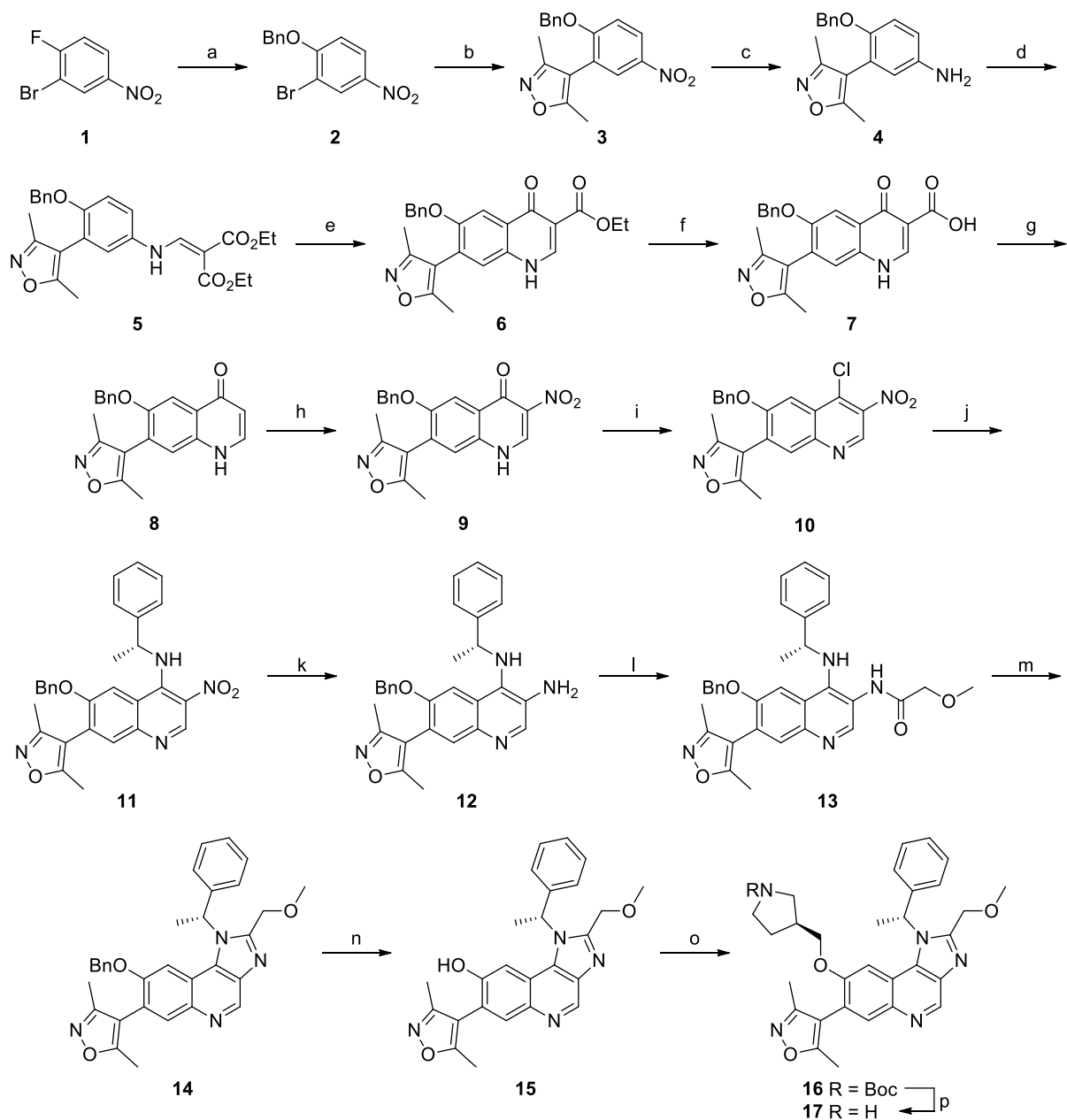
*T_{max} expressed as median and range. **n= 2.

Supplementary methods – Chemistry

Chemistry Synthesis iBET-BD1 (GSK778)



Synthesis:



Reagents and conditions: (a) NaH, BnOH, DMA, 0 °C, 1 h, 73%; (b) (3,5-dimethylisoxazol-4-yl)boronic acid, PEPPSI-IPr (2.5 mol%), Cs₂CO₃, DME, H₂O, 90 °C, 5 h, 86%; (c) Fe, NH₄Cl, EtOH, H₂O, rt, 15 h, 98%; (d) diethyl 2-(ethoxymethylene)malonate, 130 °C, 1 h, 74%; (e) Ph₂O, 260 °C, 20 min, 90%; (f) 2 M NaOH, EtOH, 95 °C, 3 h, 99%; (g) Ph₂O, 260 °C, 20 min, 89%; (h) HNO₃, EtCO₂H, 100 °C, 1.5 h, 57%; (i) POCl₃, 100 °C, 1 h, 96%; (j) (*R*)- α -methylbenzylamine, ⁱPr₂NEt, NMP, rt, 2.5 h, 99%; (k) Fe, AcOH, rt, 1 h, 83%; (l) 2-methoxyacetyl chloride, pyridine, DCM, rt, 3.5 h, 98%; (m) EtCO₂H, 140 °C, 2 h, 90%; (n) 5% Pd/C, H₂, EtOH, 35 h, 62%; (o) (*S*)-*tert*-butyl 3-[(methylsulfonyl)oxy]methyl}pyrrolidine-1-carboxylate, K₂CO₃, DMF, 100 °C, 3 h, 57%; (p) 4 M HCl in 1,4-dioxane, 1,4-dioxane, rt, 1 h, 96%.

1-(Benzyloxy)-2-bromo-4-nitrobenzene (2). To a slurry of NaH (60% dispersion in mineral oil) (2.8 g, 70.0 mmol) and DMA (60 mL) was added benzyl alcohol (4.75 mL, 45.7 mmol) dropwise with stirring under nitrogen. The mixture was stirred for 2 h at rt and then cooled to 0 °C. 2-Bromo-1-fluoro-4-nitrobenzene **1** (11 g, 50.0 mmol) was added to the cooled solution and the mixture stirred for 1 h. The reaction mixture was poured onto sat. NH₄Cl (aq) (80 mL), stirred for 10 min, filtered and washed with water. The solid was triturated with diethyl ether (25 mL) and filtered to give the title compound as a tan solid (11.25 g, 36.5 mmol, 73%). ¹H NMR (400 MHz, DMSO-*d*₆) δ 8.45 (d, *J* = 2.8 Hz, 1H), 8.28 (dd, *J* = 9.1, 2.8 Hz, 1H), 7.53–7.47 (m, 2H), 7.47–7.40 (m, 3H), 7.40–7.34 (m, 1H), 5.39 (s, 2H); LC-MS (Method A) no mass ion detected, *R*_t 1.30 min, 100% purity.

4-[2-(Benzyloxy)-5-nitrophenyl]-3,5-dimethylisoxazole (3). Nitrogen was bubbled through a mixture of 1-(benzyloxy)-2-bromo-4-nitrobenzene **2** (10.73 g, 34.8 mmol), cesium carbonate (23 g, 70.6 mmol), DME (100 mL) and water (40 mL) for 30 min. (3,5-Dimethylisoxazol-4-yl)boronic acid (9.75 g, 69.2 mmol) and PEPPSI-IPr catalyst (0.6 g, 0.883 mmol) was added and the mixture stirred at 90 °C for 5 h under nitrogen. The reaction was allowed to cool to rt then EtOAc (150 mL) and water (75 mL) added. The layers were separated and the organic layer washed with 10% Na₂SO₃ (aq) (75 mL) followed by brine (75 mL). The organic layer was dried over MgSO₄, filtered and concentrated under reduced pressure. The solid was triturated with diethyl ether (50 mL), filtered and washed with cyclohexane (100 mL). The solid was dried in a vacuum oven to give the title compound as a light brown solid (9.72 g, 30.0 mmol, 86%). ¹H NMR (400 MHz, CDCl₃) δ 8.26 (dd, *J* = 9.1, 2.8 Hz, 1H), 8.07 (d, *J* = 2.8 Hz, 1H), 7.41–7.31 (m, 3H), 7.30–7.25 (m, 2H), 7.13 (d, *J* = 9.1 Hz, 1H), 5.19 (s, 2H), 2.30 (s, 3H), 2.16 (s, 3H); LC-MS (Method A) [M + H]⁺ = 325, *R*_t 1.19 min, 100% purity.

4-(Benzyloxy)-3-(3,5-dimethylisoxazol-4-yl)aniline (4). A mixture of 4-[2-(benzyloxy)-5-nitrophenyl]-3,5-dimethylisoxazole **3** (9.2 g, 28.4 mmol), iron powder (6.0 g, 107 mmol) and ammonium chloride (12 g, 224 mmol) was suspended in EtOH (400 mL) and water (100 mL) and stirred at r.t for 15 h. The reaction mixture was filtered through a pad of Celite and the solid washed with EtOH. The filtrate was evaporated under vacuum and the residue partitioned between EtOAc (150 mL) and water (150 mL). The organic layer was separated, washed with further water (100 mL) and dried over MgSO₄. The solvent was removed under vacuum to give the title compound as a dark brown oil (8.2 g, 27.9 mmol, 98%). ¹H NMR (400 MHz, CDCl₃) δ 7.37–7.25 (m, 3H), 7.25–7.20 (m, 2H), 6.91 (d, *J* = 8.6 Hz, 1H), 6.69 (dd, *J* = 8.6, 2.9 Hz, 1H), 6.51 (d, *J* = 2.9 Hz, 1H), 4.92 (s, 2H), 3.53 (br s, 2H), 2.29 (s, 3H), 2.18 (s, 3H); LC-MS (Method A) [M + H]⁺ = 295, *R*_t 0.75 min, 85% purity (10% starting material remains).

Diethyl 2-({4-(benzyloxy)-3-(3,5-dimethylisoxazol-4-yl)phenyl}amino)methylene)malonate (5). A mixture of 4-(benzyloxy)-3-(3,5-dimethylisoxazol-4-yl)aniline **4** (8.2 g, 27.9 mmol) and diethyl 2-(ethoxymethylene)malonate (5.6 mL, 28.0 mmol) was stirred at 130 °C for 1 h. The brown oil was concentrated under reduced pressure. The residue was loaded in DCM (20 mL) and purified on a 330 g silica cartridge using a gradient of 0–100 % EtOAc in DCM over 10 column volumes. The appropriate fractions were combined and the solvent removed by rotary evaporation. The resulting solid was triturated with cyclohexane, filtered and dried in a vacuum oven to give the title compound as a light brown solid (9.6 g, 20.67 mmol, 74%). ¹H NMR (400 MHz, CDCl₃) δ 11.02 (d, *J* = 13.5 Hz, 1H), 8.44 (d, *J* = 13.5 Hz, 1H), 7.40–7.24 (m, 5H), 7.15 (dd, *J* = 8.8, 2.9 Hz, 1H), 7.07 (d, *J* = 8.8 Hz, 1H), 6.94 (d, *J* = 2.9 Hz, 1H), 5.06 (s, 2H), 4.32 (q, *J* = 7.1 Hz, 2H), 4.26 (q, *J* = 7.1 Hz, 2H), 2.31 (s, 3H), 2.18 (s, 3H), 1.40 (t, *J* = 7.1 Hz, 3H), 1.34 (t, *J* = 7.1 Hz, 3H); LC-MS (Method A) [M + H]⁺ = 465, *R*_t 1.30 min, 100% purity.

Ethyl 6-(benzyloxy)-7-(3,5-dimethylisoxazol-4-yl)-4-oxo-1,4-dihydroquinoline-3-carboxylate

(6). Diphenyl ether (75 mL) was heated with stirring to 260 °C (internal). Solid diethyl 2-([4-(benzyloxy)-3-(3,5-dimethylisoxazol-4-yl)phenyl]amino)methylene)malonate **5** (9.6 g, 20.67 mmol) was added in portions, followed by diphenyl ether (10 mL). The mixture was stirred for 20 min. The mixture was allowed to cool to rt and diluted with DCM (20 mL). The solution was loaded onto a 330 g silica cartridge and purified using a gradient of 0–20 % MeOH in DCM over 10 column volumes. The appropriate fractions were combined and the solvent removed by rotary evaporation to give the title compound as a light brown solid (7.8 g, 18.64 mmol, 90%). ¹H NMR (400 MHz, DMSO-*d*₆) δ 12.27 (br s, 1H), 8.55 (s, 1H), 7.82 (s, 1H), 7.53 (s, 1H), 7.40–7.29 (m, 5H), 5.24 (s, 2H), 4.22 (q, *J* = 7.1 Hz, 2H), 2.30 (s, 3H), 2.10 (s, 3H), 1.29 (t, *J* = 7.1 Hz, 3H); LC-MS (Method A) [M + H]⁺ = 419, *R*_t 0.93 min, 85% purity (9% decarboxylated material present).

6-(Benzyloxy)-7-(3,5-dimethylisoxazol-4-yl)-4-oxo-1,4-dihydroquinoline-3-carboxylic acid

(7). To ethyl 6-(benzyloxy)-7-(3,5-dimethylisoxazol-4-yl)-4-oxo-1,4-dihydroquinoline-3-carboxylate **6** (7.8 g, 18.64 mmol) was added EtOH (50 mL) and 2 M NaOH (aq) (30 mL, 60.0 mmol) and the mixture stirred at 95 °C for 3 h. The reaction was allowed to cool to rt and the volatiles evaporated under vacuum. The remaining mixture was acidified to pH = 1 with 12.5% HCl (aq) (~30 mL) and the resulting precipitate isolated by vacuum filtration. The solid was washed with water (200 mL) and diethylether (50 mL), and then dried in a vacuum oven overnight to give the title compound as an off-white solid (7.2 g, 18.44 mmol, 99%). ¹H NMR (400 MHz, DMSO-*d*₆) δ 15.64 (br s, 1H), 8.85 (s, 1H), 7.90 (s, 1H), 7.76 (s, 1H), 7.43–7.30 (m, 5H), 5.31 (s, 2H), 2.31 (s, 3H), 2.12 (s, 3H); LC-MS (Method A) [M + H]⁺ = 391, *R*_t 1.00 min, 82% purity (10% decarboxylated material present).

6-(Benzyloxy)-7-(3,5-dimethylisoxazol-4-yl)quinolin-4(1H)-one (8). Diphenyl ether (70 mL) was heated with stirring to 260 °C (internal). Solid 6-(benzyloxy)-7-(3,5-dimethylisoxazol-4-yl)-4-oxo-1,4-dihydroquinoline-3-carboxylic acid **7** (7.2 g, 18.44 mmol) was added in one portion followed by diphenyl ether (10 mL). The mixture stirred for 20 min. The reaction was allowed to cool to rt and the solution applied to a 330 g silica cartridge with DCM (20 mL). The mixture was purified using a gradient of 0–20 % MeOH in DCM over 10 column volumes. The appropriate fractions were combined and the solvent removed by rotary evaporation to give the title compound as a brown solid (5.7 g, 16.46 mmol, 89%). ¹H NMR (400 MHz, DMSO-*d*₆) δ 11.72 (br s, 1H), 7.92–7.86 (m, 1H), 7.75 (s, 1H), 7.44 (s, 1H), 7.41–7.29 (m, 5H), 6.03 (d, *J* = 7.2 Hz, 1H), 5.21 (s, 2H), 2.29 (s, 3H), 2.11 (s, 3H); LC-MS (Method A) [M + H]⁺ = 347, *R*_t 0.83 min, 89% purity.

6-(Benzyloxy)-7-(3,5-dimethylisoxazol-4-yl)-3-nitroquinolin-4(1H)-one (9). To a 500 mL round bottomed flask containing 6-(benzyloxy)-7-(3,5-dimethylisoxazol-4-yl)quinolin-4(1H)-one **8** (5.7 g, 16.46 mmol) was added propionic acid (75 mL, 1002 mmol) followed by 70% nitric acid (1.6 mL, 35.8 mmol). A suspension formed which was stirred at 100 °C for 1.5 h. The reaction mixture was allowed to cool to rt, filtered under vacuum and washed with cyclohexane (100 mL). The solid was dried in a vacuum oven to give the title compound as a tan solid (3.7 g, 9.45 mmol, 57%). ¹H NMR (400 MHz, DMSO-*d*₆) δ 12.97 (br s, 1H), 9.18 (s, 1H), 7.91 (s, 1H), 7.63 (s, 1H), 7.42–7.29 (m, 5H), 5.29 (s, 2H), 2.30 (s, 3H), 2.11 (s, 3H); LC-MS (Method A) [M + H]⁺ = 392, *R*_t 0.94 min, 98% purity.

4-[6-(Benzyloxy)-4-chloro-3-nitroquinolin-7-yl]-3,5-dimethylisoxazole (10). To 6-(benzyloxy)-7-(3,5-dimethylisoxazol-4-yl)-3-nitroquinolin-4(1H)-one **9** (3.53 g, 9.02 mmol) was added POCl₃ (20 mL, 215 mmol) and the suspension stirred at 100 °C under nitrogen for 1 h. The reaction mixture was allowed to cool to rt and evaporated under vacuum. Toluene (20 mL) was

added and the mixture evaporated. The residue was dissolved in DCM (25 mL) and sat. NaHCO₃ (aq) (25 mL) was added. The mixture was stirred vigorously for 30 min and the organic layer separated. The aqueous layer was extracted with DCM (25 mL), the organics combined and passed through a hydrophobic frit. The solvent was removed under vacuum and the resulting solid triturated with cyclohexane:diethylether (8:2) (40 mL). The solid was dried *in vacuo* to give the title compound as a light brown solid (3.54 g, 8.64 mmol, 96%). mp 230–232 °C; IR (solid) ν (cm⁻¹) 3130, 1619, 1556, 1526, 1420, 1381, 1331, 1227, 1023, 739; ¹H NMR (400 MHz, CDCl₃) δ 9.16 (s, 1H), 8.01 (s, 1H), 7.82 (s, 1H), 7.47–7.33 (m, 5H), 5.32 (s, 2H), 2.37 (s, 3H), 2.23 (s, 3H); ¹³C NMR (100 MHz, CDCl₃) δ 167.1, 159.3, 157.3, 144.9, 142.6, 141.7, 135.0, 134.2, 133.0, 129.2, 128.9 (2 C), 128.7, 127.4 (2 C), 126.7, 111.7, 104.7, 71.3, 12.0, 10.9; LC-MS (Method A) [M + H]⁺ = 410, 412, R_t 1.32 min, 98% purity; HRMS [M + H]⁺ calcd for C₂₁H₁₇³⁵ClN₃O₄ 410.0902, found 410.0897.

6-(Benzyloxy)-7-(3,5-dimethylisoxazol-4-yl)-3-nitro-N-[(R)-1-phenylethyl]quinolin-4-amine (11). A solution of 4-[6-(benzyloxy)-4-chloro-3-nitroquinolin-7-yl]-3,5-dimethylisoxazole **10** (5 g, 12.20 mmol) in anhydrous NMP (25 mL) was treated with ^tPr₂NEt (4.26 mL, 24.40 mmol) followed by (R)-1-phenylethanamine (1.712 mL, 13.42 mmol). The solution was stirred under nitrogen at rt for 2.5 h. The reaction mixture was diluted with water (50 mL) and extracted with EtOAc (75 mL). The organic layer was washed with a 10% aqueous solution of LiCl (2 x 50 mL) followed by water (50 mL), and passed through a hydrophobic frit. The solvent was removed *in vacuo* and dried in a vacuum oven to give the title compound as a yellow foam (5.96 g, 12.05 mmol, 99%). ¹H NMR (400 MHz, CDCl₃) δ 9.54 (d, *J* = 7.8 Hz, 1H), 9.27 (s, 1H), 7.70 (s, 1H), 7.53–7.46 (m, 2H), 7.44–7.37 (m, 3H), 7.36–7.29 (m, 1H), 7.28–7.21 (m, 3H), 7.00–6.95 (m, 2H), 5.32 (dq, *J* = 7.8, 6.7 Hz, 1H), 4.46 (d, *J* = 11.8 Hz, 1H), 4.07 (d, *J* = 11.8 Hz, 1H), 2.20 (s, 3H),

2.07 (s, 3H), 1.69 (d, $J = 6.7$ Hz, 3 H); LC-MS (Method A) $[M + H]^+ = 495$, R_t 1.31 min, 100% purity.

6-(Benzyloxy)-7-(3,5-dimethylisoxazol-4-yl)- N^4 -[(*R*)-1-phenylethyl]quinoline-3,4-diamine

(12). Iron powder (5.36 g, 96 mmol) was added to a solution of 6-(benzyloxy)-7-(3,5-dimethylisoxazol-4-yl)-3-nitro-*N*-[(*R*)-1-phenylethyl]quinolin-4-amine **11** (5.93 g, 11.99 mmol) in acetic acid (50 mL). The mixture was stirred in an open vessel at rt for 1 h. EtOAc (50 mL) was added to the flask and the mixture stirred for 1 h. The mixture was filtered through a Celite cartridge which was washed with further EtOAc (100 mL). The filtrate was washed with 0.5 M aqueous NaOH (2 x 100 mL) and water (100 mL). The organic layer was separated, passed through a hydrophobic frit and the solvent removed by rotary evaporation. The resulting foam was dissolved in MeOH (10 mL) and applied to a MeOH-preconditioned 50 g aminopropyl cartridge. The cartridge was washed with MeOH (160 mL) and the solvent evaporated under vacuum to give the title compound as a light brown foam (4.62 g, 9.94 mmol, 83%). $^1\text{H NMR}$ (400 MHz, CDCl_3) δ 8.38 (s, 1H), 7.73 (s, 1H), 7.41–7.25 (m, 10H), 6.99 (s, 1H), 5.02–4.93 (m, 2H), 4.52 (q, $J = 6.7$ Hz, 1H), 3.69 (br s, 2H), 3.56 (br s, 1H), 2.34 (s, 3H), 2.21 (s, 3H), 1.61 (d, $J = 6.7$ Hz, 3H); LC-MS (Method A) $[M + H]^+ = 465$, R_t 0.99 min, 95% purity.

***N*-[6-(Benzyloxy)-7-(3,5-dimethylisoxazol-4-yl)-4-[(*R*)-1-phenylethyl]amino}quinolin-3-yl]-**

2-methoxyacetamide (13). A solution of 6-(benzyloxy)-7-(3,5-dimethylisoxazol-4-yl)- N^4 -[(*R*)-1-phenylethyl]quinoline-3,4-diamine **12** (1.89 g, 4.07 mmol) and pyridine (0.50 mL, 6.18 mmol) in DCM (20 mL) was cooled to 0 °C and 2-methoxyacetyl chloride (0.41 mL, 4.48 mmol) added. The mixture was stirred under nitrogen at 0 °C for 10 min and allowed to warm to rt over 3.5 h. The reaction mixture was washed sequentially with 0.5 M aqueous HCl (20 mL) and water (2 x 20 mL). The organic layer was separated, passed through a hydrophobic frit and the solvent removed

by rotary evaporation to give the title compound as a light brown foam (2.14 g, 3.99 mmol, 98%). ¹H NMR (400 MHz, CDCl₃) δ 8.80 (s, 1H), 8.25 (s, 1H), 7.82 (s, 1H), 7.40–7.29 (m, 8H), 7.26–7.21 (m, 3H), 4.92–4.85 (m, 2H), 4.62 (dq, *J* = 8.6, 6.8 Hz, 1H), 4.27 (d, *J* = 8.6 Hz, 1H), 4.10 (s, 2H), 3.53 (s, 3H), 2.34 (s, 3H), 2.21 (s, 3H), 1.61 (d, *J* = 6.8 Hz, 3H); LC-MS (Method A) [M + H]⁺ = 537, *R*_t 0.91 min, 100% purity.

4-{8-(Benzyloxy)-2-(methoxymethyl)-1-[(*R*)-1-phenylethyl]-1*H*-imidazo[4,5-*c*]quinolin-7-yl}-3,5-dimethylisoxazole (14). A solution of *N*-[6-(benzyloxy)-7-(3,5-dimethylisoxazol-4-yl)-4-{{(*R*)-1-phenylethyl}amino}quinolin-3-yl]-2-methoxyacetamide **13** (2.14 g, 3.99 mmol) in propionic acid (6.0 mL, 80 mmol) was stirred at 140 °C under nitrogen for 2 h. The reaction mixture was allowed to cool to rt and the solvent removed *in vacuo*. The residue was dissolved in DCM (25 mL) and washed with 1 M NaOH (aq) (25 mL). The aqueous layer was extracted with DCM (25 mL), the organic layers combined and passed through a hydrophobic frit. The solvent was removed by rotary evaporation, the foam dissolved in DCM (5 mL) and purified on a 100 g silica cartridge using a gradient of 0–15 % MeOH in DCM over 12 column volumes. The appropriate fractions were combined and the solvent was removed by rotary evaporation to give the title compound as a light brown foam (1.87 g, 3.61 mmol, 90%). ¹H NMR (400 MHz, DMSO-*d*₆, 393 K) δ 9.15 (s, 1H), 7.96 (s, 1H), 7.46–7.30 (m, 8 H), 7.24–7.20 (m, 2H), 7.09 (s, 1H), 6.47 (q, *J* = 7.1 Hz, 1H), 4.88–4.85 (m, 2H), 4.80 (d, *J* = 11.9 Hz, 1H), 4.41 (d, *J* = 11.9 Hz, 1H), 3.40 (s, 3H), 2.24 (s, 3H), 2.07–2.03 (m, 6H) ; LC-MS (Method A) [M + H]⁺ = 519, *R*_t 1.08 min, 96% purity.

7-(3,5-Dimethylisoxazol-4-yl)-2-(methoxymethyl)-1-[(*R*)-1-phenylethyl]-1*H*-imidazo[4,5-*c*]quinolin-8-ol (15). A solution of 4-{8-(benzyloxy)-2-(methoxymethyl)-1-[(*R*)-1-phenylethyl]-1*H*-imidazo[4,5-*c*]quinolin-7-yl}-3,5-dimethylisoxazole **14** (1.81 g, 3.49 mmol) in EtOH (20 mL) was added to 5% palladium on carbon (180 mg, 1.692 mmol) and stirred at rt under atmospheric

hydrogen for 15 h. The reaction mixture was filtered through Celite and the cake washed with EtOH (50 mL). The filtrate was evaporated under vacuum and the residue dissolved in EtOH (40 mL). The solution was added to 5% palladium on carbon (360 mg, 3.38 mmol) and stirred at rt under atmospheric hydrogen for 20 h. The reaction mixture was filtered through Celite and the cake washed with EtOH (50 mL). The filtrate was evaporated under vacuum and the residue dissolved in DCM (8 mL). The solution was loaded onto a 220 g silica cartridge and purified using a gradient of 0–15 % MeOH in DCM over 10 column volumes. The appropriate fractions were combined and the solvent removed by rotary evaporation to give an off-white solid which was purified by MDAP using Method B. The appropriate fractions were combined and the solvent removed by rotary evaporation to give the title compound as a light yellow solid (923 mg, 2.154 mmol, 62%). ¹H NMR (400 MHz, DMSO-*d*₆, 393 K) δ 9.50 (br s, 1H), 9.04 (s, 1H), 7.89 (s, 1H), 7.45–7.23 (m, 6H), 6.51 (q, *J* = 7.1 Hz, 1H), 4.66 (ABq, 2H, Δδ_{AB} = 0.07, *J*_{AB} = 12.9 Hz), 3.33 (s, 3H), 2.31 (s, 3H), 2.17 (d, *J* = 7.1 Hz, 3H), 2.14 (s, 3H); LC-MS (Method A) [M + H]⁺ = 429, *R*_t 0.72 min, 96% purity.

Fractions containing a minor peak were combined and the solvent removed by rotary evaporation to give (*R*)-1-{2-(methoxymethyl)-8-methyl-1-(1-phenylethyl)-1*H*-furo[2,3-*g*]imidazo[4,5-*c*]quinolin-7-yl}ethanone **15** as a light yellow foam (129 mg, 0.312 mmol, 9%). ¹H NMR (400 MHz, DMSO-*d*₆, 393 K) δ 9.24 (s, 1H), 8.71 (s, 1H), 7.70 (s, 1H), 7.44–7.36 (m, 2H), 7.36–7.25 (m, 3H), 6.57 (q, *J* = 7.1 Hz, 1H), 4.82 (s, 2H), 3.38 (s, 3H), 2.79 (s, 3H), 2.67 (s, 3H), 2.13 (d, *J* = 7.1 Hz, 3H); LC-MS (Method A) [M + H]⁺ = 414, *R*_t 0.81 min, 96% purity.

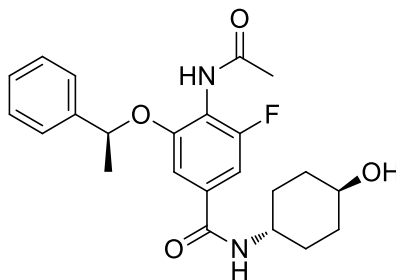
(3*S*)-tert-Butyl 3-[(7-(3,5-dimethylisoxazol-4-yl)-2-(methoxymethyl)-1-((*R*)-1-phenylethyl)-1*H*-imidazo[4,5-*c*]quinolin-8-yl)oxy)methyl]pyrrolidine-1-carboxylate (16). A mixture of 7-(3,5-dimethylisoxazol-4-yl)-2-(methoxymethyl)-1-((*R*)-1-phenylethyl)-1*H*-imidazo[4,5-

c]quinolin-8-ol **15** (233 mg, 0.544 mmol), potassium carbonate (107 mg, 0.778 mmol) and (*S*)-*tert*-butyl 3-[[[(methylsulfonyl)oxy]methyl]pyrrolidine-1-carboxylate (190 mg, 0.680 mmol) in anhydrous DMF (1.2 mL) was stirred at 100 °C under nitrogen for 3 h. The reaction mixture was allowed to cool to rt, diluted with 10 % LiCl (aq) (10 mL) and extracted with EtOAc (3 x 10 mL). The organic layers were combined and passed through a hydrophobic frit. The solvent was removed by rotary evaporation and the residue purified by MDAP using Method B. The appropriate fractions were combined and evaporated *in vacuo* to give the title compound as an off-white solid (191 mg, 0.312 mmol, 57% yield). ¹H NMR (400 MHz, DMSO-*d*₆, 373 K) δ 9.15 (s, 1H), 7.93 (s, 1H), 7.44–7.38 (m, 2H), 7.37–7.31 (m, 3H), 6.92 (s, 1H), 6.49 (q, *J* = 7.0 Hz, 1H), 4.93 (d, *J* = 13.0 Hz, 1H), 4.88 (d, *J* = 13.0 Hz, 1H), 3.71 (dd, *J* = 9.4, 6.4 Hz, 1H), 3.41 (s, 3H), 3.39–3.25 (m, 3H), 3.13–3.07 (m, 1H), 2.93–2.91 (m, 1H), 2.49–2.41 (m, 1H), 2.27 (s, 3H), 2.11 (d, *J* = 7.0 Hz, 3H), 2.08 (s, 3H), 2.00–1.89 (m, 1H), 1.65–1.54 (m, 1H), 1.46 (s, 9H); LC-MS (Method A) [M + H]⁺ = 612, *R*_t 1.08 min, 100% purity; HRMS [M + H]⁺ calcd for C₃₅H₄₂N₅O₅ 612.3181, found 612.3170.

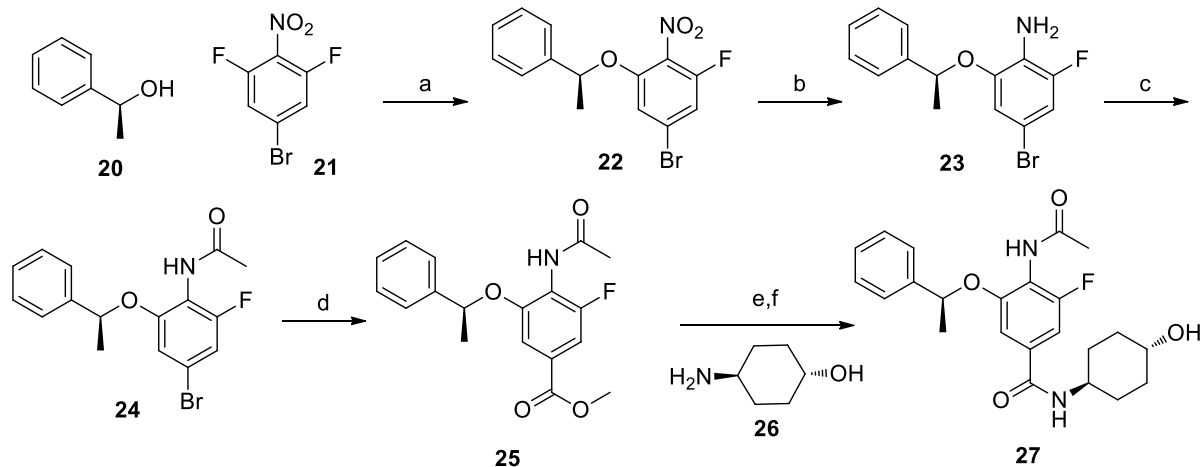
4-{2-(Methoxymethyl)-1-[(*R*)-1-phenylethyl]-8-[(*S*)-pyrrolidin-3-ylmethoxy]-1*H*-imidazo[4,5-*c*]quinolin-7-yl}-3,5-dimethylisoxazole (17**). A solution of (*3S*)-*tert*-Butyl 3-[[[(7-(3,5-dimethylisoxazol-4-yl)-2-(methoxymethyl)-1-[(*R*)-1-phenylethyl]-1*H*-imidazo[4,5-*c*]quinolin-8-yl)oxy)methyl]pyrrolidine-1-carboxylate **16** (186 mg, 0.304 mmol) in anhydrous 1,4-dioxane (2 mL) was treated with 4 M HCl in 1,4-dioxane (2 mL, 8.00 mmol) and the mixture allowed to stand in a stoppered vessel for 1 h. The reaction mixture was evaporated *in vacuo* and the solid dissolved in MeOH (2 mL). The solution was applied to a MeOH-preconditioned 5 g SCX-2 cartridge which was then washed with MeOH (30 mL) followed by 2 M ammonia in MeOH solution (30 mL). The basic wash was evaporated *in vacuo* to give the title compound as an off-**

white solid (150 mg, 0.293 mmol, 96 % yield). mp 130–132 °C; $[\alpha]_D^{21} -27$ (*c* 0.5, CHCl₃); IR (solid) ν (cm⁻¹) 2929, 1618, 1495, 1444, 1393, 1367, 1215, 1095. ¹H NMR (400 MHz, DMSO-*d*₆, 393 K) δ 9.13 (s, 1H), 7.92 (s, 1H), 7.44–7.37 (m, 2H), 7.37–7.29 (m, 3H), 6.95 (s, 1H), 6.48 (q, *J* = 7.0 Hz, 1H), 4.91 (d, *J* = 13.0 Hz, 1H), 4.87 (d, *J* = 13.0 Hz, 1H), 3.65 (dd, *J* = 9.3, 6.3 Hz, 1H), 3.41 (s, 3H), 3.19–3.12 (m, 1H), 2.92–2.81 (m, 3H), 2.44 (dd, *J* = 10.6, 6.0 Hz, 1H), 2.34–2.22 (m, 4H), 2.11 (d, *J* = 7.0 Hz, 3H), 2.07 (s, 3H), 1.85–1.74 (m, 1H), 1.40–1.29 (m, 1H), NH not resolved; ¹³C NMR (100 MHz, DMSO-*d*₆, 393 K) δ 165.2, 158.3, 153.9, 151.8, 142.7, 139.7, 139.6, 137.1, 132.5, 132.4, 128.6 (2C), 127.0, 125.1 (2C), 120.2, 117.4, 111.8, 104.1, 71.3, 66.8, 57.5, 54.1, 49.4, 45.6, 38.1, 28.5, 18.7, 10.6, 9.5; >99% d.e. determined by HPLC analysis on a Chiralpak AD column (250 x 4.6 mm, 10 μ m), elution with 20% EtOH in heptane containing 0.1% isopropylamine, flow rate 1 mL/min, UV detection at 235 nm; LC-MS (Method A) $[M + H]^+ = 512$, *R*_t 0.59 min, 100% purity; HRMS $[M + H]^+$ calcd for C₃₀H₃₄N₅O₃ 512.2656, found 512.2650.

iBET-BD2 (GSK046)



Synthesis:



Reagents and conditions: (a) LiHMDS, THF, rt to 110°C, 1 h, 62%; (b) Fe(0), NH₄Cl, EtOH/water, reflux, 1 h, 81%; (c) Ac₂O, rt, 16 h, 81%; (d), Pd(OAc)₂, XantPhos, NEt₃, CO, DMF, EtOH, 70 °C, 1 h, 90%; (e) NaOH, THF/EtOH/water, rt, 2 h, 96%; (f) HATU, **26**, DIPEA, CH₂Cl₂, rt, 1.5 h, 84%.

Procedure:

(S)-5-Bromo-1-fluoro-2-nitro-3-(1-phenylethoxy)benzene (22). A solution of (S)-1-phenylethanol (5.33 mL, 44.1 mmol) and 5-bromo-1,3-difluoro-2-nitrobenzene (10 g, 42.0 mmol) in THF (200 mL) at room temperature under Nitrogen was treated with LiHMDS (1N in THF, 46.2 mL, 46.2 mmol) over 5 min and the resulting mixture was stirred at this temperature for 30 min then was quenched with a saturated NH₄Cl aqueous solution. The mixture was partitioned between EtOAc and water and the layers were separated. The aqueous phase was extracted with EtOAc and the combined organics were washed with brine, dried over Na₂SO₄ and concentrated *in vacuo* to give (S)-5-bromo-1-fluoro-2-nitro-3-(1-phenylethoxy)benzene (14.1 g, 99%) as a black oil which was used in the next step without further purification.

¹H NMR (400 MHz, CDCl₃) δ ppm 7.32-7.26 (m, 2H), 7.28-7.24 (m, 2H), 7.25-7.20 (m, 1H), 6.85 (dd, *J* = 8.5, 1.5 Hz, 1H), 6.78-6.76 (m, 1H), 5.31 (q, *J* = 6.5 Hz, 1H), 1.57 (d, *J* = 6.5 Hz, 3H).

¹³C NMR (101 MHz, CDCl₃) δ ppm 154.26 (d, *J* = 259.69 Hz, 1C), 151.26 (d, *J* = 3.00 Hz, 1C), 140.52 (s, 1C), 130.76 (br d, *J* = 15.50 Hz, 1C), 129.08 (s, 2C), 128.46 (s, 1C), 125.42 (s, 2C),

124.82 (d, $J = 11.80$ Hz, 1C), 114.72 (d, $J = 3.50$ Hz, 1C), 112.28 (d, $J = 22.80$ Hz, 1C), 79.11 (s, 1C), 24.05 (s, 1C).

LCMS (method high pH): Retention time 1.42 min, no mass.

(S)-4-Bromo-2-fluoro-6-(1-phenylethoxy)aniline (23). A solution of (S)-5-bromo-1-fluoro-2-nitro-3-(1-phenylethoxy)benzene (44.8 g, 132 mmol) and NH_4Cl (35.2 g, 659 mmol) in EtOH (440 mL) and H_2O (147 mL) at room temperature was treated with Fe(0) (22.07 g, 395 mmol) and the resulting mixture was refluxed for 1 h then was cooled to room temperature and partitioned between water (500 mL) and EtOAc (500 mL). The mixture was filtered through celite and the layers were separated. The aqueous phase was extracted with EtOAc (2 * 500 mL) and the combined organics were washed with brine, dried over Na_2SO_4 and concentrated *in vacuo* to give (S)-4-bromo-2-fluoro-6-(1-phenylethoxy)aniline (34.5 g, 82%) as a colourless liquid. This was used in the next step without further purification.

^1H NMR (400 MHz, CDCl_3) δ ppm 7.36-7.34 (m, 2H), 7.35-7.33 (m, 2H), 7.31-7.26 (m, 1H), 6.78 (dd, $J = 9.8, 2.1$ Hz, 1H), 6.59 (t, $J = 1.8$ Hz, 1H), 5.28 (q, $J = 6.4$ Hz, 1H), 1.65 (d, $J = 6.5$ Hz, 3H).

^{13}C NMR (101 MHz, CDCl_3) δ ppm 151.32 (d, $J = 240.6$ Hz, 1C), 147.03 (d, $J = 8.1$ Hz, 1C), 142.03 (s, 1C), 128.83 (s, 2C), 127.96 (s, 1C), 125.43 (s, 2C), 124.67 (d, $J = 14.7$ Hz, 1C), 112.86 (d, $J = 2.9$ Hz, 1C), 111.71 (d, $J = 22.7$ Hz, 1C), 107.57 (d, $J = 11.7$ Hz, 1C), 77.45 (s, 1C), 24.17 (s, 1C).

LCMS (method high pH): Retention time 1.34 min, $[\text{M}+\text{H}]^+ = 312.1$ (1 Br)

(S)-N-(4-Bromo-2-fluoro-6-(1-phenylethoxy)phenyl)acetamide (24). To neat (S)-4-bromo-2-fluoro-6-(1-phenylethoxy)aniline (34.0 g, 106 mmol) at room temperature was added neat acetic

anhydride (523 mL, 5541 mmol) in one charge and the resulting mixture was stirred at this temperature for 16 h then was concentrated *in vacuo*.

The residue obtained was triturated with n-pentane (2 x 100 mL). The solid obtained was filtered through a Buchner funnel, rinsed with n-pentane, and dried under reduced pressure to give (S)-N-(4-bromo-2-fluoro-6-(1-phenylethoxy)phenyl)acetamide (30.8 g, 81%) as a white solid which was used in the next step without further purification.

¹H NMR (400 MHz, DMSO-*d*₆) δ ppm, 9.28 (br s, 1H), 7.46-7.41 (m, 2H) 7.38-7.32 (m, 2H), 7.31-7.24 (m, 1H), 7.09 (dd, *J* = 9.0, 1.6 Hz, 1H), 6.99 - 6.91 (m, 1H), 5.59 (q, *J* = 6.2 Hz, 1H), 2.08 (br s, 3H), 1.52 (d, *J* = 6.2 Hz, 3H).

¹³C NMR (101 MHz, DMSO-*d*₆) δ ppm 168.69 (br s, 1C), 158.66 (d, *J* = 249.4 Hz, 1C), 155.11 (br d, *J* = 5.9 Hz, 1C), 142.57 (s, 1C), 128.99 (s, 2C), 128.12 (s, 1C), 126.08 (s, 2C), 119.06 (br d, *J* = 12.5 Hz, 1C), 115.78 (br d, *J* = 15.4 Hz, 1C), 114.17 (s, 1C), 111.82 (br d, *J* = 24.2 Hz, 1C), 76.68 (s, 1C), 24.35 (s, 1C), 22.98 (s, 1C).

LCMS (method high pH): Retention time 1.14 min, [M+H]⁺ = 352.0 (1 Br)

(S)-Methyl 4-acetamido-3-fluoro-5-(1-phenylethoxy)benzoate (25). A flask was charged with (S)-N-(4-bromo-2-fluoro-6-(1-phenylethoxy)phenyl)acetamide, Pd(OAc)₂ (0.319 g, 1.42 mmol) and Xantphos (0.821 g, 1.420 mmol) and purged with nitrogen, then was filled with DMF (40 mL) and MeOH (20 mL) and the resulting mixture was treated with NEt₃ (6.00 mL, 43.0 mmol) before being purged with carbon monoxide from a balloon (about 1 L volume). A fresh balloon was fitted and the mixture was stirred at 70°C for 4 h, then was cooled to room temperature and diluted with EtOAc (100 mL). The organic phase was washed with a 10% w/w LiCl aqueous solution (2 x 100 mL) dried over Na₂SO₄ and concentrated *in vacuo*. Purification of the residue by flash

chromatography on silica gel (100 g column, gradient: 10-100% EtOAc in cyclohexane gave methyl (S)-4-acetamido-3-fluoro-5-(1-phenylethoxy)benzoate (4.5 g, 96%) as a pale yellow foam.

^1H NMR (400 MHz, DMSO-*d*₆) δ ppm 9.50 (s, 1H), 7.49-7.44 (m, 2H), 7.38-7.33 (m, 2H), 7.32-7.28 (m, 1H), 7.29-7.28 (m, 1H), 7.28-7.24 (m, 1H), 5.61 (q, $J = 6.4$ Hz, 1H), 3.79 (s, 3H), 2.11 (s, 3H), 1.56 (d, $J = 6.4$ Hz, 3H).

^{13}C NMR (101 MHz, DMSO-*d*₆) δ ppm 168.60 (s, 1C), 165.34 (d, $J = 2.9$ Hz, 1C), 157.97 (d, $J = 247.2$ Hz, 1C), 154.09 (d, $J = 5.1$ Hz, 1C), 142.69 (s, 1C), 128.99 (s, 2C), 128.61 (br d, $J = 9.5$ Hz, 1C), 128.09 (s, 1C), 126.03 (s, 2C), 120.86 (d, $J = 15.4$ Hz, 1C), 111.15 (s, 1C), 109.12 (br d, $J = 23.5$ Hz, 1C), 76.86 (s, 1C), 52.92 (s, 1C), 24.43 (s, 1C), 23.00 (s, 1C).

LCMS (method Formic): Retention time 0.97 min, $[\text{M}+\text{H}]^+ = 332.3$

(S)-4-Acetamido-3-fluoro-5-(1-phenylethoxy)benzoic acid. A solution of (S)-methyl 4-acetamido-3-fluoro-5-(1-phenylethoxy)benzoate (3.35 g, 10.1 mmol) in a mixture of THF (20 mL), MeOH (20 mL) and water (20 mL) was treated at room temperature with NaOH (2.03 g, 50.7 mmol) and the resulting mixture was stirred at room temperature for 2 h. Most of the solvent was evaporated *in vacuo* and the residue was partitioned between water (50 mL) and Et₂O (50 mL) and the layers were separated. The aqueous phase was acidified with a 2N aqueous HCl solution to pH 4, then was extracted with EtOAc (2 x 100 mL). The combined organics were dried over Na₂SO₄ and concentrated *in vacuo* to give (S)-4-acetamido-3-fluoro-5-(1-phenylethoxy)benzoic acid (3.10 g, 96%) as a colourless solid, which was used in the next step without further purification.

^1H NMR (400 MHz, DMSO-*d*₆) δ ppm 13.08 (br d, $J = 2.4$ Hz, 1H), 9.46 (br s, 1H), 7.51-7.42 (m, 2H), 7.39-7.32 (m, 2H), 7.27-7.25 (m, 1H), 7.30-7.25 (m, 1H), 7.29-7.24 (m, 1H), 5.59 (q, $J = 6.4$ Hz, 1H), 2.10 (s, 3H), 1.55 (d, $J = 5.9$ Hz, 3H).

^{13}C NMR (101 MHz, DMSO-*d*₆) δ ppm 168.63 (br s, 1C), 166.36 (s, 1C), 157.97 (d, $J = 247.2$ Hz, 1C), 154.02 (br d, $J = 5.1$ Hz, 1C), 142.81 (s, 1C), 129.98 (br d, $J = 9.5$ Hz, 1C), 128.99 (s, 2C), 128.06 (s, 1C), 126.01 (s, 2C), 120.37 (d, $J = 15.4$ Hz, 1C), 111.21 (br s, 1C), 109.14 (br d, $J = 22.7$ Hz, 1C), 76.74 (s, 1C), 24.54 (s, 1C), 23.00 (br s, 1C).

LCMS (method Formic): Retention time 0.87 min, $[\text{M}+\text{H}]^+ = 318.2$

4-Acetamido-3-fluoro-N-((1*r*,4*S*)-4-hydroxycyclohexyl)-5-((*S*)-1-phenylethoxy)benzamide

(27). A solution of (*S*)-4-acetamido-3-fluoro-5-(1-phenylethoxy)benzoic acid (10.0 g, 31.5 mmol) in CH_2Cl_2 (200 mL) at room temperature was treated with DIPEA (16.5 mL, 95.0 mmol) then HATU (18.0 g, 47.3 mmol) and the reaction was stirred at this temperature for 20 min. (1*r*,4*r*)-4-Aminocyclohexanol **26** (3.99 g, 34.7 mmol) was added and stirring at room temperature continued. After 30 min CH_2Cl_2 (100 mL) was added to aid stirring the thick suspension formed. After overall 1 h, the reaction mixture was diluted with 10% MeOH in CH_2Cl_2 (1500 mL) and washed successively with a 0.5N HCl aqueous solution (500 mL), a saturated NaHCO_3 aqueous solution (1000 mL) and brine (1000 mL) then was dried over MgSO_4 and concentrated *in vacuo*. Purification of the residue by flash chromatography on silica gel (340 g column, gradient 10-70% (3:1 EtOAc:EtOH) in cyclohexane) gave 4-acetamido-3-fluoro-N-((1*r*,4*S*)-4-hydroxycyclohexyl)-5-((*S*)-1-phenylethoxy)benzamide **27** (12.2 g, 89%) as a cream solid.

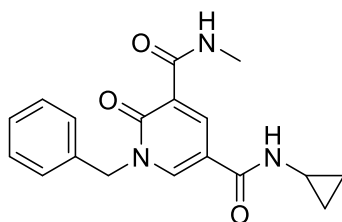
^1H NMR (400 MHz, DMSO-*d*₆) δ ppm 9.28 (br s, 1H), 7.46-7.41 (m, 2H), 7.38-7.32 (m, 2H), 7.31 - 7.24 (m, 1H), 7.09 (dd, $J = 9.0, 1.6$ Hz, 1H), 6.99-6.91 (m, 1H), 5.59 (q, $J = 6.2$ Hz, 1H), 2.08 (br s, 3H), 1.52 (d, $J = 6.2$ Hz, 3H).

^{13}C NMR (101 MHz, DMSO-*d*₆) δ ppm 168.69 (br s, 1C), 158.66 (d, $J = 249.4$ Hz, 1C), 155.11 (br d, $J = 5.9$ Hz, 1C), 142.57 (s, 1C), 128.99 (s, 2C), 128.12 (s, 1C), 126.08 (s, 2C), 119.06 (br d,

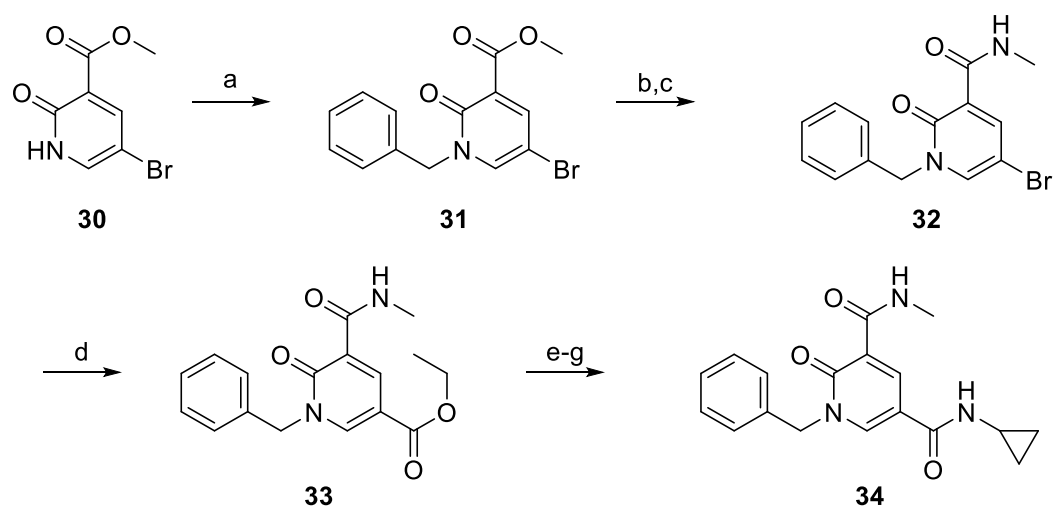
$J = 12.5$ Hz, 1C), 115.78 (br d, $J = 15.4$ Hz, 1C), 114.17 (s, 1C), 111.82 (br d, $J = 24.2$ Hz, 1C), 76.68 (s, 1C), 24.35 (s, 1C), 22.98 (s, 1C).

LCMS (method high pH): Retention time 0.82 min, $[M+H]^+ = 413.3$

GSK620



Synthesis:



Reagents and conditions: (a) NaH, BnBr, DMF/THF, 0°C, 89%; (b) LiOH, H₂O/THF/MeOH, room temperature, 78%; (c) (i) (COCl)₂, DMF, CH₂Cl₂, room temperature, (ii) NEt₃, MeNH₂, THF, 0°C, 95%; (d) NEt₃, Pd(OAc)₂, dppb, CO (50 PSI), DMSO/EtOH, 100°C, 94%; (e) NaOH/MeOH/H₂O, room temperature, 80%; (f) HATU, NEt₃, NHcPr, CH₂Cl₂, room temperature 84%; (g) EtOH, Pd scavenger, reflux, 66%.

Methyl 1-benzyl-5-bromo-2-oxo-1,2-dihydropyridine-3-carboxylate (31). Sodium hydride (5.17 g, 60% dispersion in mineral oil, 129 mmol) was added to a solution of methyl 5-bromo-2-oxo-1,2-dihydro-3-pyridinecarboxylate (**30**, 25 g, 108 mmol) in DMF (200 mL) and THF (200 mL) at 0 °C and the mixture was stirred for 30 min, giving a dense suspension. Benzyl bromide (14.10 mL, 119 mmol) was added and the mixture stirred for a further 2 h, allowing to warm to rt, then the resulting clear brown solution was added to water (400 mL) and extracted with EtOAc (2 x 300 mL). The combined organics were washed with water (2 x 200 mL), dried and evaporated *in vacuo* to give methyl 1-benzyl-5-bromo-2-oxo-1,2-dihydropyridine-3-carboxylate (**31**, 31 g, 96 mmol, 89% yield) as a beige solid. This material was carried through to the next step without purification.

LCMS (2 min High pH): Rt = 0.98 min, [MH]⁺ = 322.0 & 324.1.

¹H NMR (400 MHz, CHCl₃-*d*) δ ppm 8.16 (d, J=2.9 Hz, 1 H) 7.62 (d, J=2.9 Hz, 1 H) 7.30 - 7.43 (m, 5 H) 5.15 (s, 2 H) 3.92 (s, 3 H).

1-Benzyl-5-bromo-2-oxo-1,2-dihydropyridine-3-carboxylic acid. Lithium hydroxide (6.91 g, 289 mmol) in water (200 mL) was added to a mixture of methyl 1-benzyl-5-bromo-2-oxo-1,2-dihydropyridine-3-carboxylate (**31**, 31 g, 96 mmol), THF (200 mL) and methanol (200 mL) and the mixture was stirred at rt for 2 h, then evaporated *in vacuo* to about half volume, giving a dense suspension. This was diluted with water (200 mL) and acidified with acetic acid to pH 5, then extracted with EtOAc (2 x 300 mL). The combined organics were dried over sodium sulphate and evaporated *in vacuo* to give an off-white solid. The product was suspended in ether (200 mL), sonicated, diluted with cyclohexane (100 mL) and collected by filtration to give 1-benzyl-5-bromo-2-oxo-1,2-dihydropyridine-3-carboxylic acid (23 g, 74.6 mmol, 78% yield).

LCMS (2 min Formic): Rt = 1.01 min, [MH]⁺ = 308.0 & 310.1.

¹H NMR (400 MHz, CHCl₃-*d*) δ ppm 14.02 (br. s., 1 H) 8.55 (d, J=2.7 Hz, 1 H) 7.73 (d, J=2.7 Hz, 1 H) 7.40 - 7.47 (m, 3 H) 7.31 - 7.37 (m, 2 H) 5.25 (s, 2 H).

1-Benzyl-5-bromo-N-methyl-2-oxo-1,2-dihydropyridine-3-carboxamide (32). 1-Benzyl-5-bromo-2-oxo-1,2-dihydropyridine-3-carboxylic acid (28 g, 91 mmol) was suspended in DCM (300 mL) and oxalyl chloride (23.86 mL, 273 mmol) and DMF (0.352 mL, 4.54 mmol) were added, then the mixture was stirred for 2 h at rt. The solvent was evaporated *in vacuo* to give a brown residue, which was then dissolved in THF (300 mL) and Et₃N (12.67 mL, 91 mmol) was added. The mixture was cooled in an ice bath, then methanamine (91 mL, 2M in THF, 182 mmol) was added dropwise over 30 min and the mixture stirred for a further 1 h at 0 °C. The solvent was evaporated *in vacuo* and the solid residue was partitioned between water (300 mL) and DCM (300 mL), the organic layer was washed with brine, dried and evaporated *in vacuo* to give 1-benzyl-5-bromo-N-methyl-2-oxo-1,2-dihydropyridine-3-carboxamide (**32**, 27.6 g, 86 mmol, 95% yield) as a brown solid.

LCMS (2 min Formic): Rt = 0.97 min, [MH]⁺ = 321.0 & 323.1.

¹H NMR (400 MHz, CHCl₃-*d*) δ ppm 9.57 (br. s., 1 H) 8.60 (d, J=2.9 Hz, 1 H) 7.62 (d, J=2.9 Hz, 1 H) 7.34 - 7.48 (m, 3 H) 7.29 - 7.33 (m, 2 H) 5.20 (s, 2 H) 3.00 (d, J=4.9 Hz, 3 H).

Ethyl 1-benzyl-5-(methylcarbamoyl)-6-oxo-1,6-dihydropyridine-3-carboxylate (33). 1-Benzyl-5-bromo-N-methyl-2-oxo-1,2-dihydropyridine-3-carboxamide (**32**, 23 g, 71.6 mmol), DMSO (60 mL), ethanol (70 g, 1519 mmol), Et₃N (19.96 mL, 143 mmol), dppb (3.05 g, 7.16 mmol) and palladium acetate (1.608 g, 7.16 mmol) were placed in a steel Parr vessel, which was then purged with carbon monoxide by filling to 50 psi, then releasing the pressure, then refilled to 50 psi and heated overnight at 100 °C. The mixture was diluted with water (200 mL) and extracted with EtOAc (2 x 300 mL), the organic layer washed with water (2 x 300 mL), then dried and

evaporated *in vacuo* and the residue was triturated with ether (200 mL) and the solid collected by filtration to give ethyl 1-benzyl-5-(methylcarbamoyl)-6-oxo-1,6-dihydropyridine-3-carboxylate (**33**, 21.2 g, 67.4 mmol, 94% yield).

LCMS (2 min Formic): Rt = 0.99 min, [MH]⁺ = 315.2.

¹H NMR (400 MHz, CHCl₃-*d*) δ ppm 9.37 (br. s., 1 H) 9.03 (d, *J*=2.4 Hz, 1 H) 8.38 (d, *J*=2.7 Hz, 1 H) 7.34 - 7.42 (m, 3 H) 7.28 - 7.34 (m, 2 H) 5.25 (s, 2 H) 4.35 (q, *J*=7.1 Hz, 2 H) 2.99 (d, *J*=4.9 Hz, 3 H) 1.37 (t, *J*=7.2 Hz, 3 H).

1-Benzyl-5-(methylcarbamoyl)-6-oxo-1,6-dihydropyridine-3-carboxylic acid. Sodium hydroxide (99 mL, 199 mmol, 2M aq.) was added to a solution of ethyl 1-benzyl-5-(methylcarbamoyl)-6-oxo-1,6-dihydropyridine-3-carboxylate (**33**, 20.8 g, 66.2 mmol) in a mixture of methanol (100 mL) and THF (100 mL) and the resulting solution was stirred for 2 h at rt, then evaporated *in vacuo* to approximately 100 mL volume. The mixture was diluted with water (200 mL), then filtered to remove a dark grey solid, the filtrate was washed with MTBE (200 mL), then acidified to pH 4 with 2M HCl and the resulting suspension stirred for 2 h, then filtered and the product washed with water, then dried in the vacuum oven to give 1-benzyl-5-(methylcarbamoyl)-6-oxo-1,6-dihydropyridine-3-carboxylic acid (15.2 g, 53.1 mmol, 80% yield).

LCMS (2 min High pH): Rt = 0.58 min, [MH]⁺ = 287.2.

¹H NMR (400 MHz, DMSO-*d*₆) δ ppm 13.19 (br. s., 1 H) 9.14 - 9.34 (m, 1 H) 8.88 (d, *J*=2.7 Hz, 1 H) 8.70 (d, *J*=2.7 Hz, 1 H) 7.25 - 7.42 (m, 5 H) 5.33 (s, 2 H) 2.82 (d, *J*=4.6 Hz, 3 H).

¹³C NMR (151 MHz, DMSO-*d*₆) δ ppm 165.2, 163.3, 161.9, 147.0, 142.4, 136.6, 129.1 (2C), 128.3, 128.3 (2C), 120.1, 110.8, 53.2, 26.4.

1-Benzyl-*N*⁵-cyclopropyl-*N*³-methyl-2-oxo-1,2-dihydropyridine-3,5-dicarboxamide (34**).** 1-Benzyl-5-(methylcarbamoyl)-6-oxo-1,6-dihydropyridine-3-carboxylic acid (5.5 g, 19.21 mmol)

was suspended in DCM (100 mL) and Et₃N (3.21 mL, 23.05 mmol), HATU (9.50 g, 24.98 mmol) and cyclopropylamine (1.625 mL, 23.05 mmol) were added, then the mixture was stirred for 2 h at rt. The mixture was washed with water (100 mL), 0.5 M HCl (100 mL) and saturated sodium bicarbonate solution (100 mL) and the organic layer was dried and evaporated *in vacuo* to give a pale yellow solid. The solid was suspended in ether (20 mL) and sonicated, then filtered and the solid dried in the vacuum oven to give 1-benzyl-*N*⁵-cyclopropyl-*N*³-methyl-2-oxo-1,2-dihydropyridine-3,5-dicarboxamide (5.25 g, 16.14 mmol, 84 % yield) as a colourless solid. The product was combined with another batch, prepared by a similar method (2.4 g), the combined material was dissolved by refluxing in ethanol (200 mL) for 20 min, then Silicycle thiourea palladium scavenging resin (10 g) was added and the mixture heated for a further 30 min. The mixture was filtered into a Buchner flask and allowed to cool to rt over 1 h, then cooled in an ice bath for 1 h and the resulting solid collected by filtration and dried in the vacuum oven to give 1-benzyl-*N*⁵-cyclopropyl-*N*³-methyl-2-oxo-1,2-dihydropyridine-3,5-dicarboxamide (**34**, 6.76 g, 20.78 mmol, 66% yield) as a colourless solid.

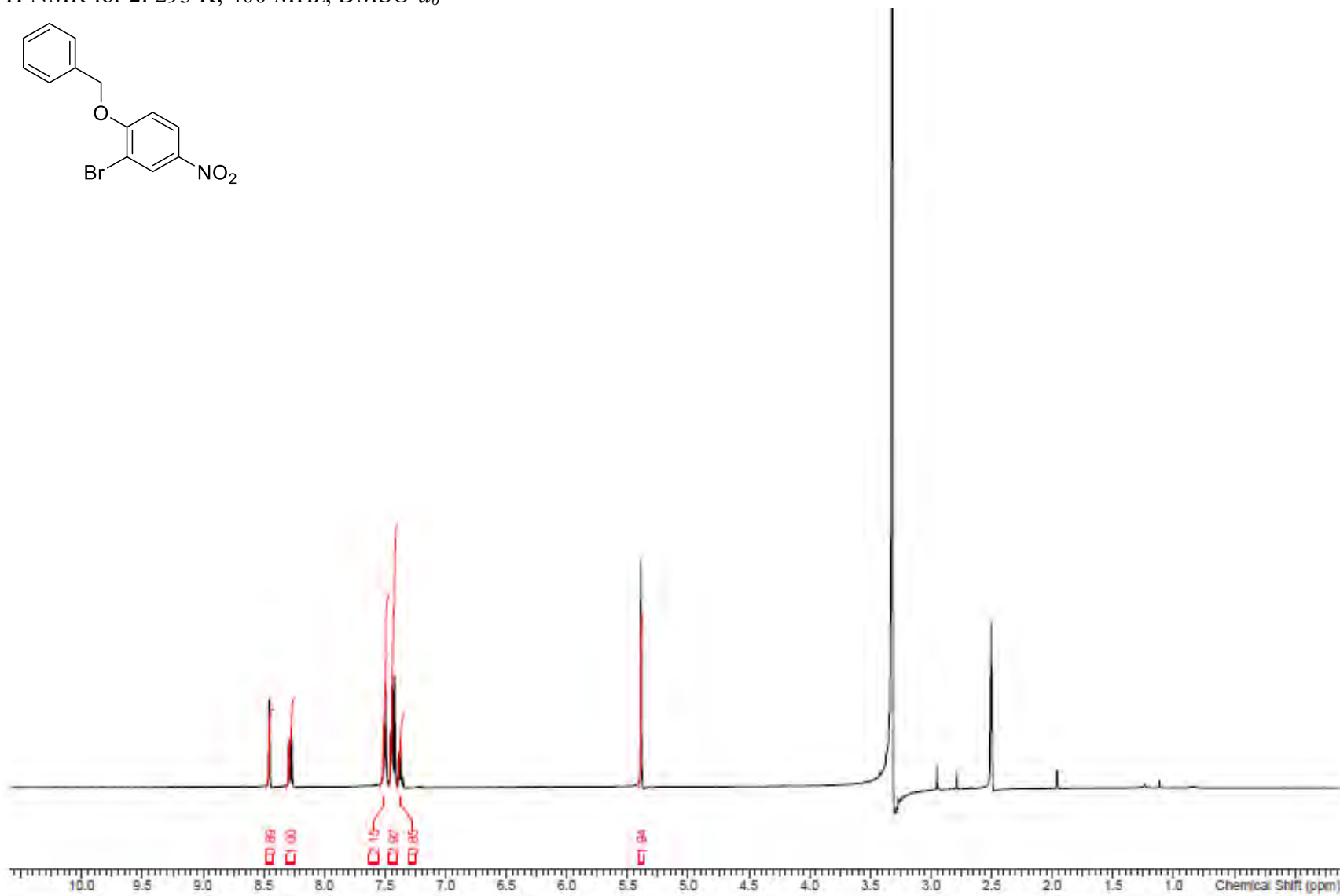
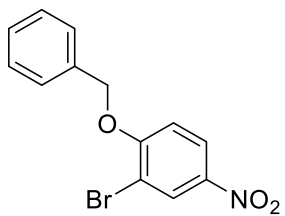
LCMS (2 min high pH): Rt = 0.84 min, [MH]⁺ = 326.

HRMS (C₁₈H₁₉N₃O₃): [M+H]⁺ calculated 326.1499, found 326.1499.

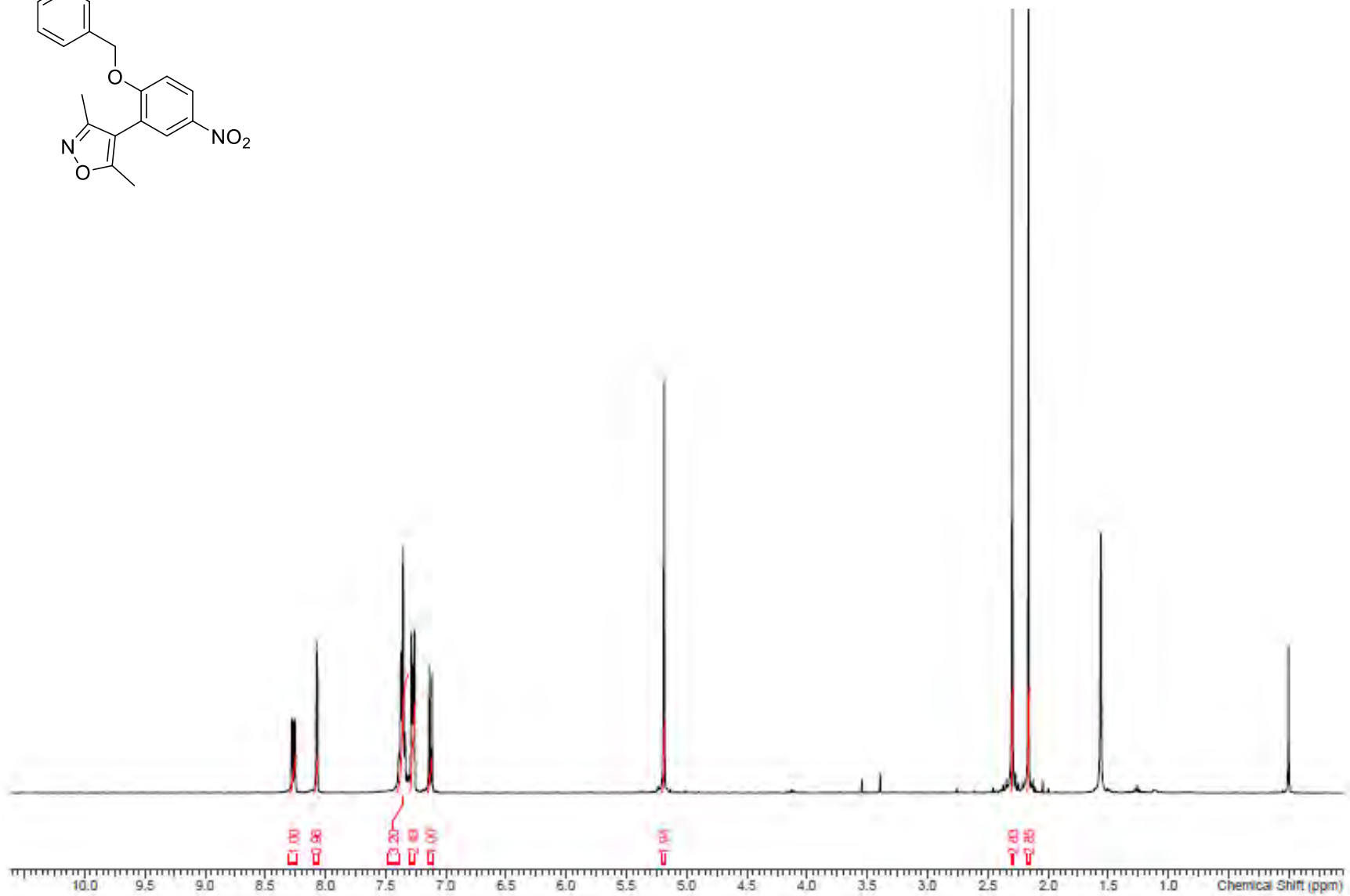
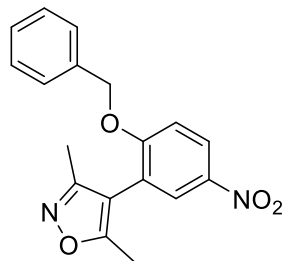
¹H NMR (400 MHz, DMSO-*d*₆) δ ppm 9.35 (d, *J*=4.9 Hz, 1 H) 8.80 (d, *J*=2.7 Hz, 1 H) 8.72 (d, *J*=2.7 Hz, 1 H) 8.54 (d, *J*=3.9 Hz, 1 H) 7.25 - 7.42 (m, 5 H) 5.29 (s, 2 H) 2.75 - 2.89 (m, 4 H) 0.65 - 0.72 (m, 2 H) 0.53 - 0.59 (m, 2 H).

¹³C NMR (151 MHz, DMSO-*d*₆) δ ppm 163.9, 163.1, 161.1, 144.0, 140.8, 136.2, 128.6 (2C), 127.7, 127.7 (2C), 119.3, 113.5, 52.8, 25.8, 22.9, 5.5 (2C).

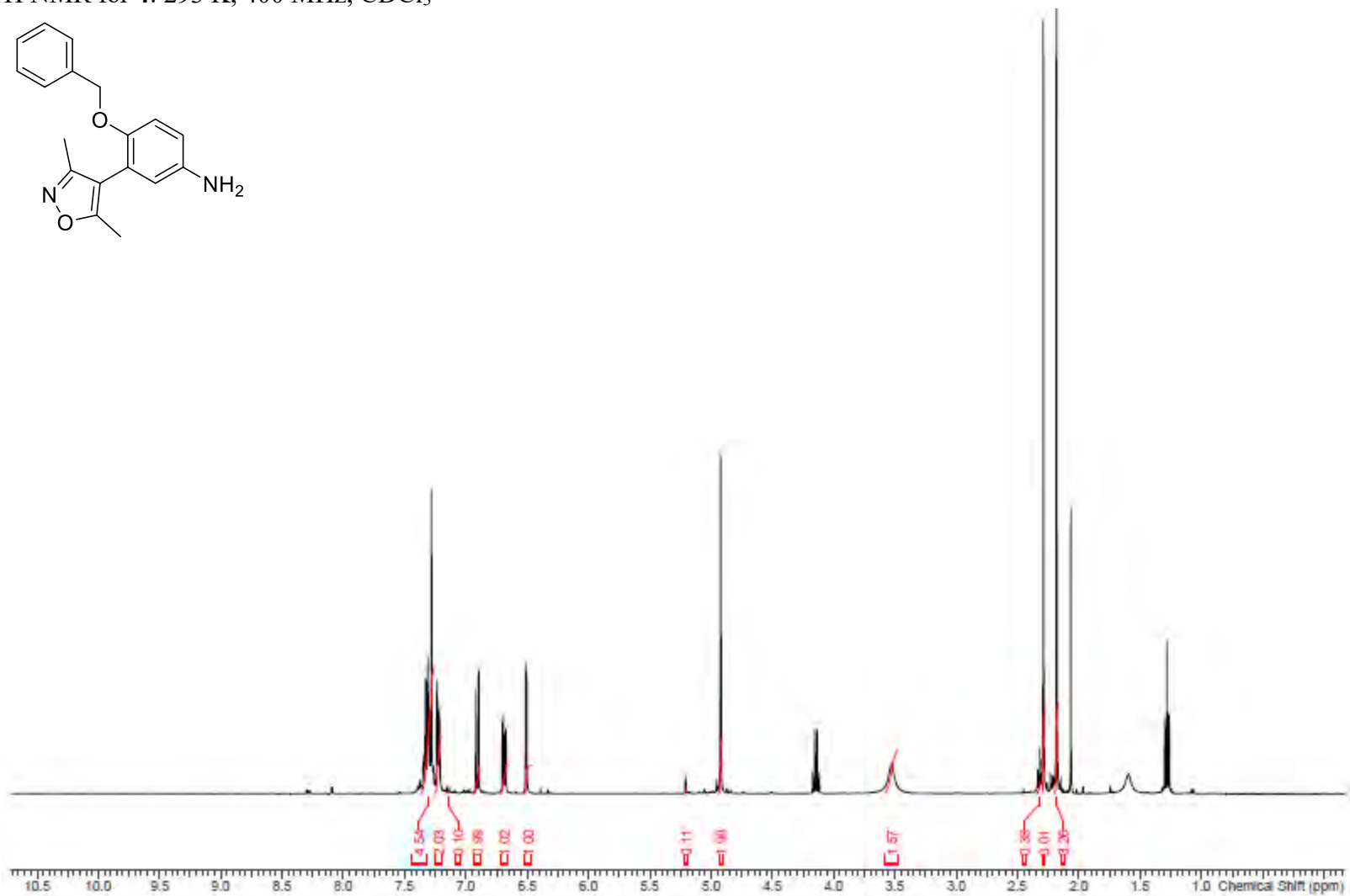
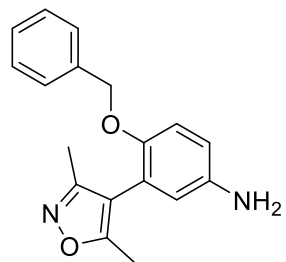
¹H NMR for **2**: 293 K, 400 MHz, DMSO-*d*₆



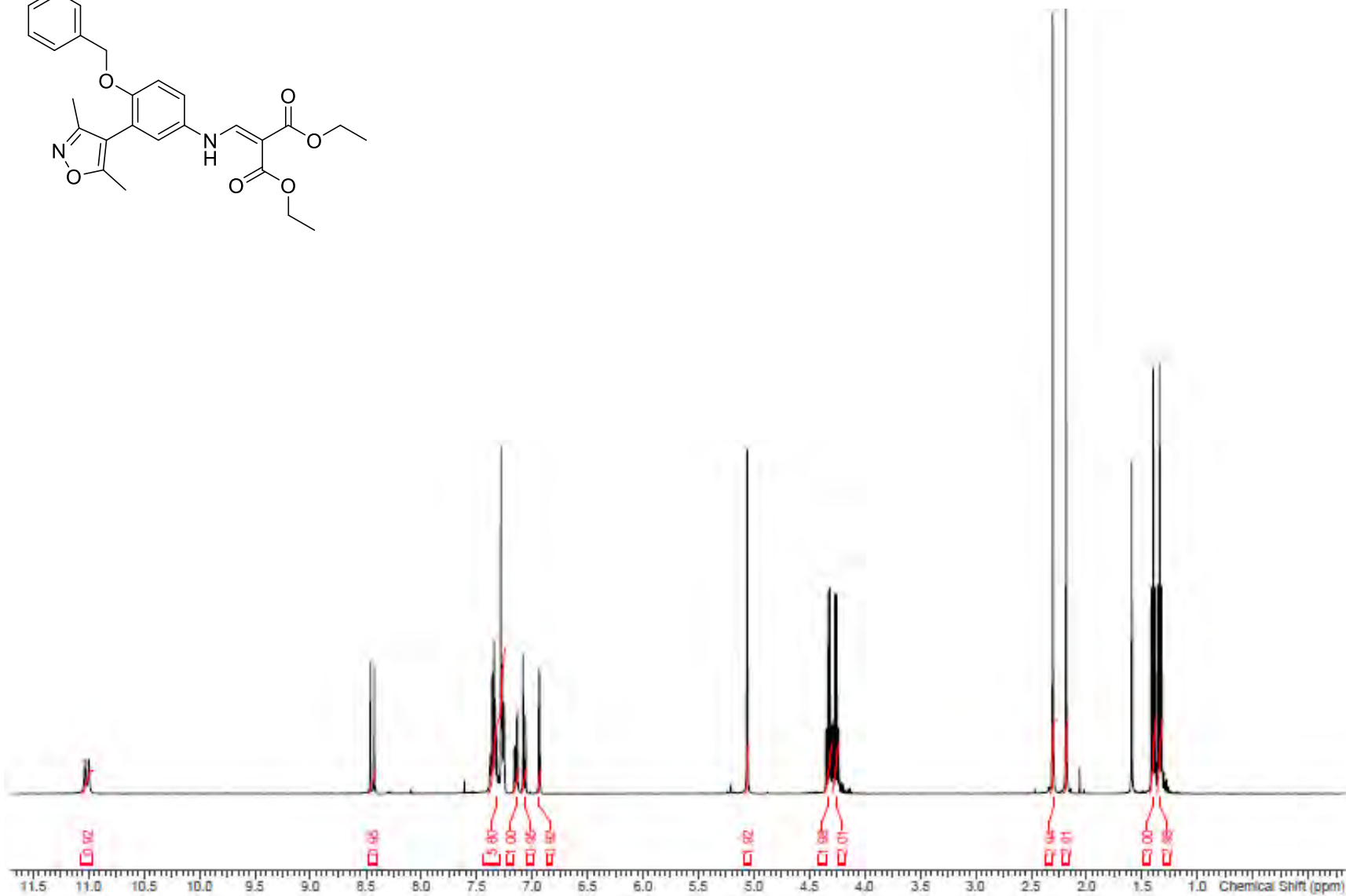
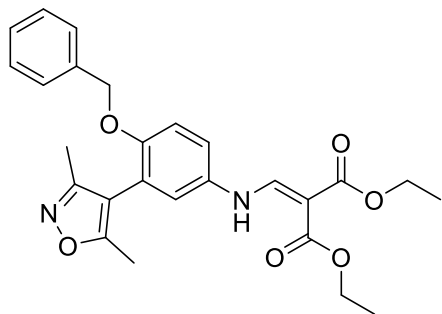
^1H NMR for **3**: 293 K, 400 MHz, CDCl_3



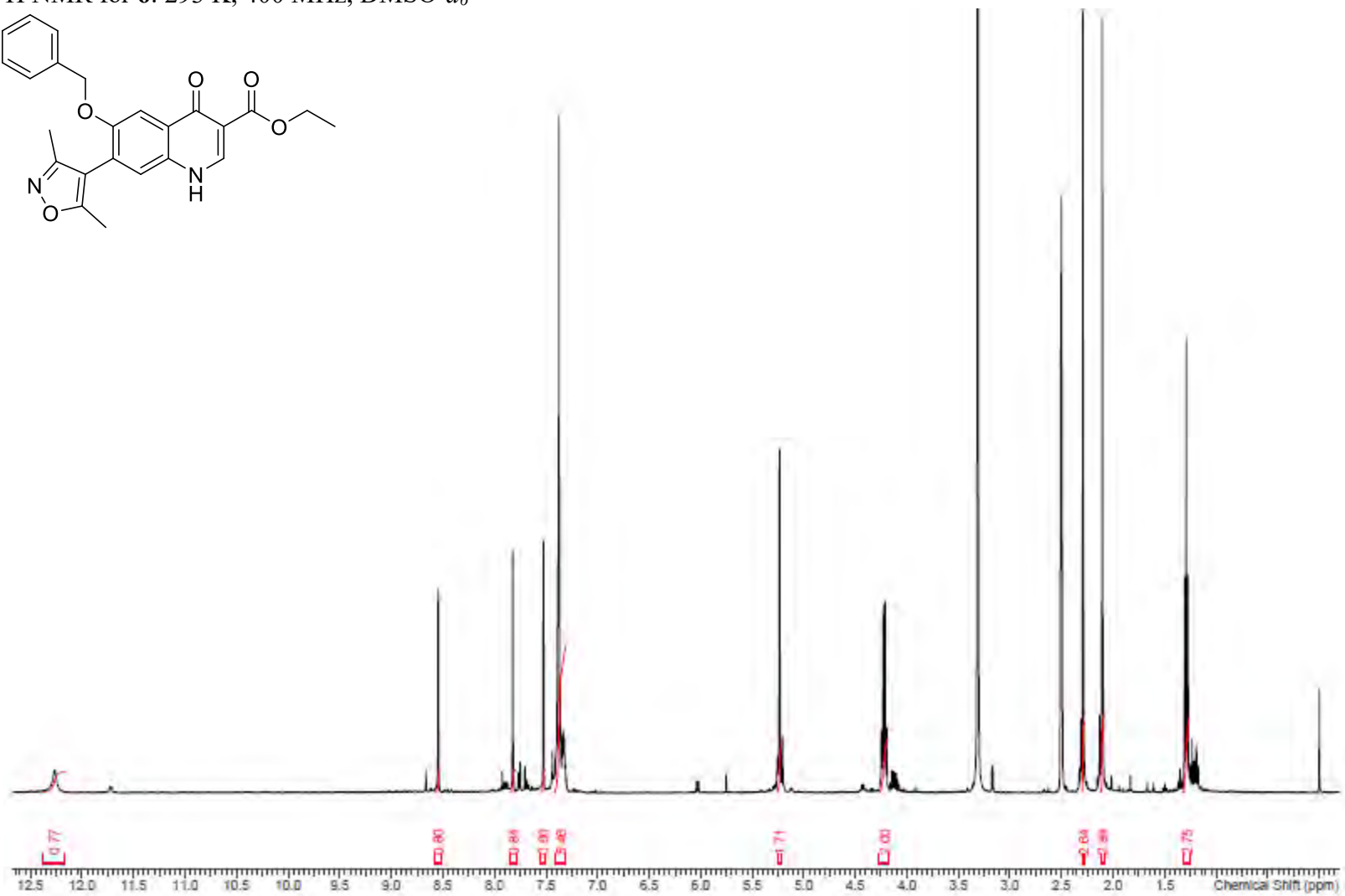
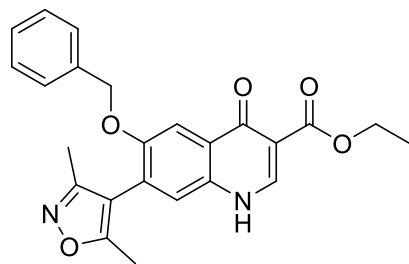
^1H NMR for **4**: 293 K, 400 MHz, CDCl_3



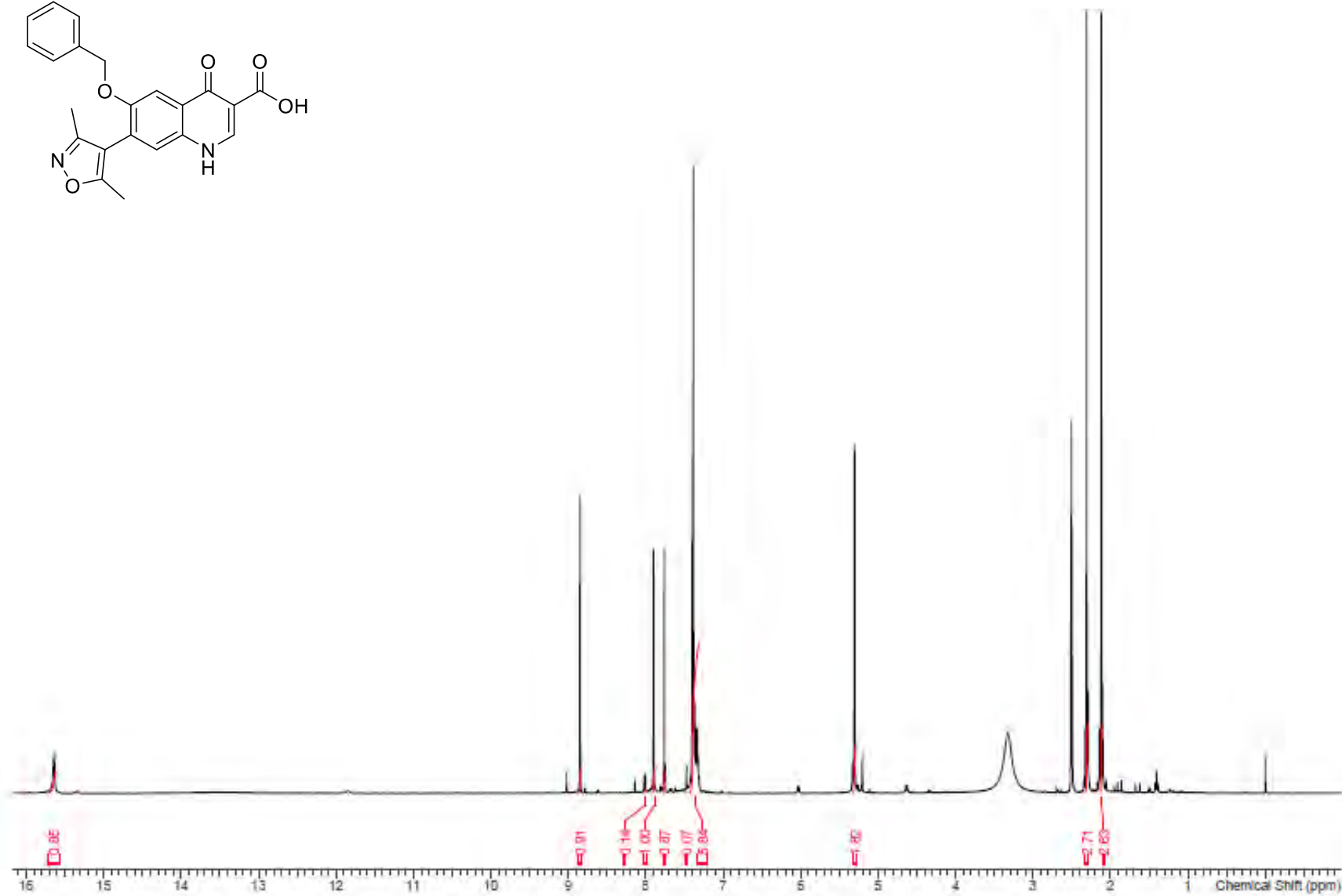
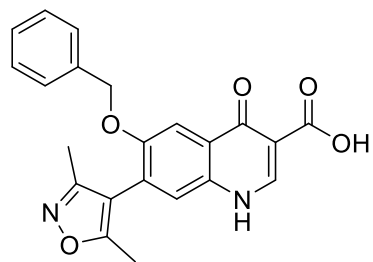
^1H NMR for **5**: 293 K, 400 MHz, CDCl_3



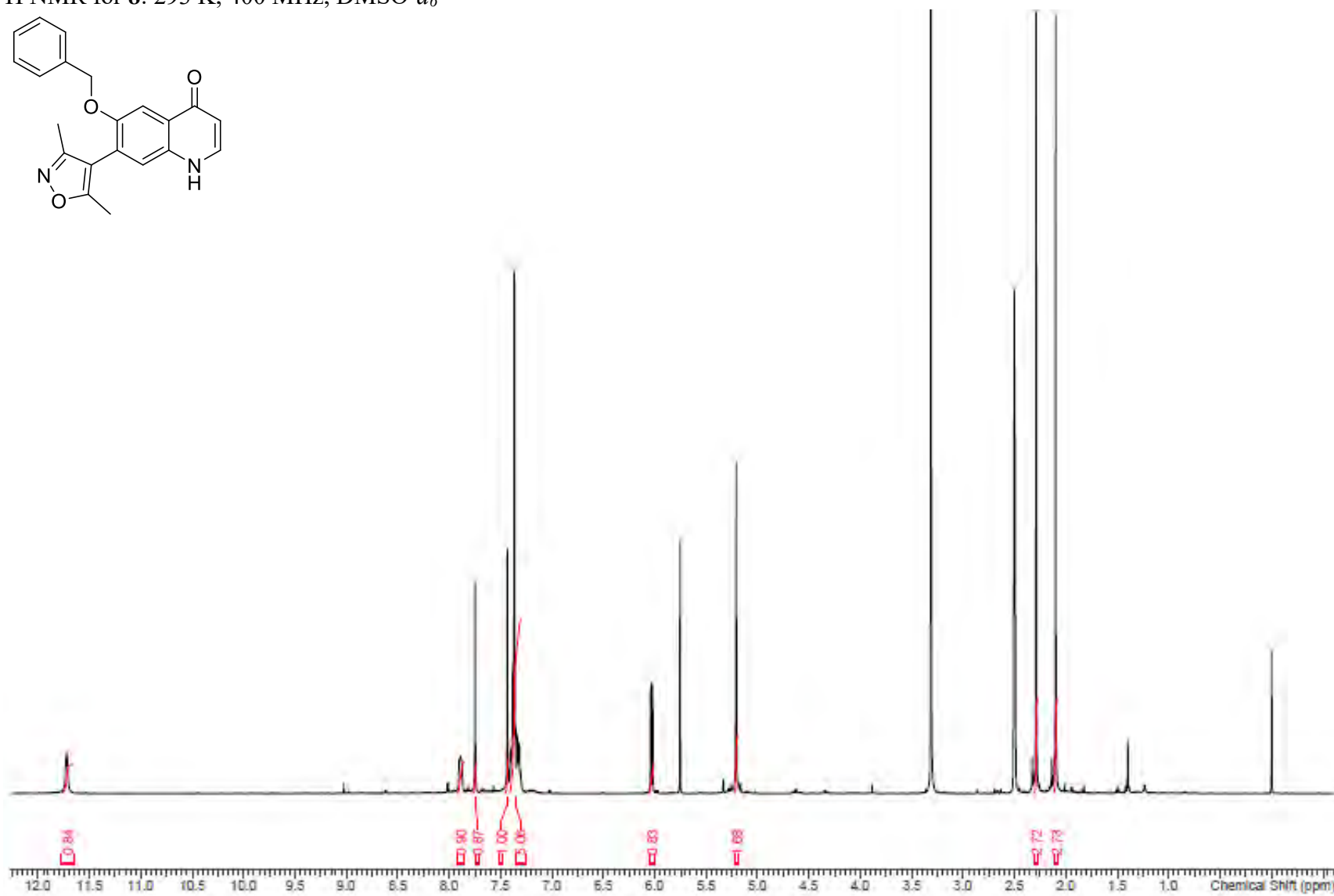
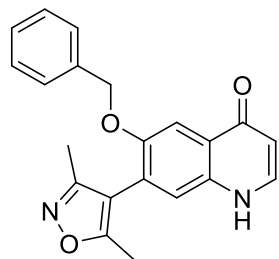
^1H NMR for **6**: 293 K, 400 MHz, $\text{DMSO-}d_6$



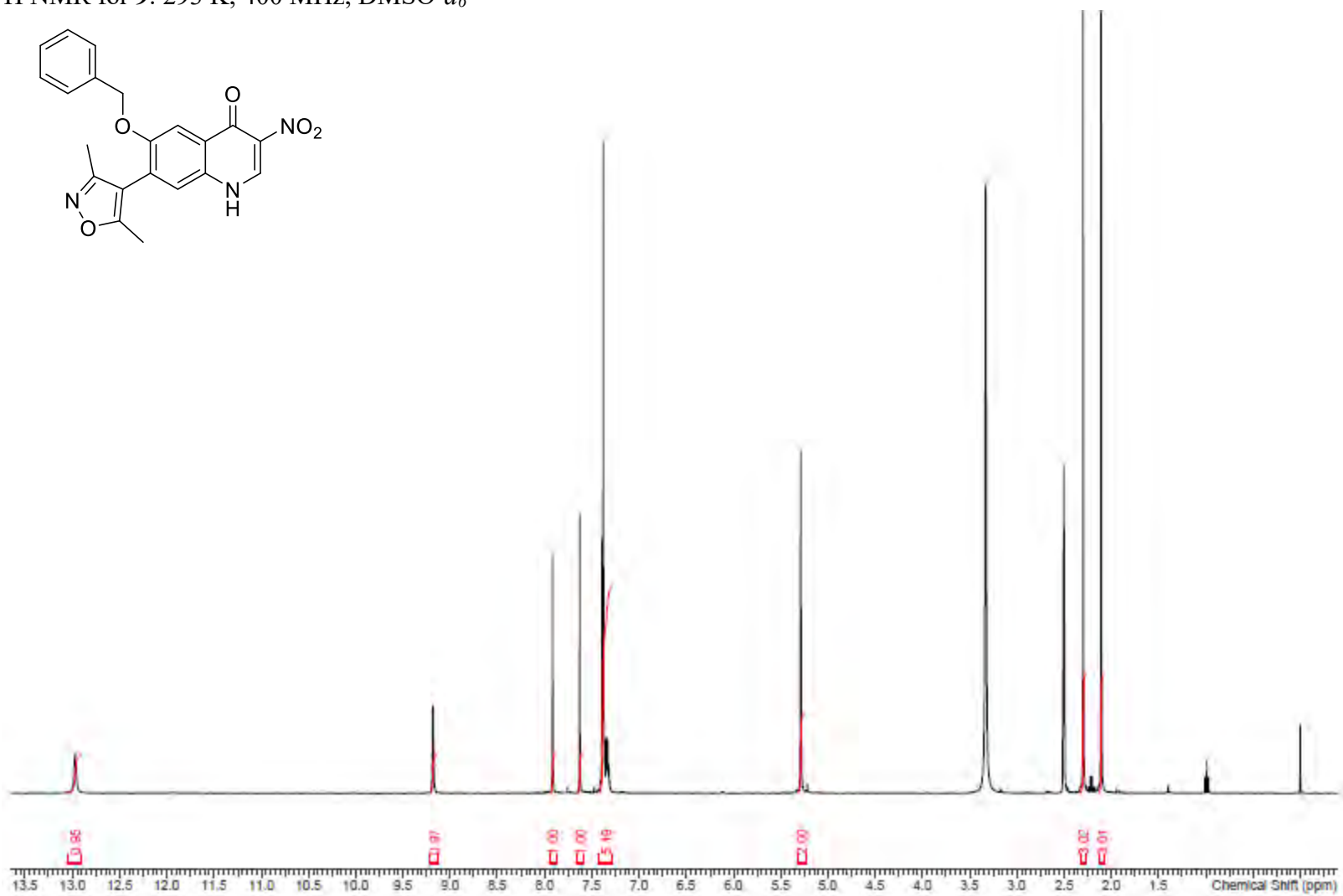
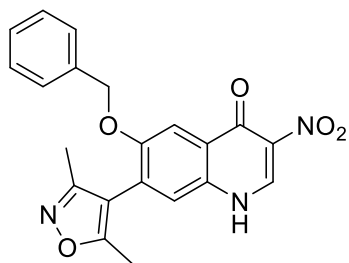
^1H NMR for 7: 293 K, 400 MHz, $\text{DMSO-}d_6$



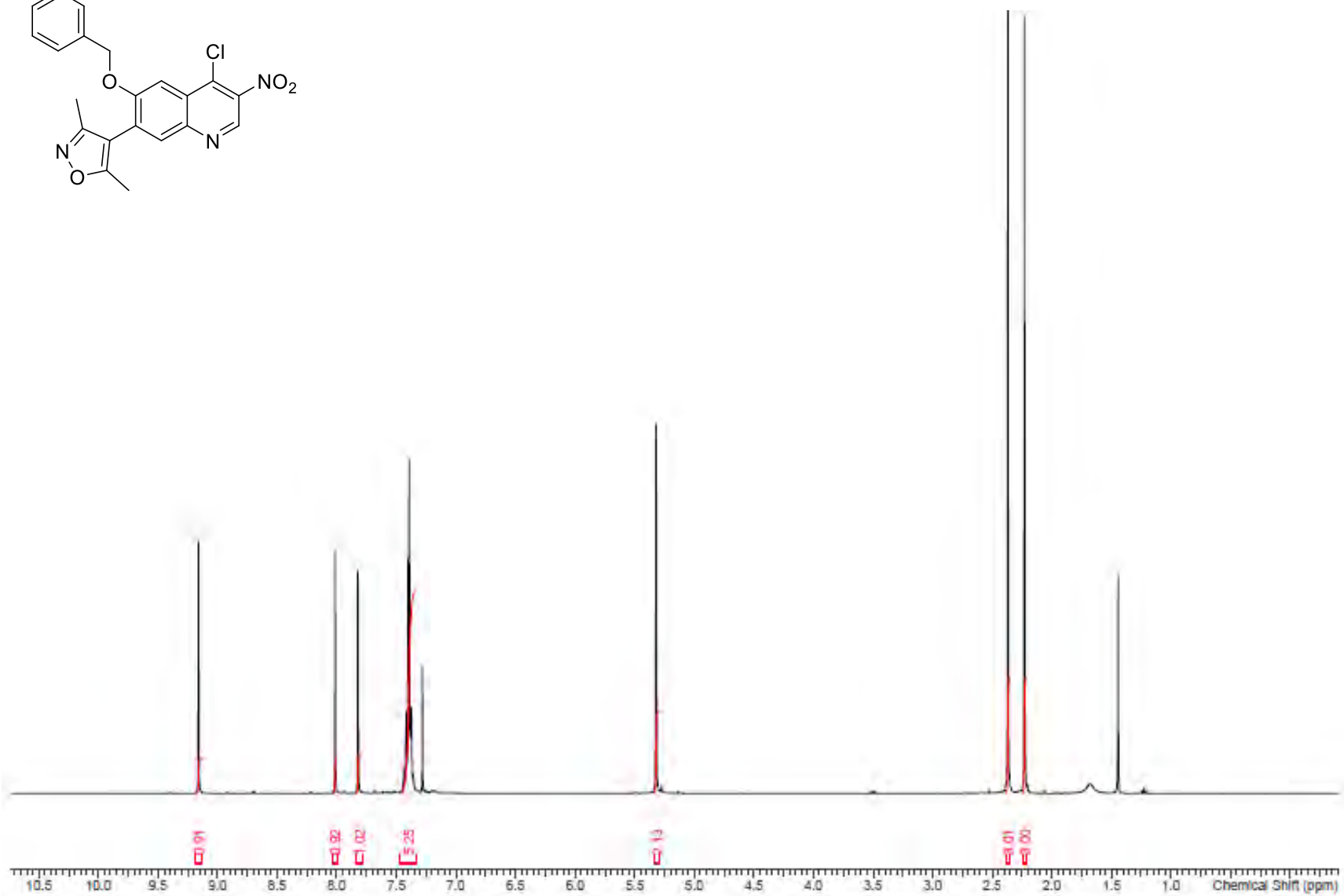
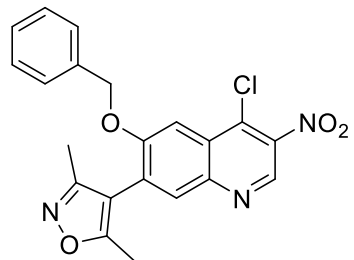
^1H NMR for **8**: 293 K, 400 MHz, $\text{DMSO-}d_6$



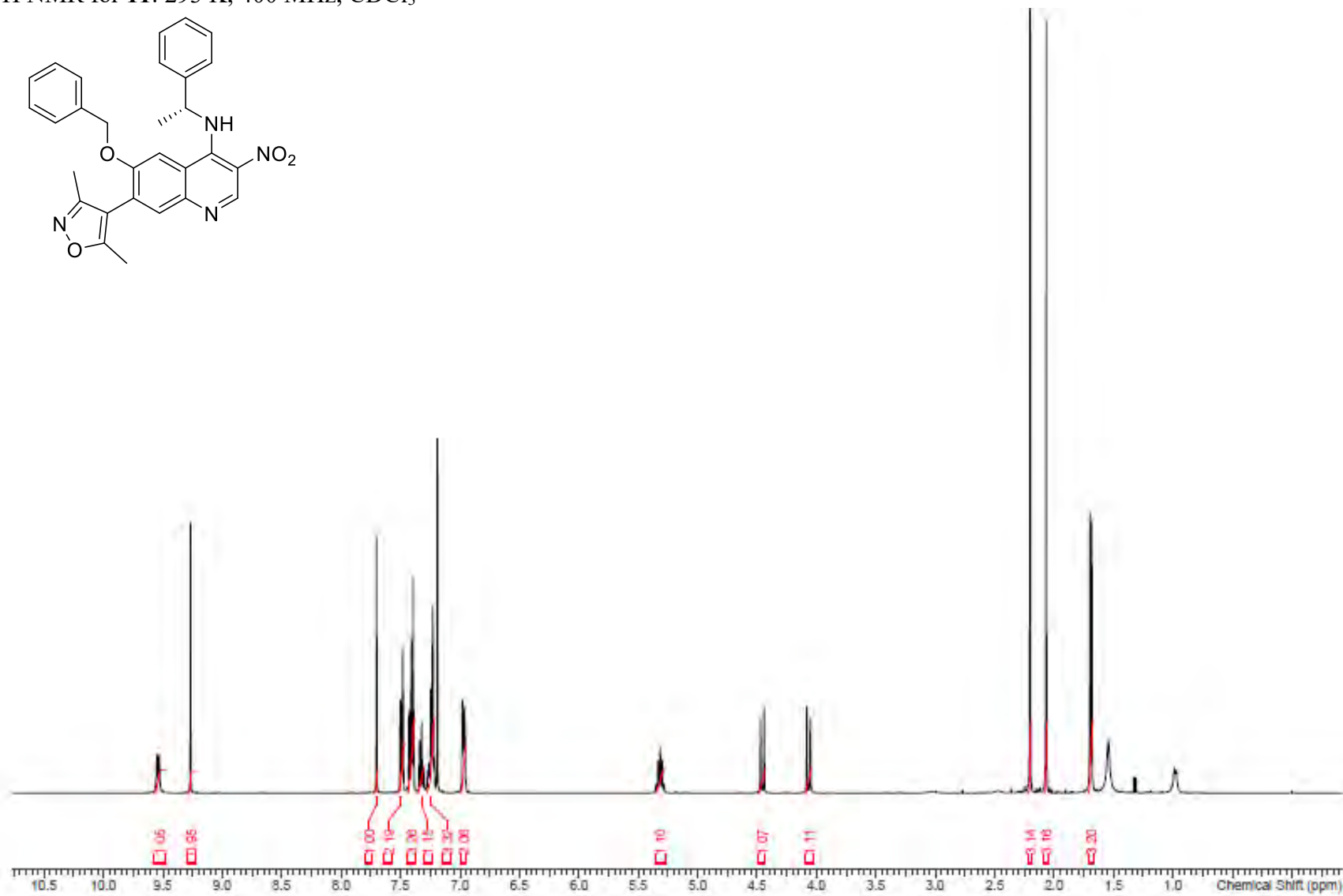
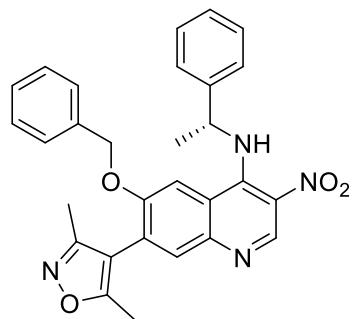
^1H NMR for **9**: 293 K, 400 MHz, $\text{DMSO-}d_6$



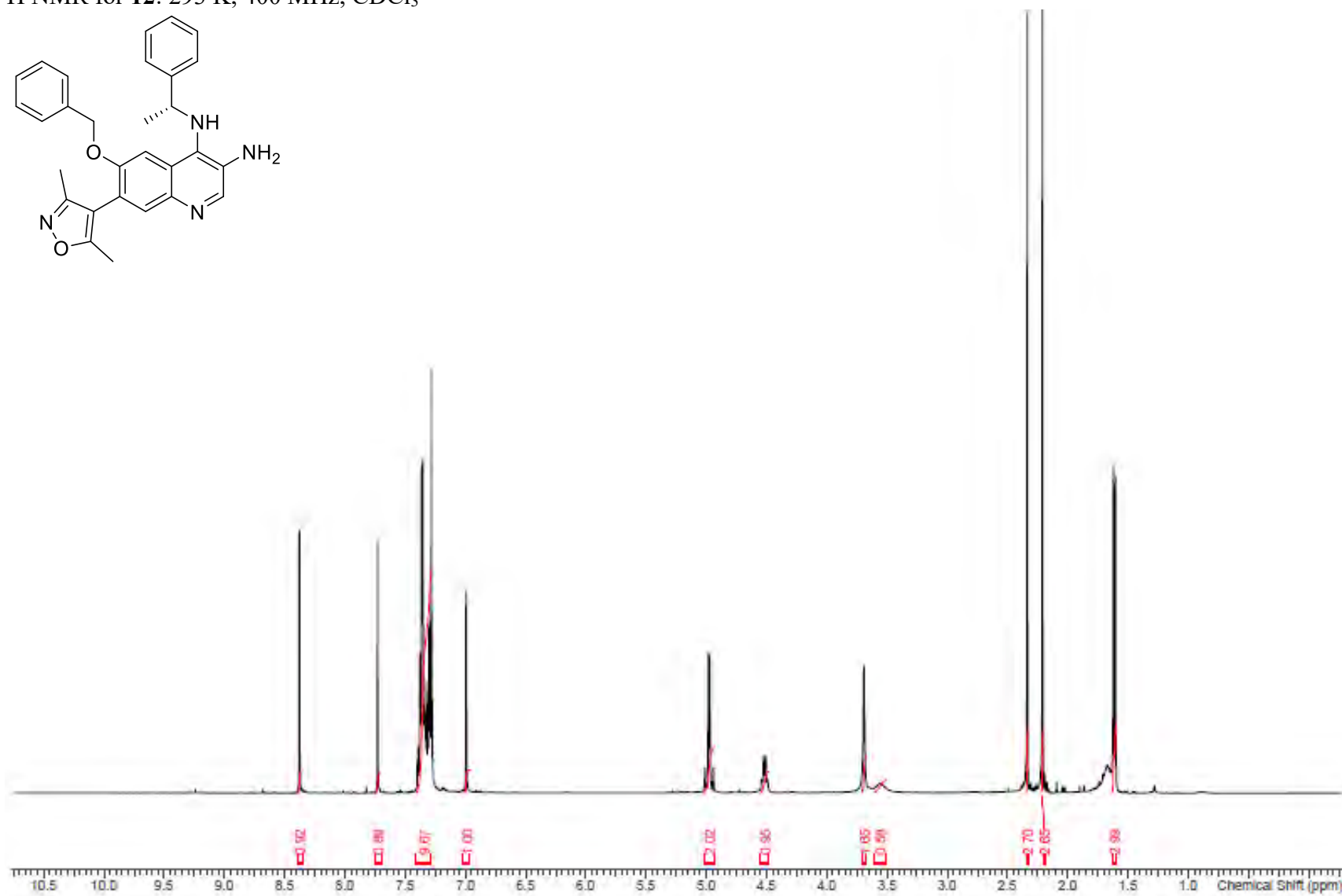
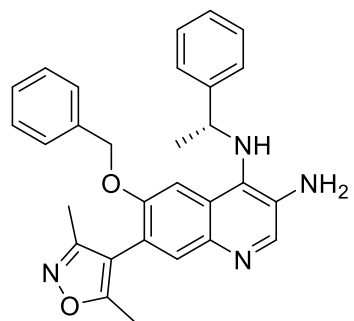
^1H NMR for **10**: 293 K, 400 MHz, CDCl_3



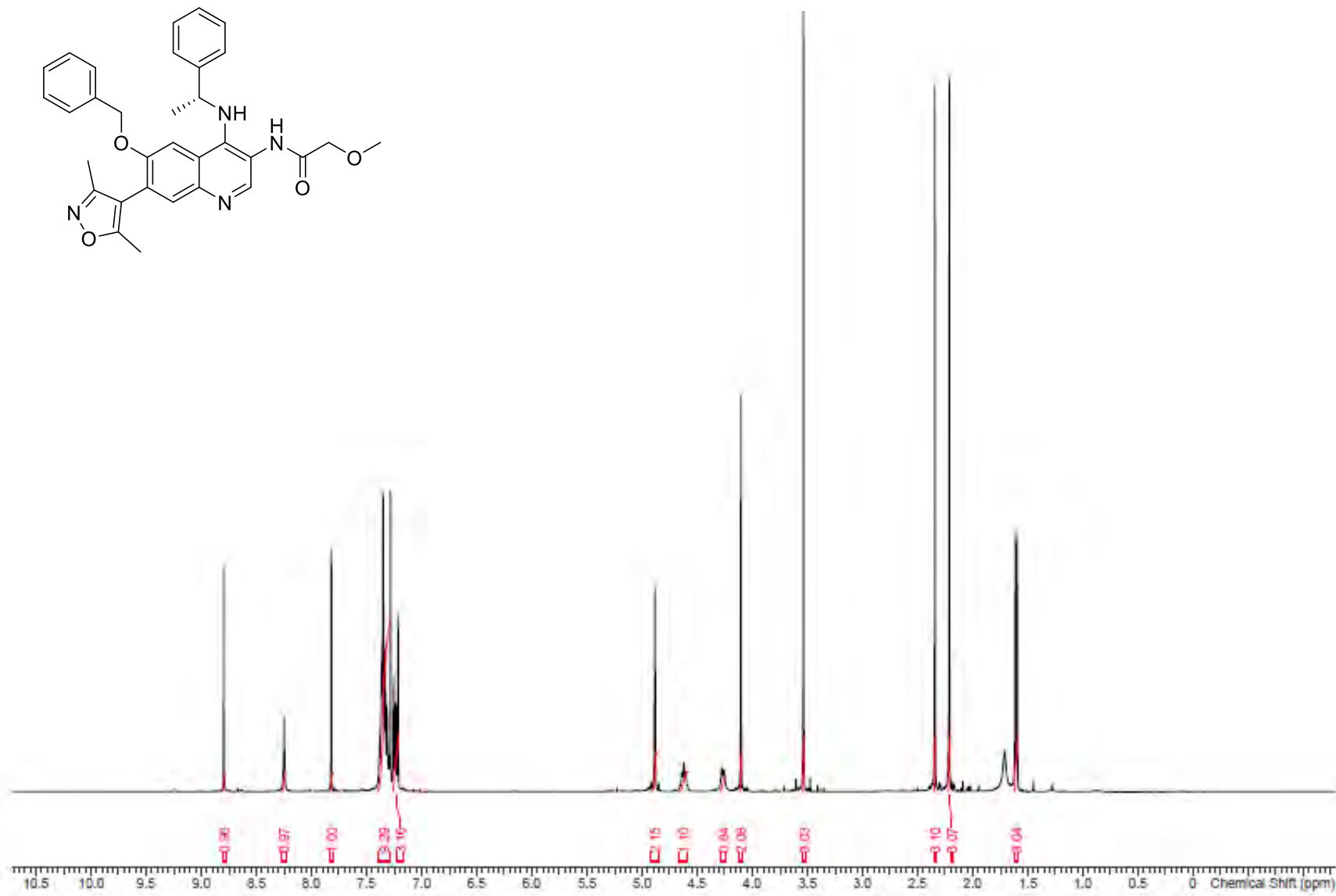
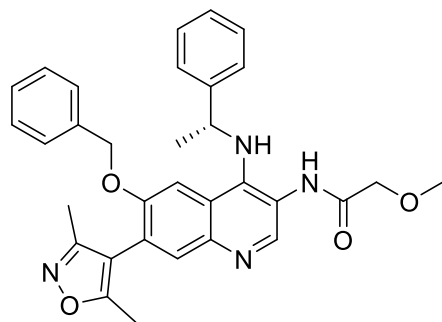
^1H NMR for **11**: 293 K, 400 MHz, CDCl_3



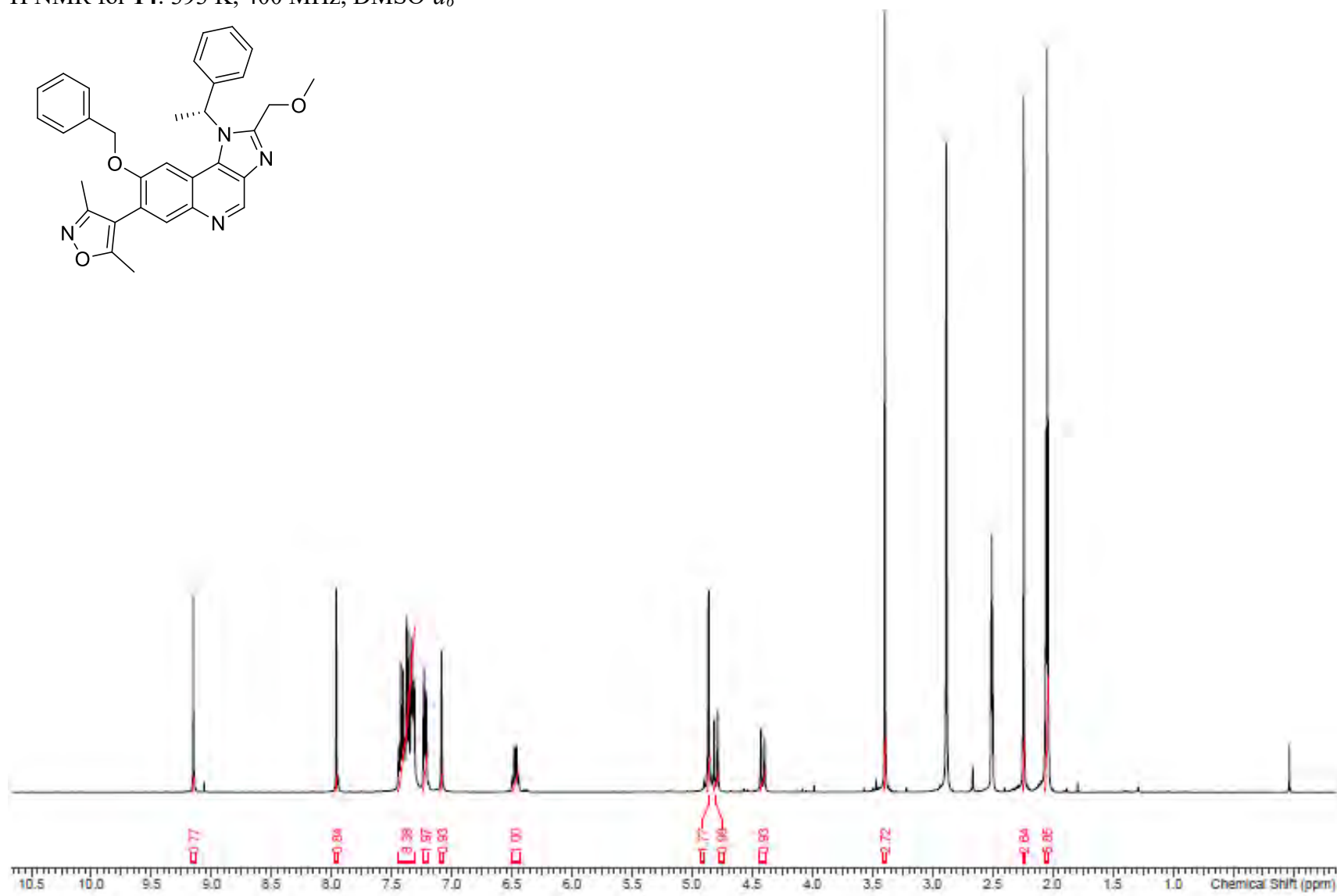
^1H NMR for **12**: 293 K, 400 MHz, CDCl_3



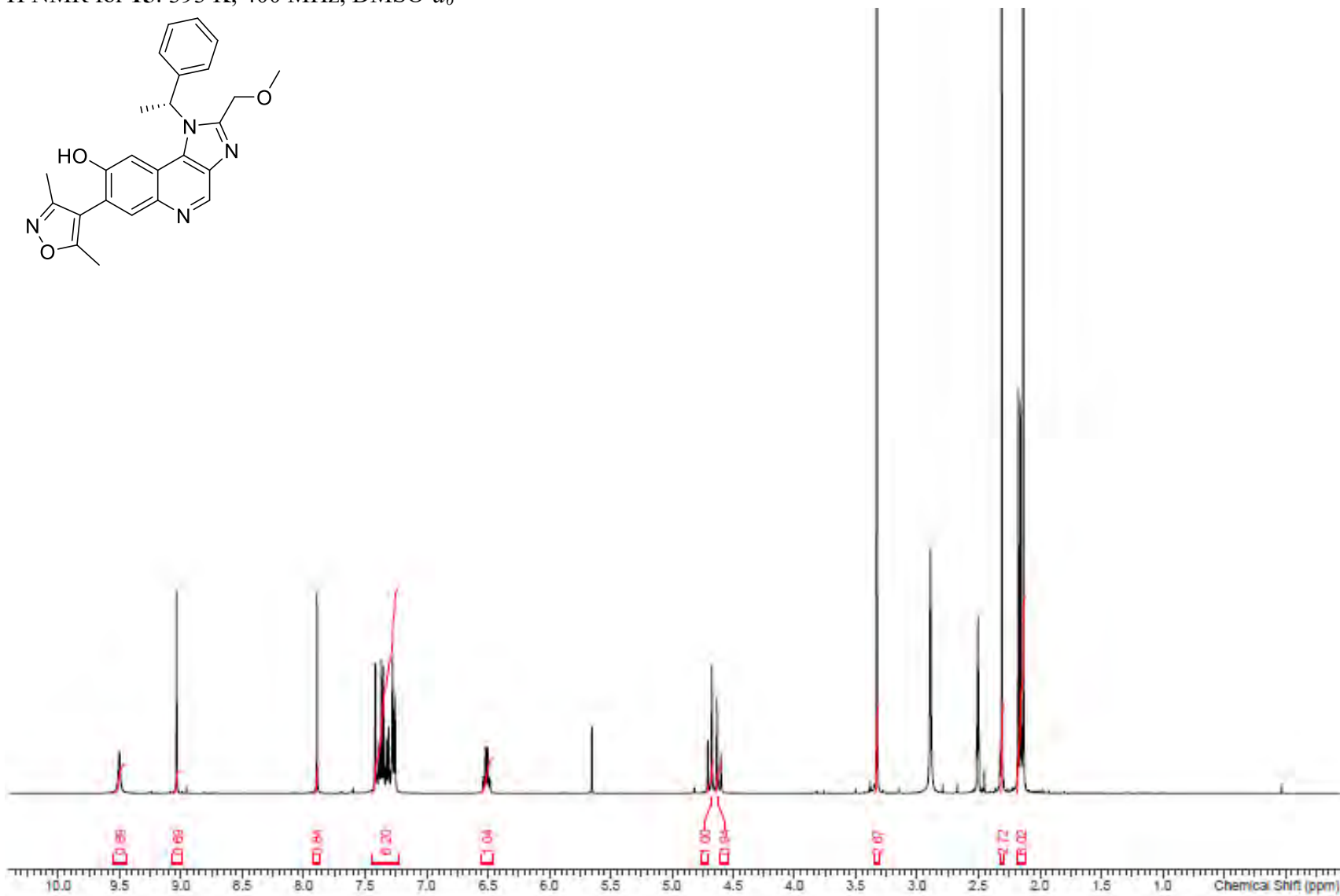
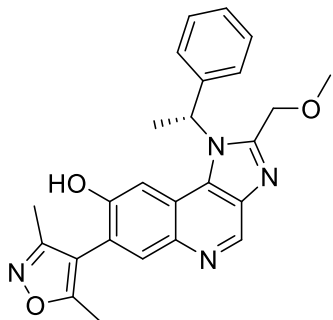
^1H NMR for **13**: 293 K, 400 MHz, CDCl_3



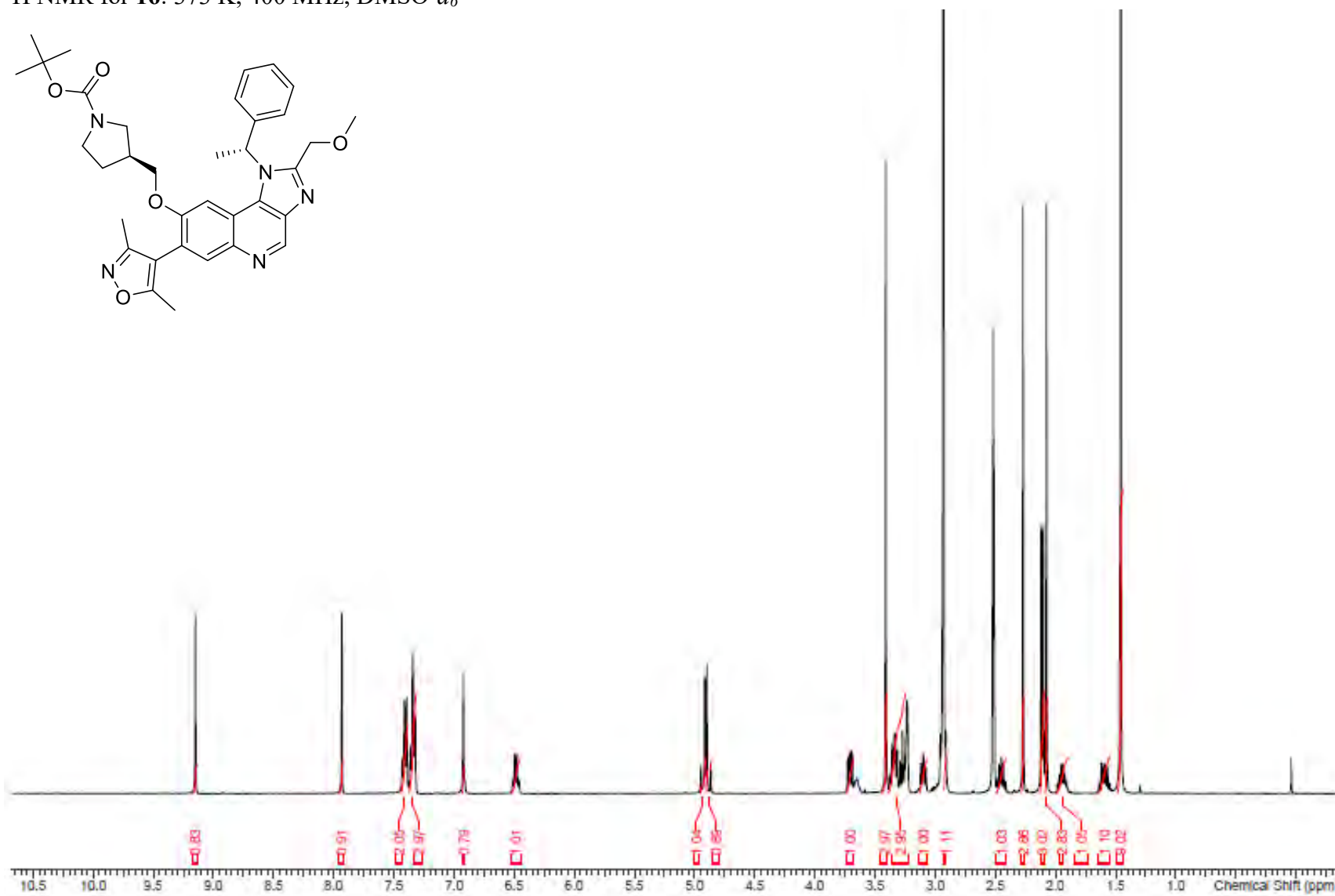
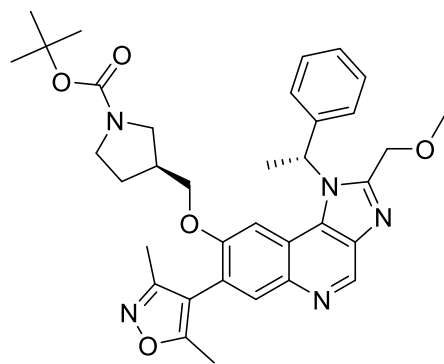
¹H NMR for **14**: 393 K, 400 MHz, DMSO-*d*₆



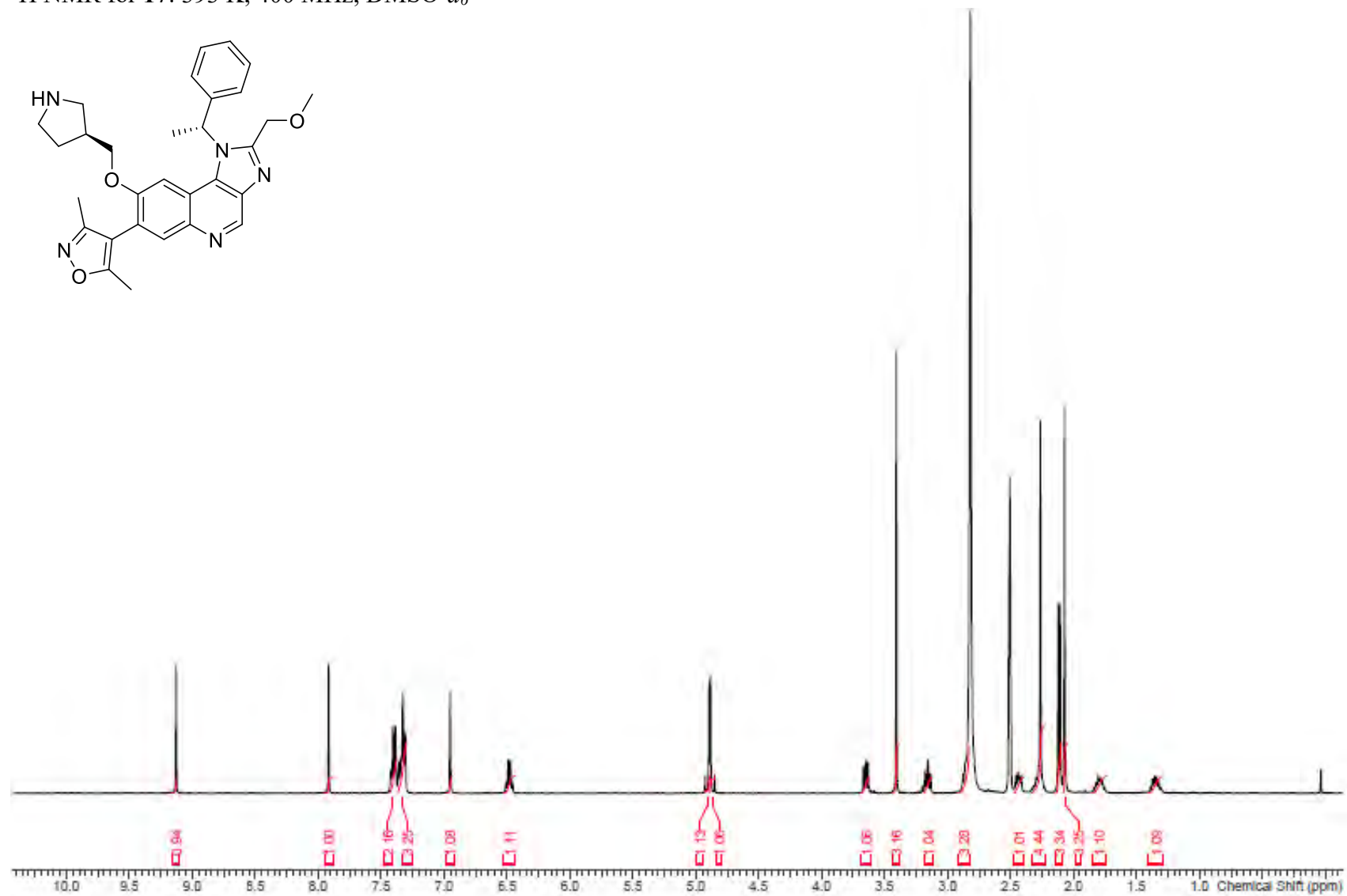
^1H NMR for **15**: 393 K, 400 MHz, $\text{DMSO-}d_6$



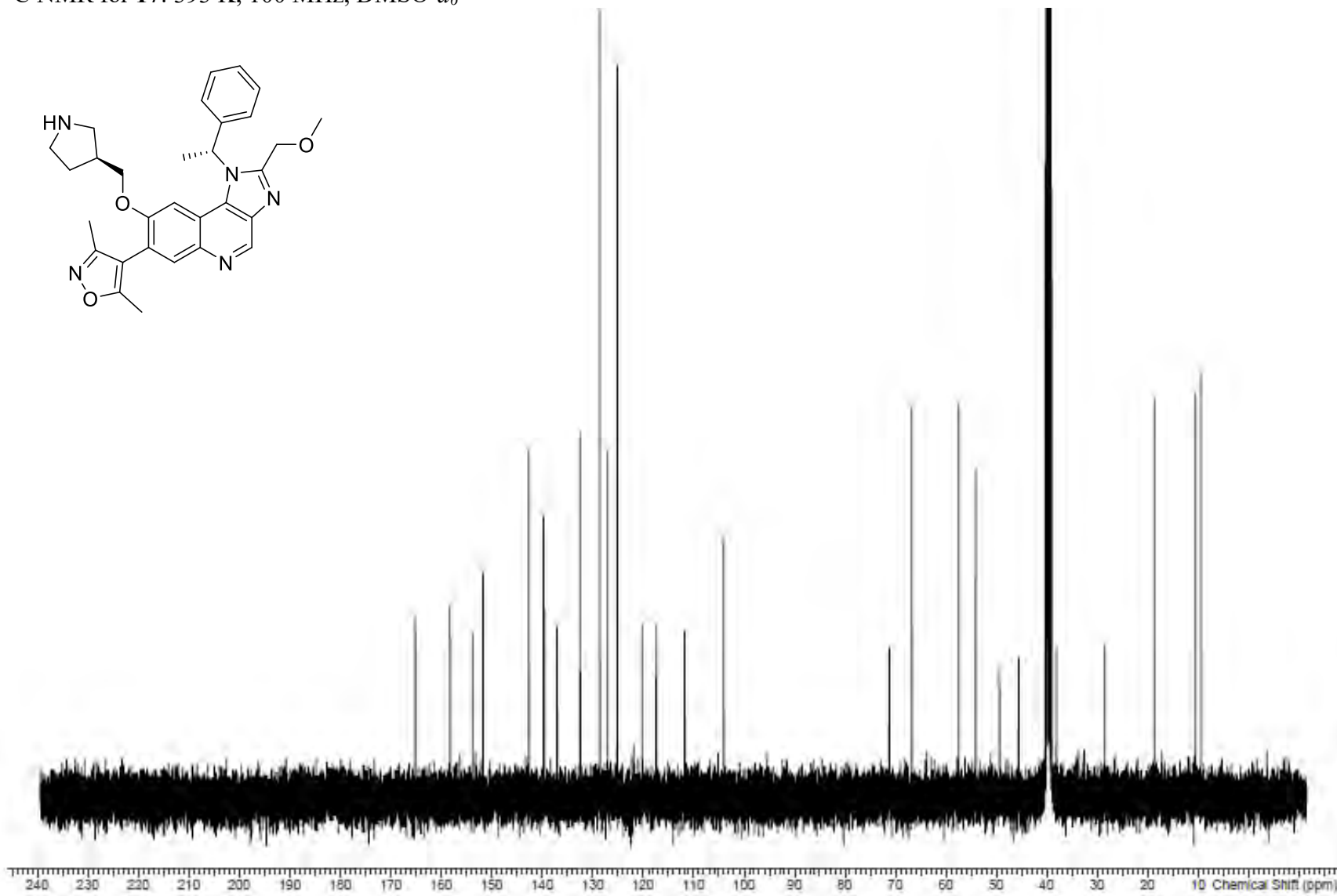
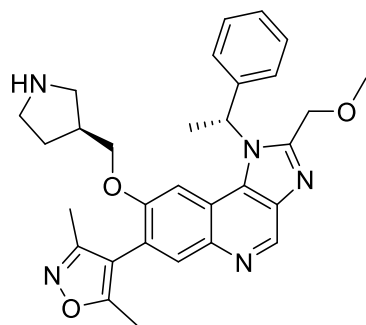
^1H NMR for **16**: 373 K, 400 MHz, $\text{DMSO-}d_6$



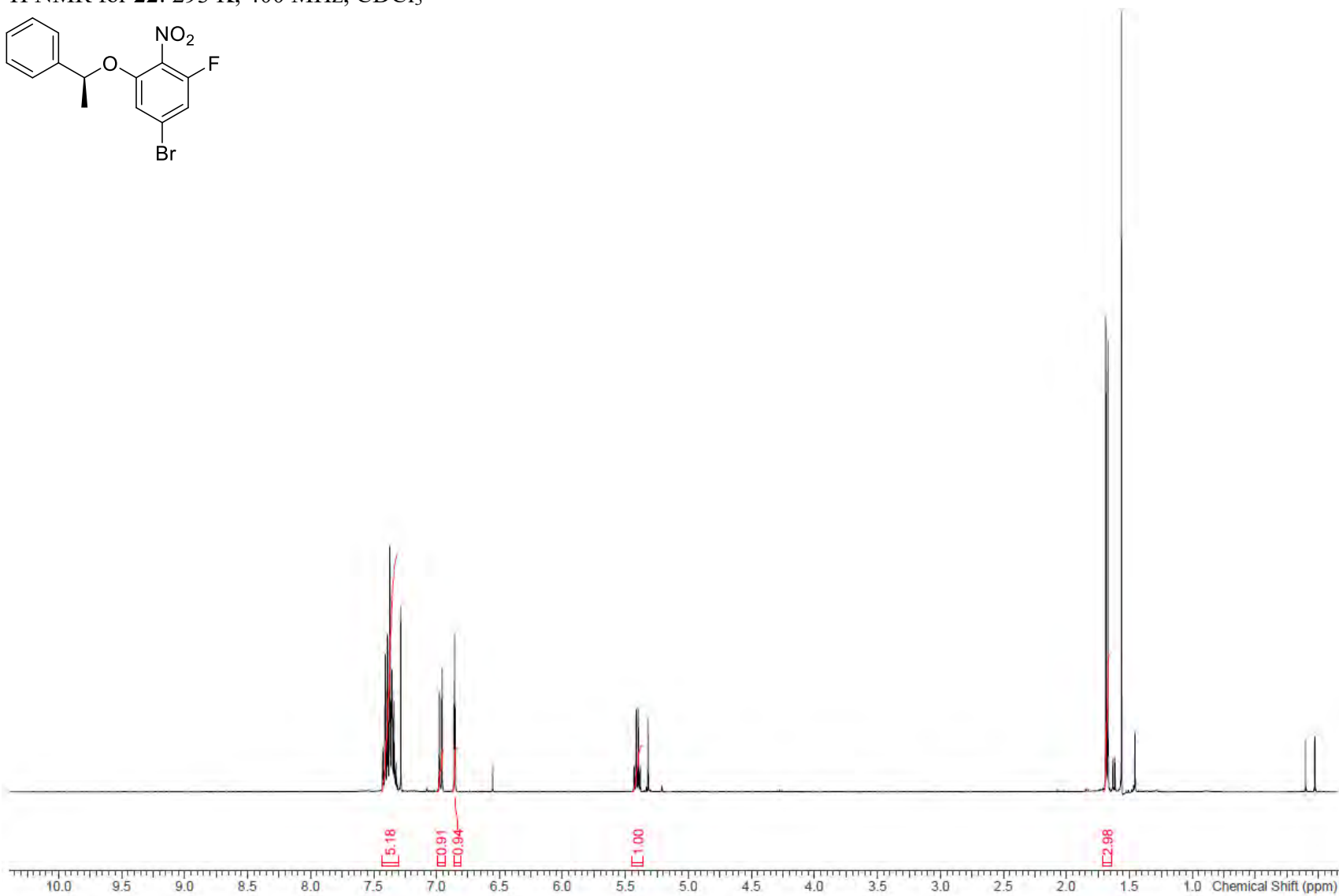
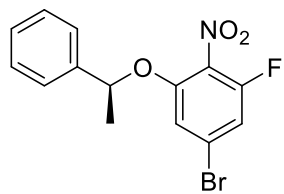
^1H NMR for **17**: 393 K, 400 MHz, $\text{DMSO-}d_6$



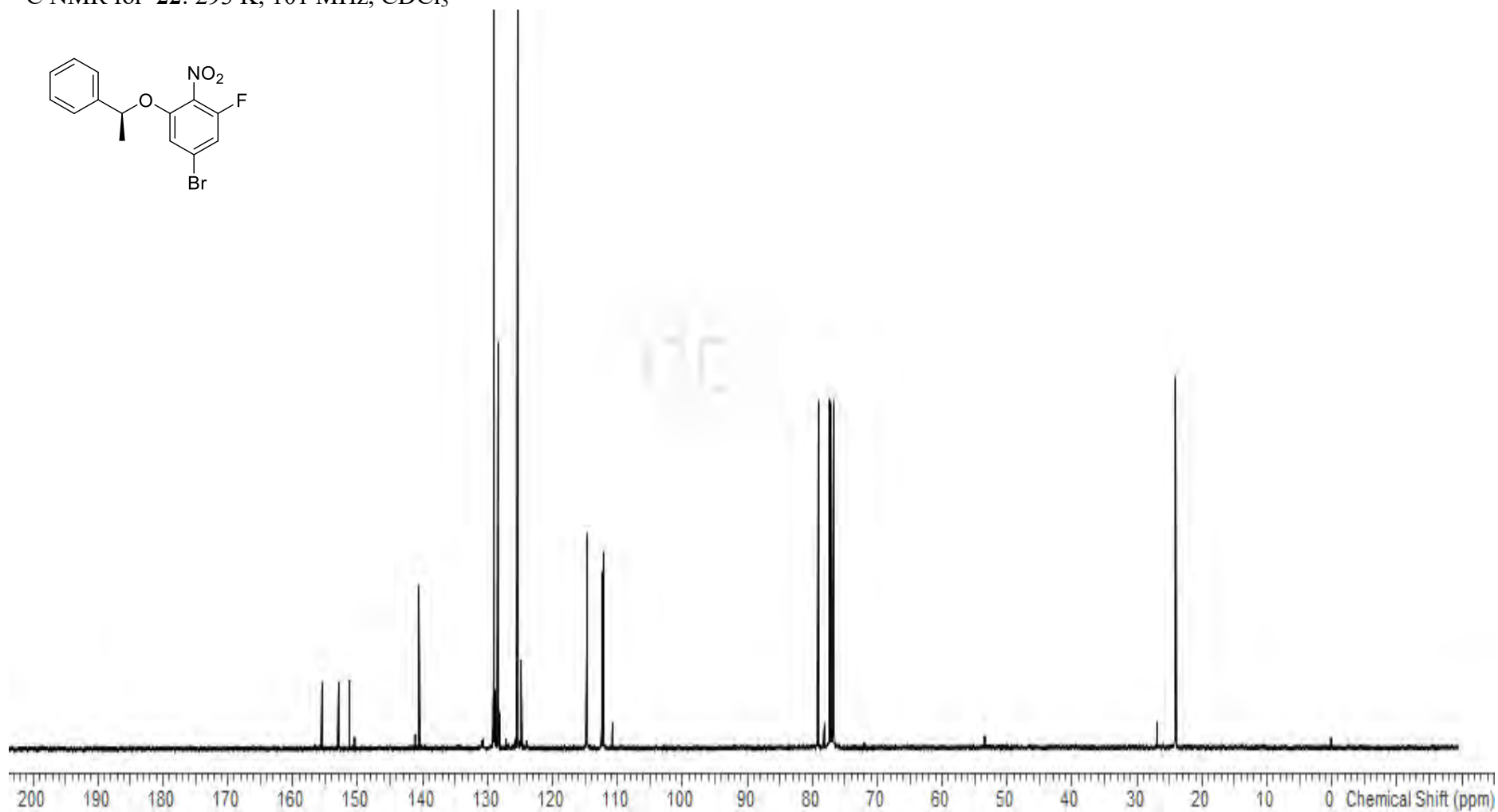
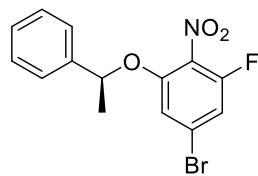
^{13}C NMR for **17**: 393 K, 100 MHz, $\text{DMSO-}d_6$



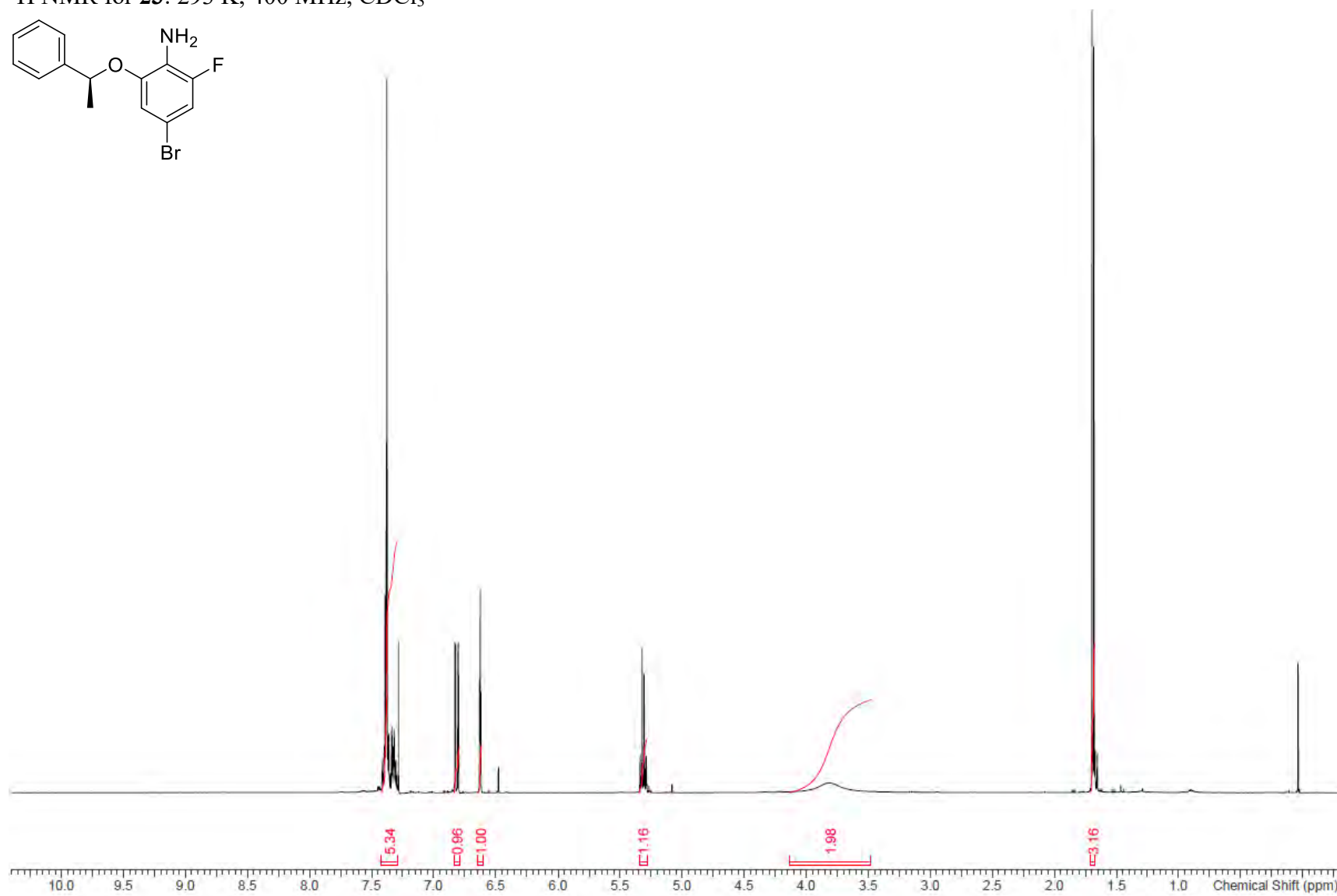
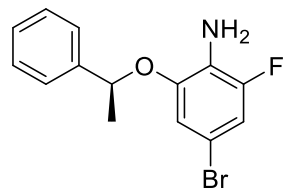
¹H NMR for **22**: 293 K, 400 MHz, CDCl₃



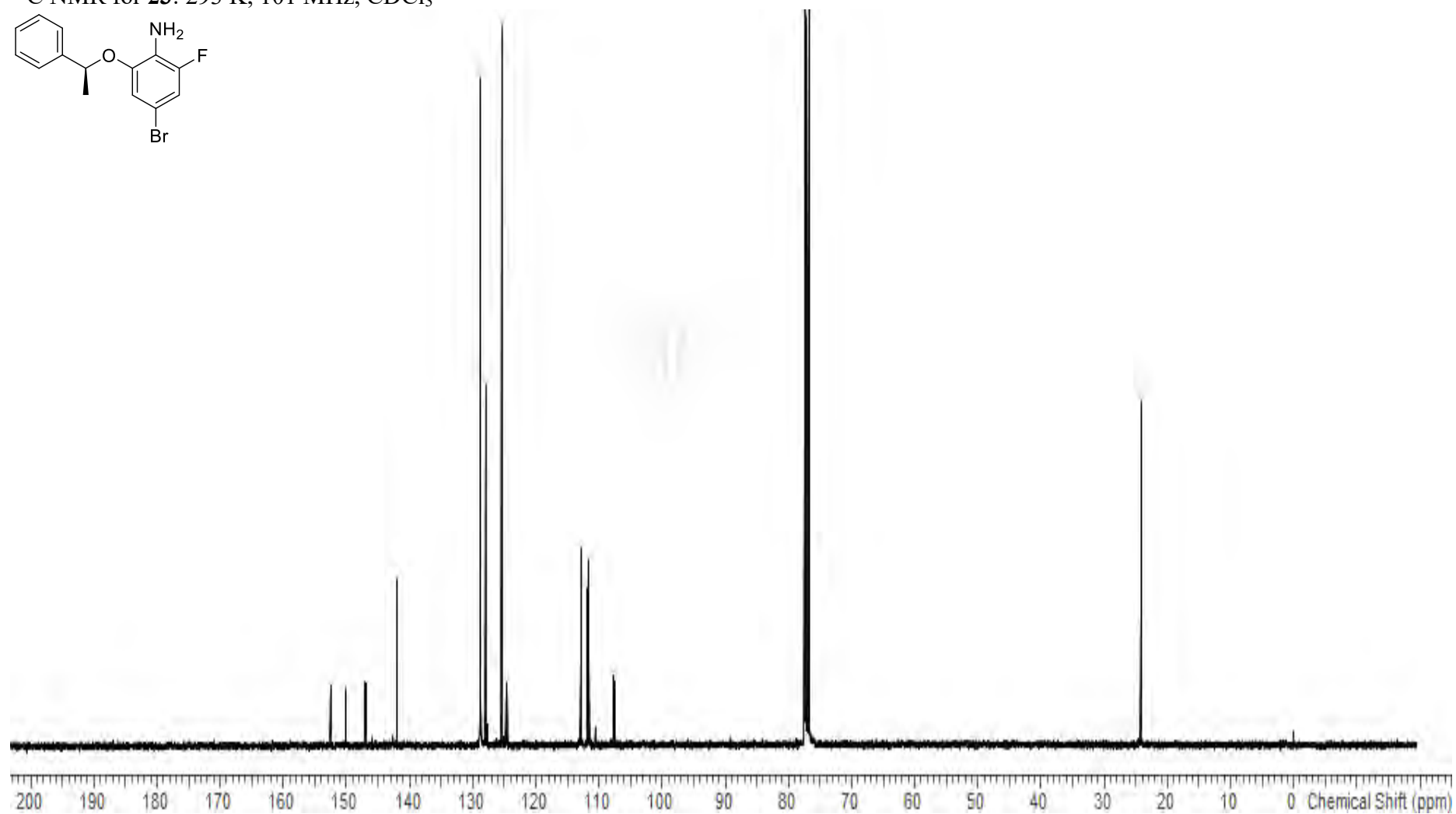
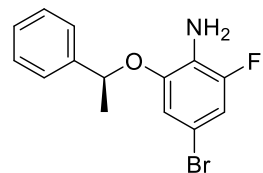
^{13}C NMR for **22**: 293 K, 101 MHz, CDCl_3



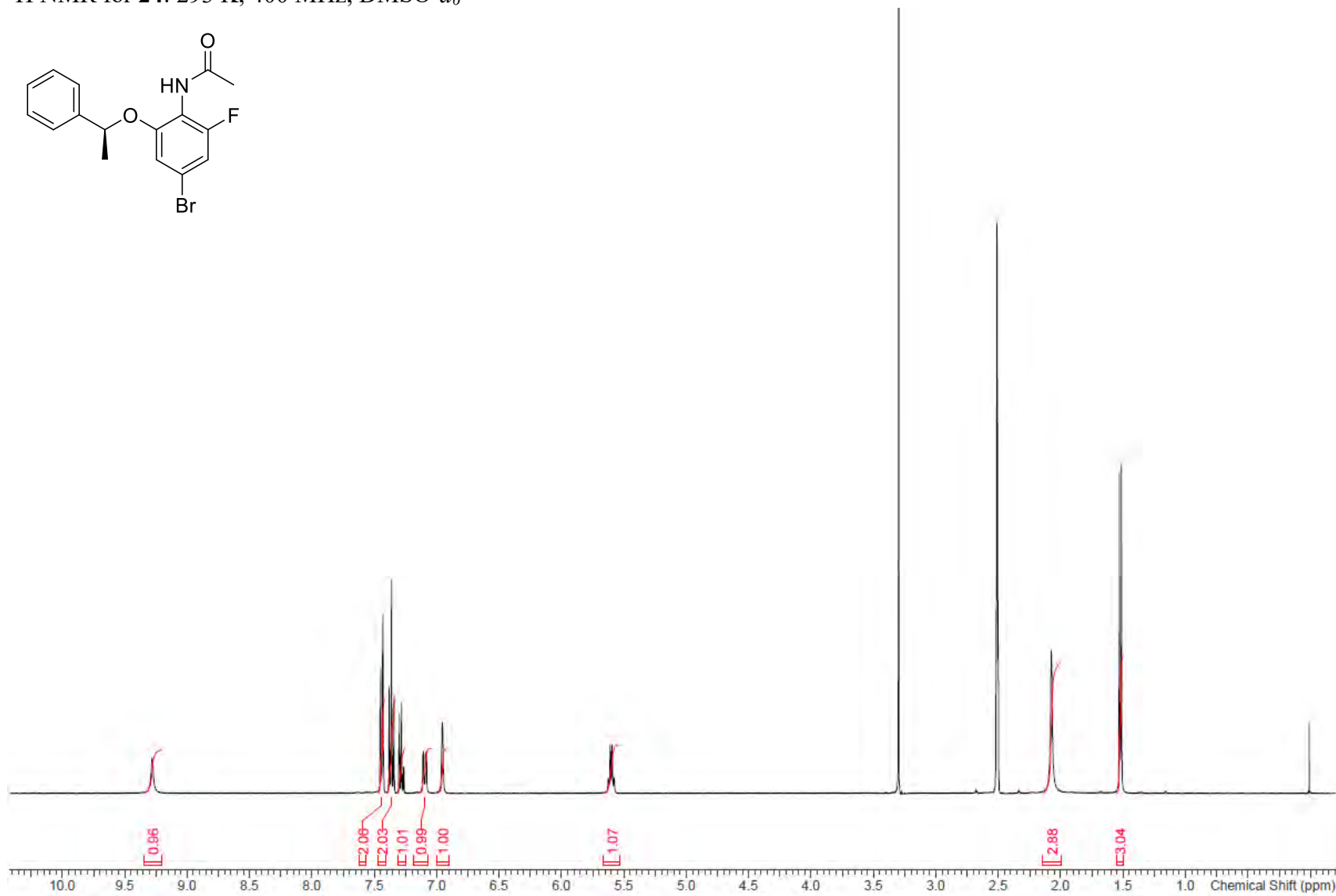
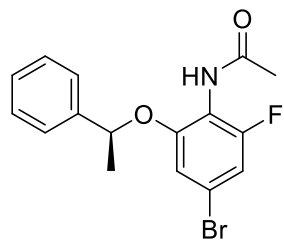
^1H NMR for **23**: 293 K, 400 MHz, CDCl_3



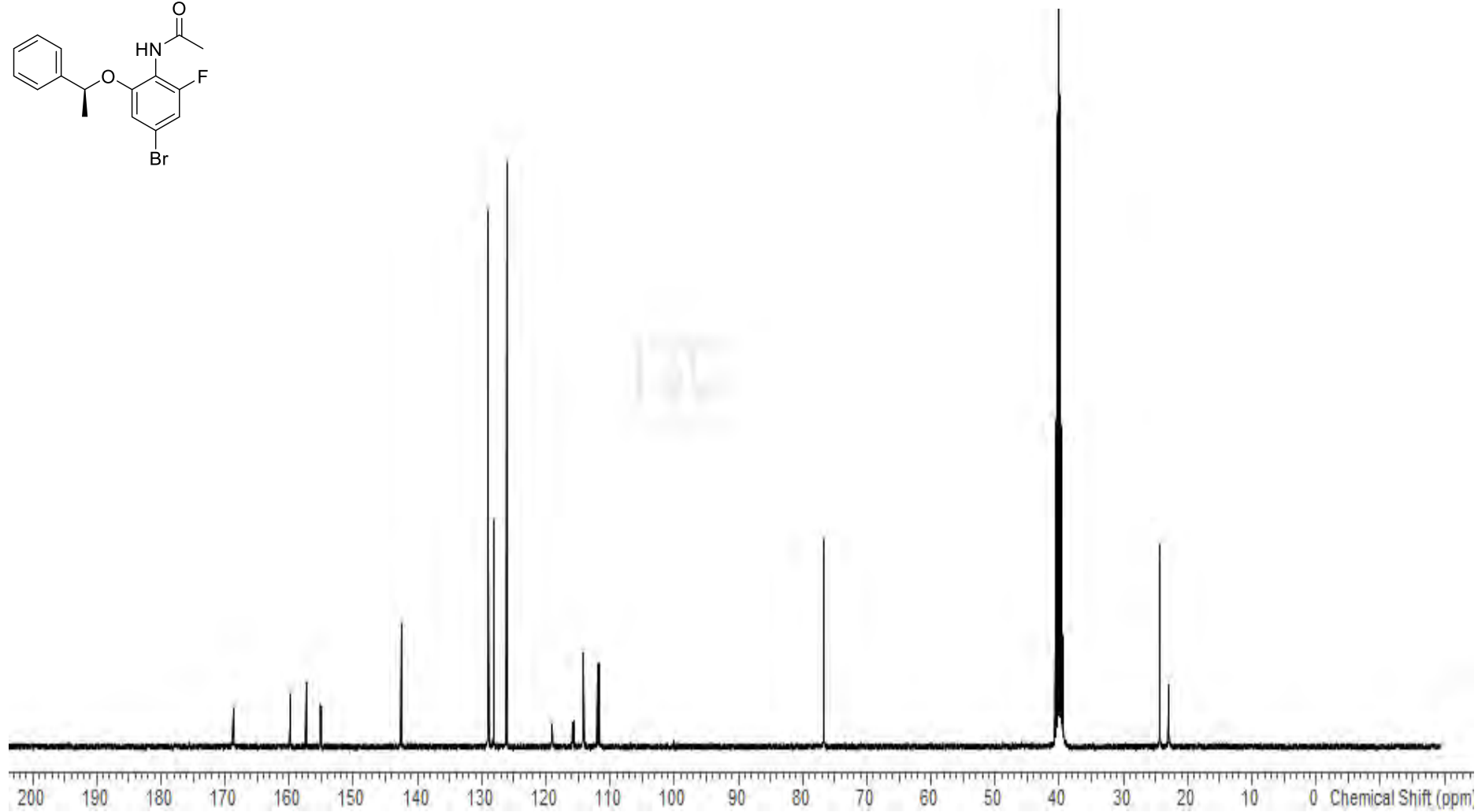
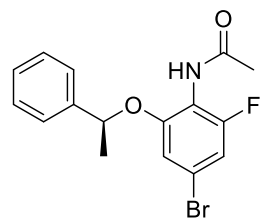
^{13}C NMR for **23**: 293 K, 101 MHz, CDCl_3



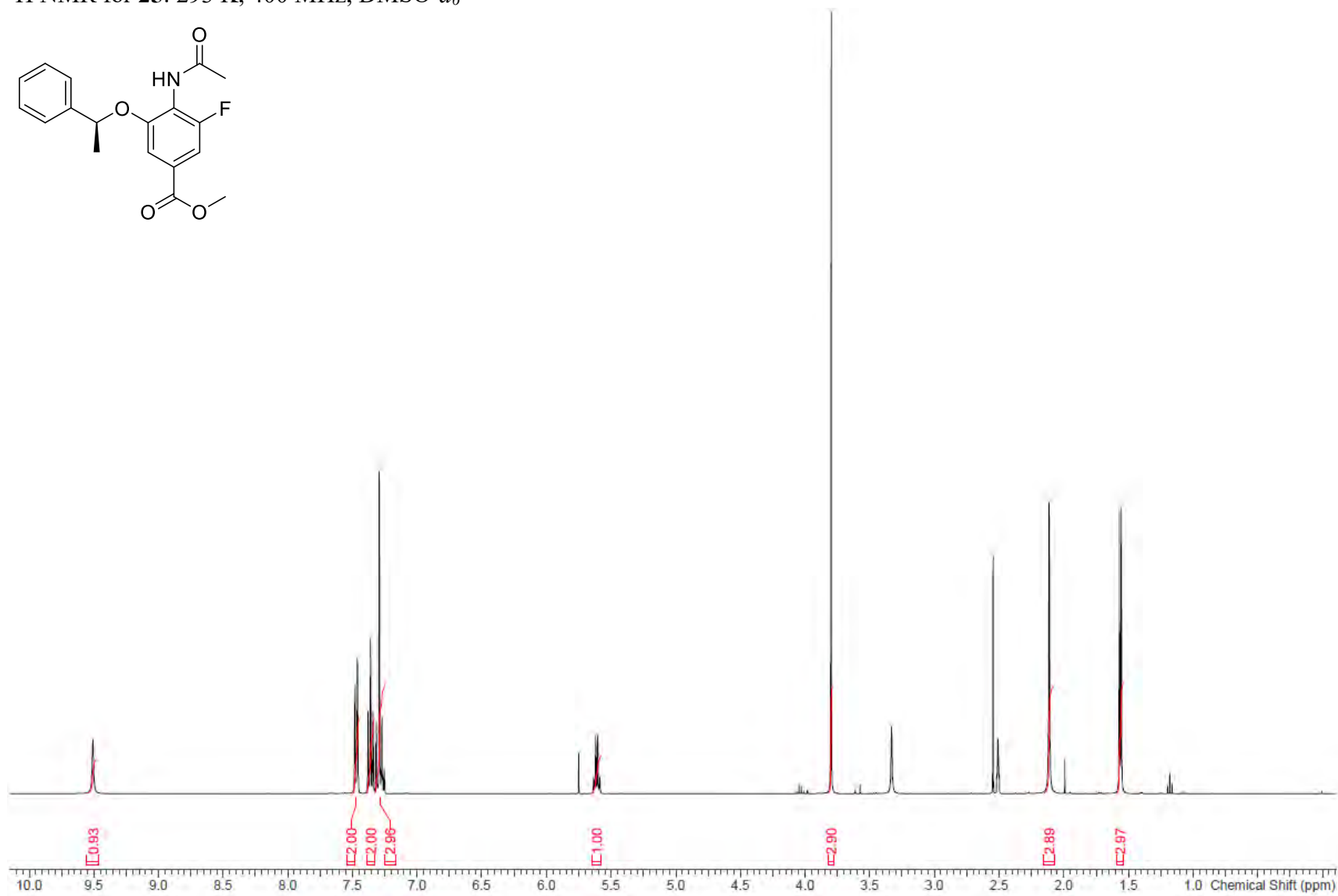
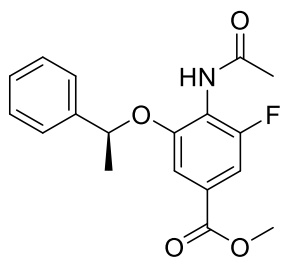
^1H NMR for **24**: 293 K, 400 MHz, $\text{DMSO-}d_6$



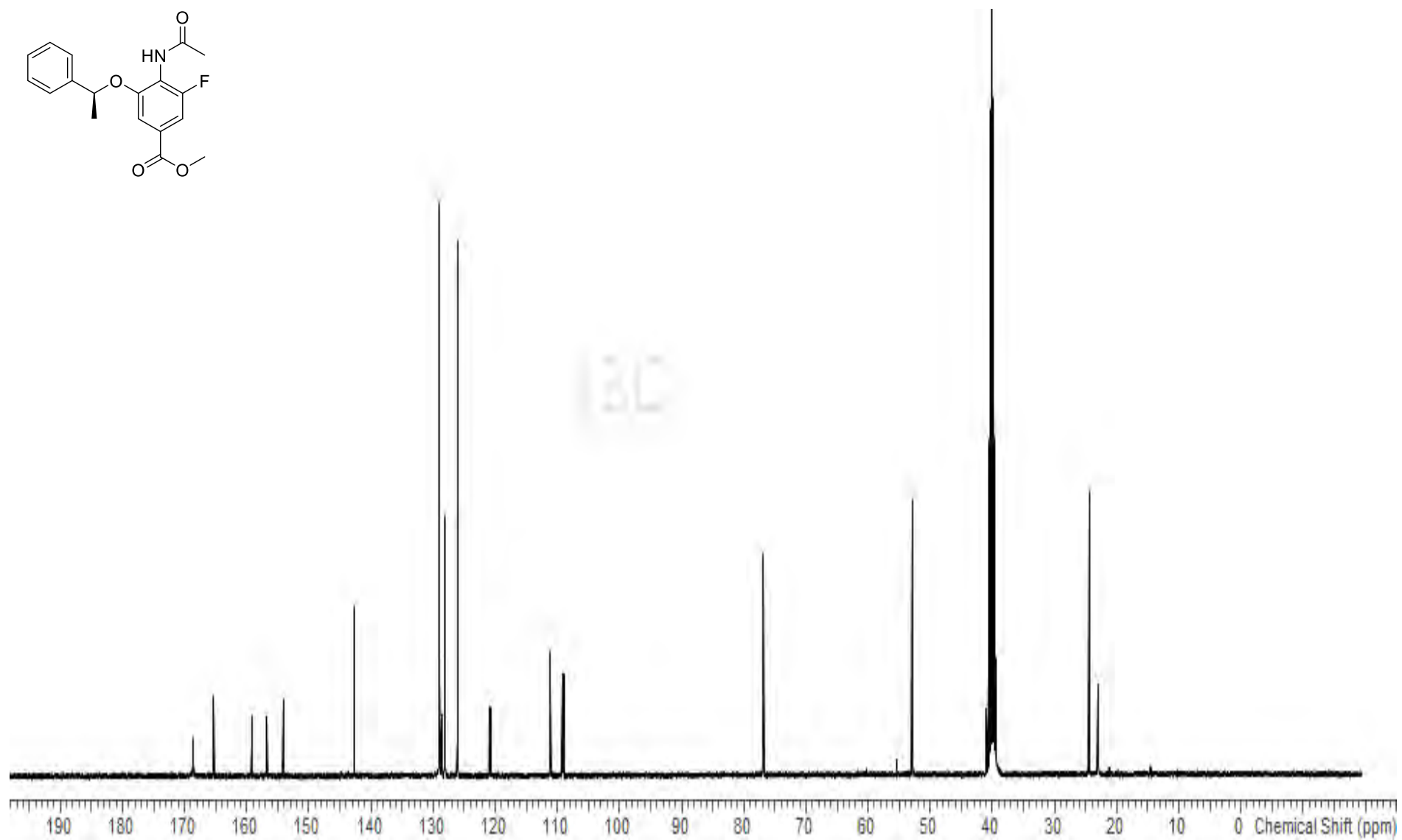
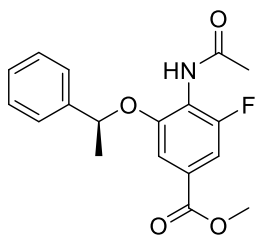
^{13}C NMR for **24**: 293 K, 101 MHz, $\text{DMSO-}d_6$



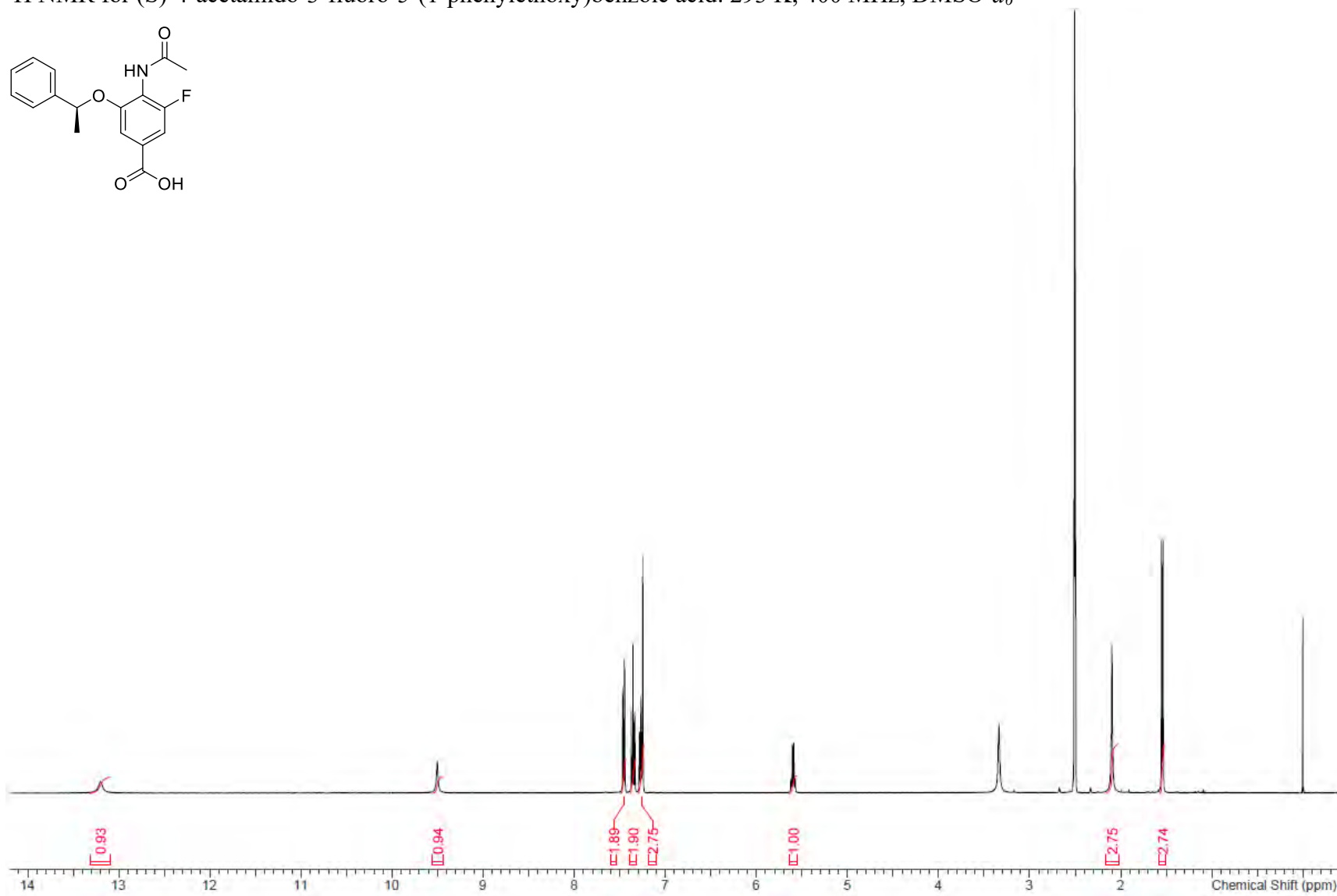
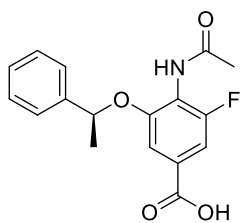
^1H NMR for **25**: 293 K, 400 MHz, $\text{DMSO-}d_6$



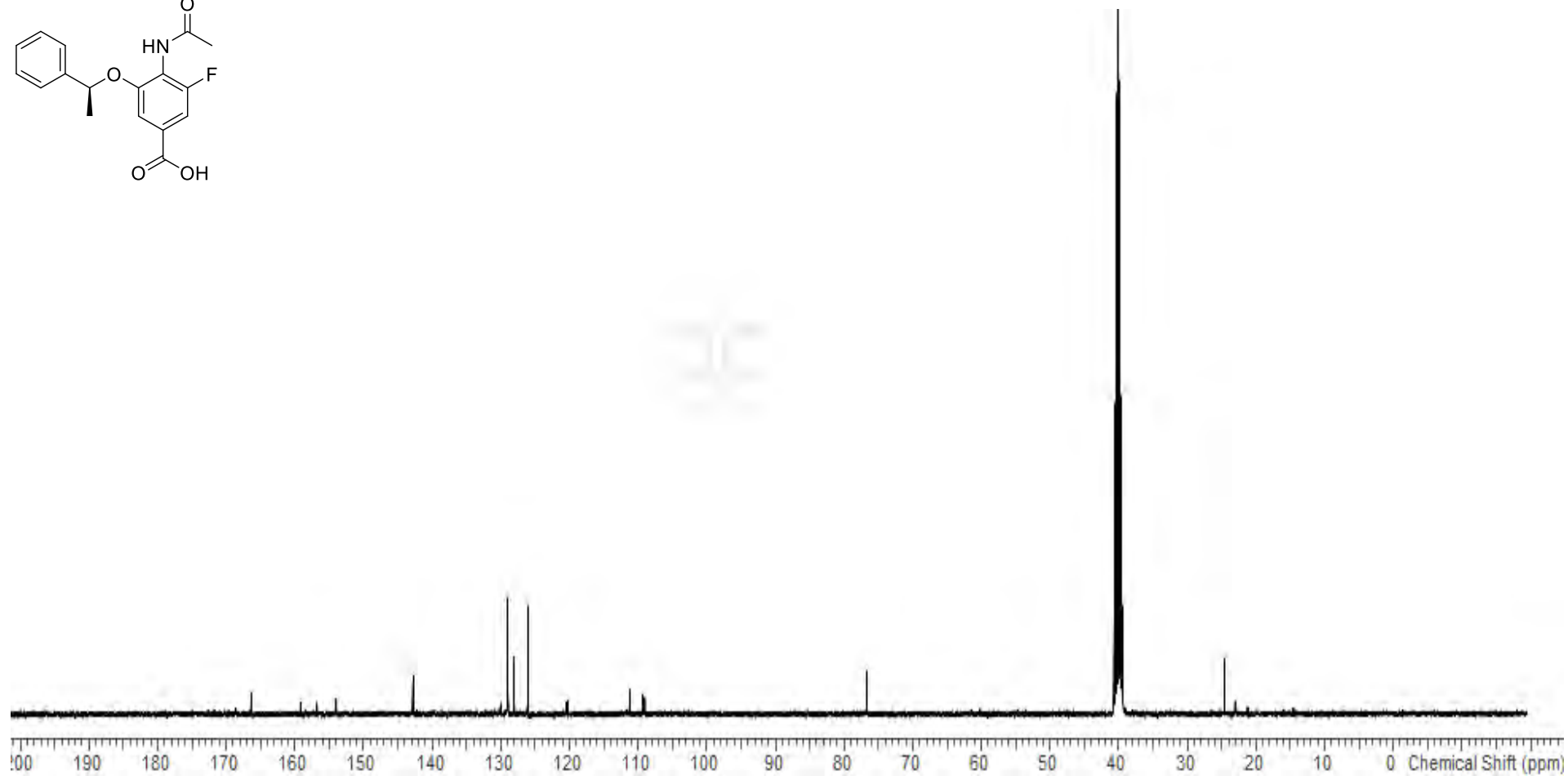
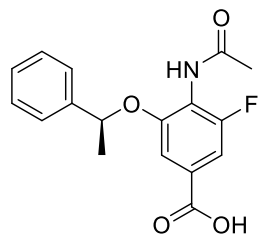
^{13}C NMR for **25**: 293 K, 101 MHz, $\text{DMSO-}d_6$



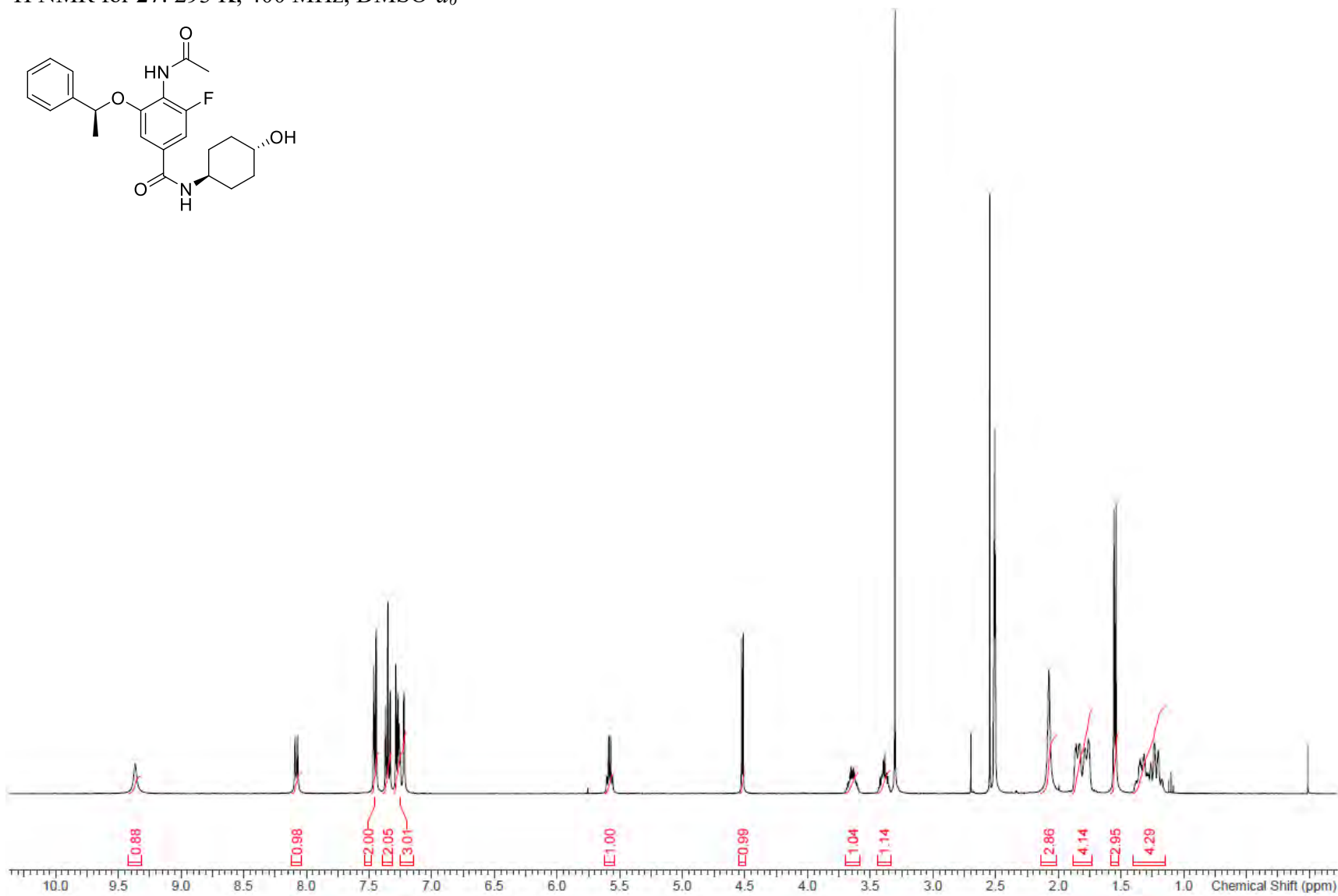
^1H NMR for (S)-4-acetamido-3-fluoro-5-(1-phenylethoxy)benzoic acid: 293 K, 400 MHz, $\text{DMSO-}d_6$



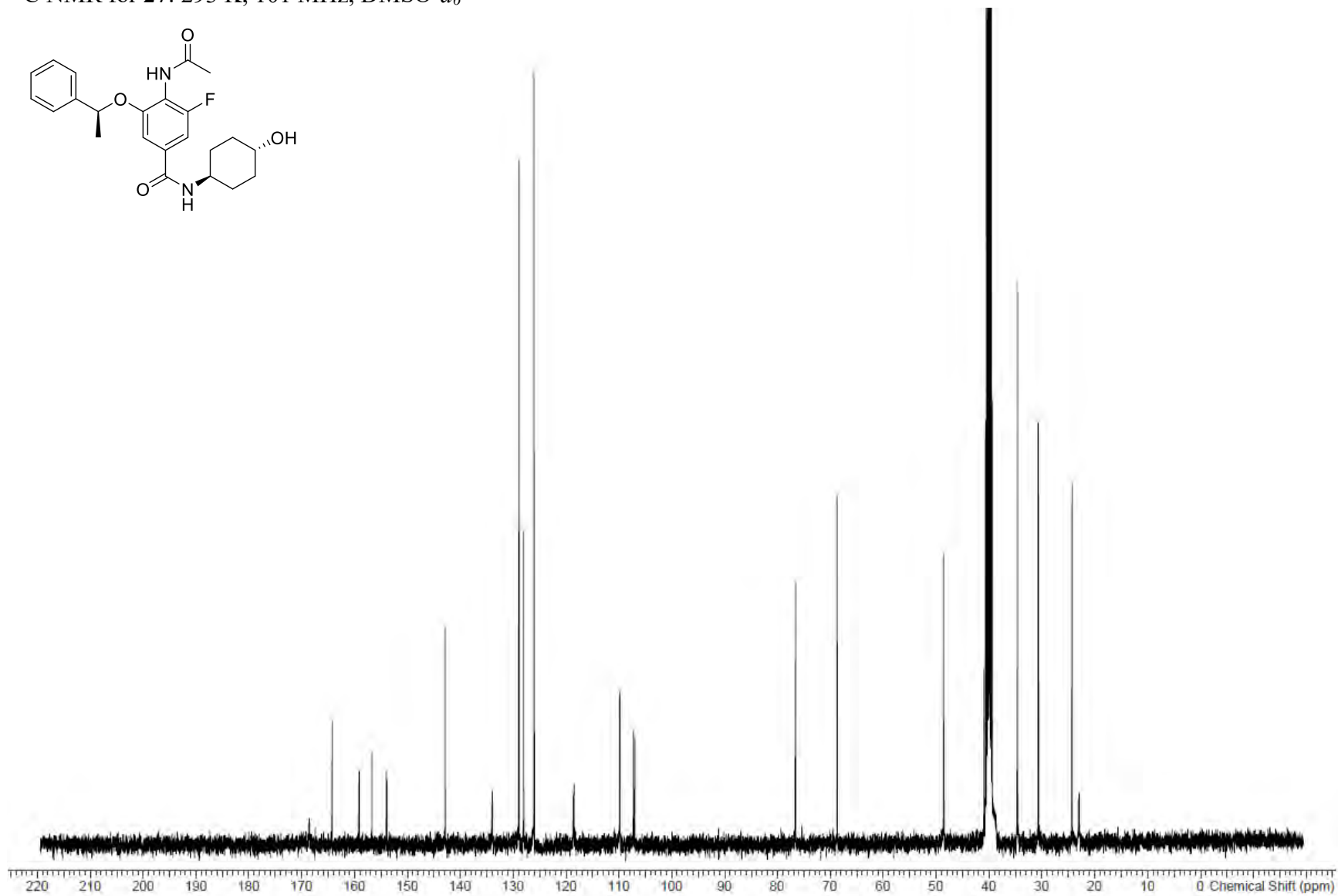
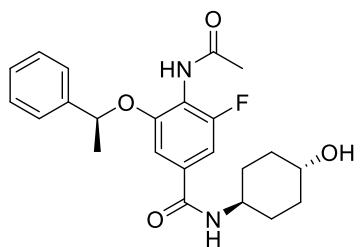
^{13}C NMR for (S)-4-Acetamido-3-fluoro-5-(1-phenylethoxy)benzoic acid: 293 K, 101 MHz, $\text{DMSO-}d_6$



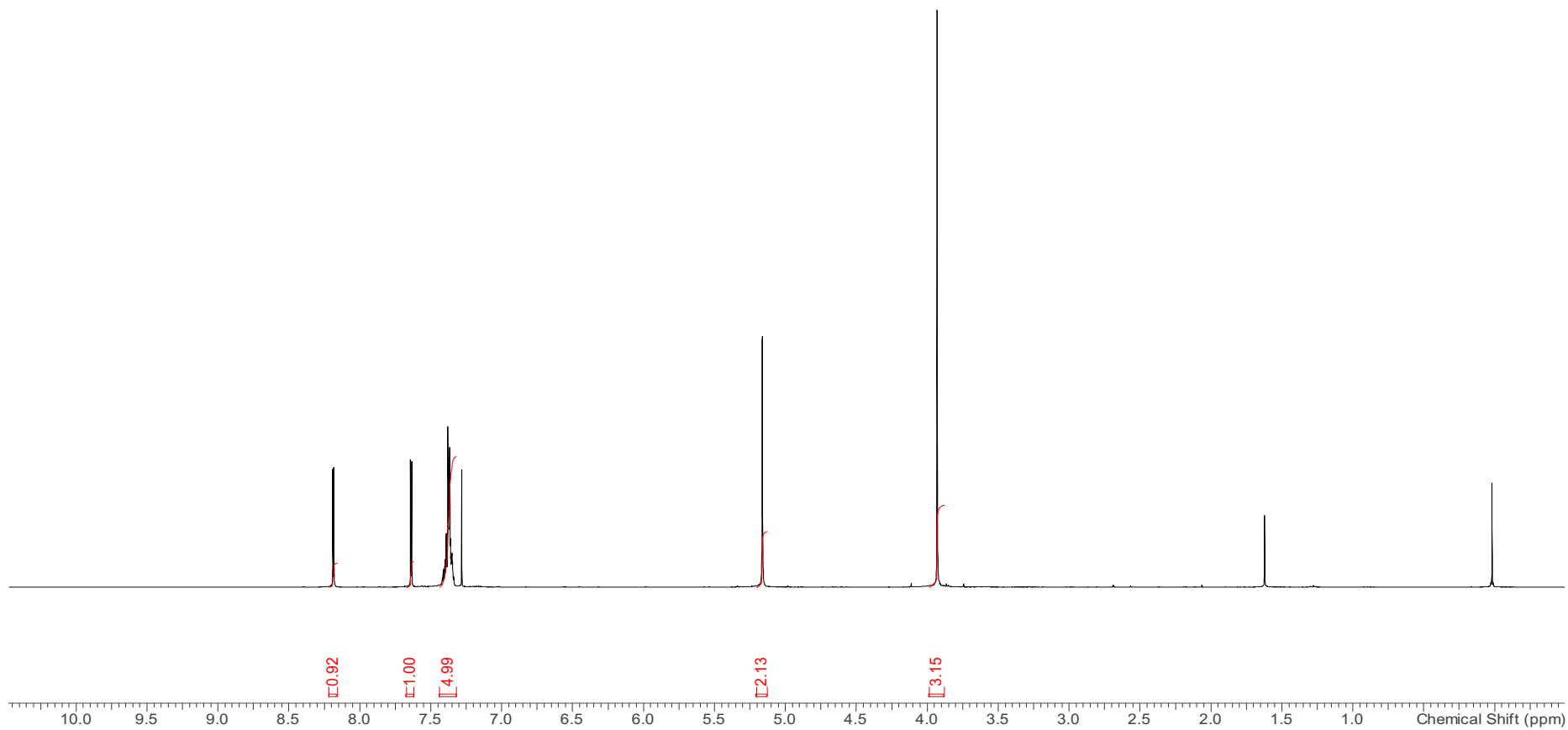
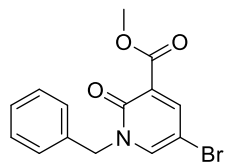
^1H NMR for **27**: 293 K, 400 MHz, $\text{DMSO-}d_6$



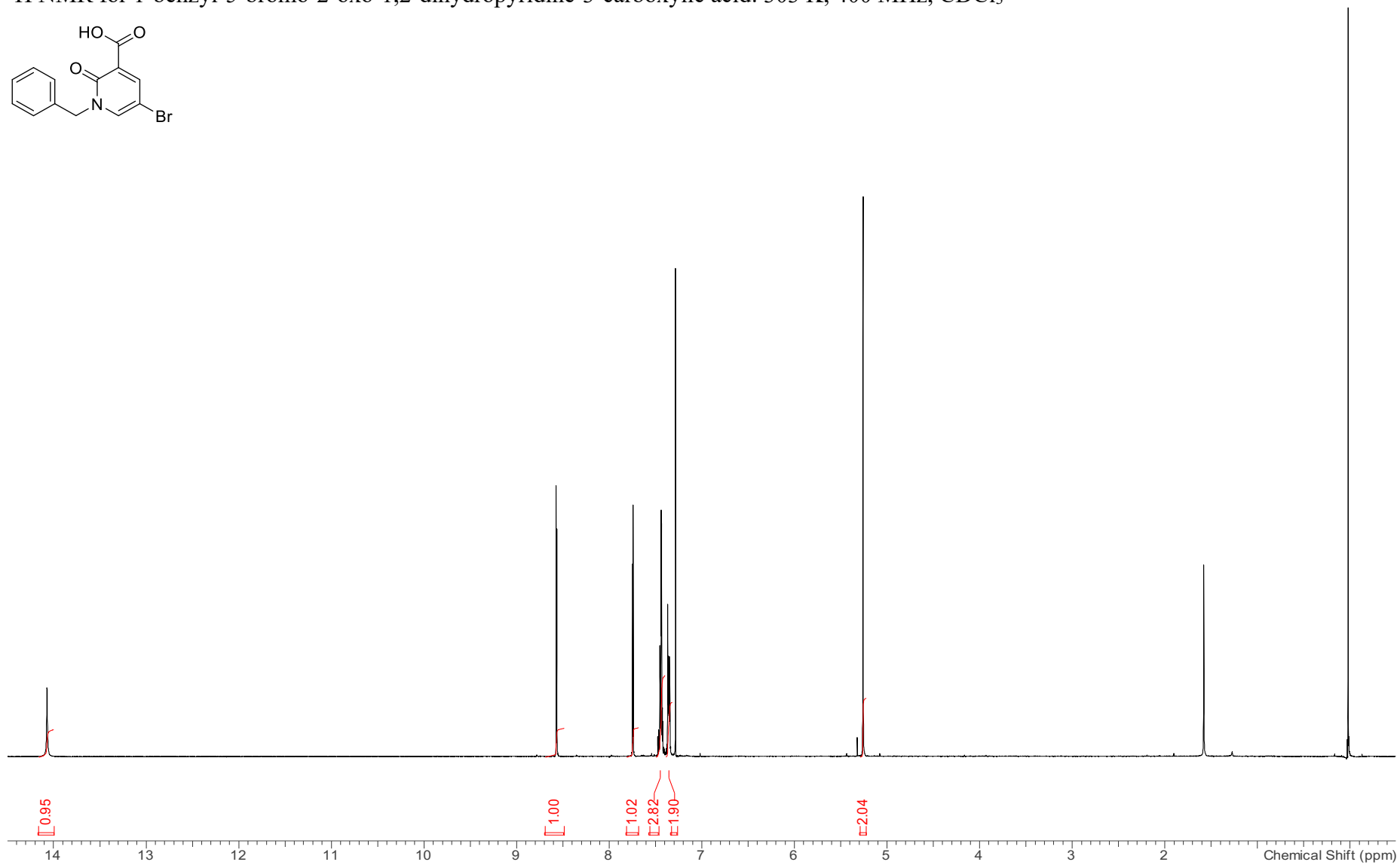
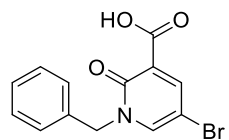
^{13}C NMR for **27**: 293 K, 101 MHz, $\text{DMSO-}d_6$



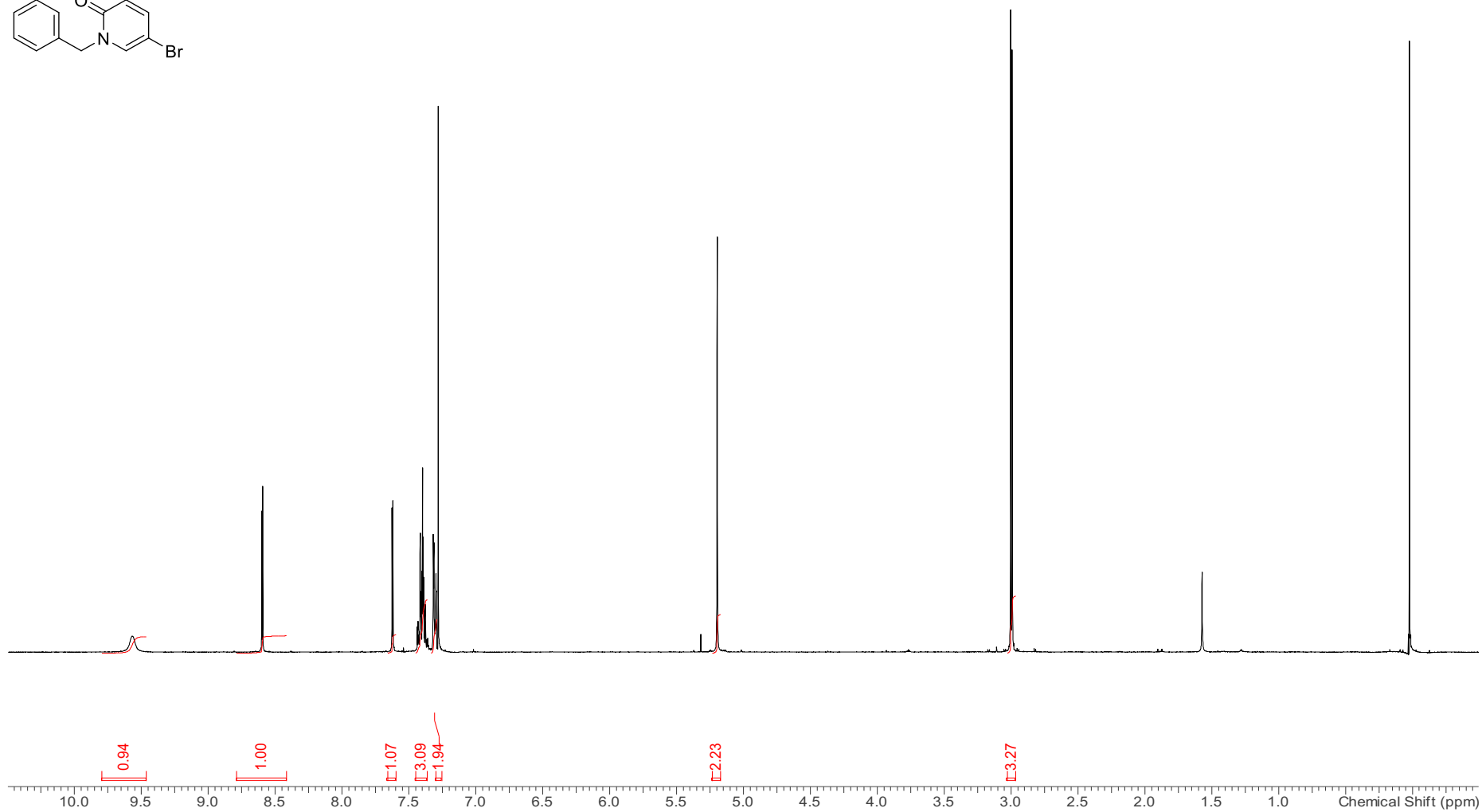
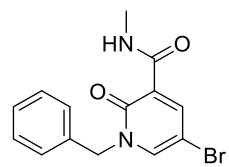
^1H NMR for **31**: 303 K, 400 MHz, CDCl_3



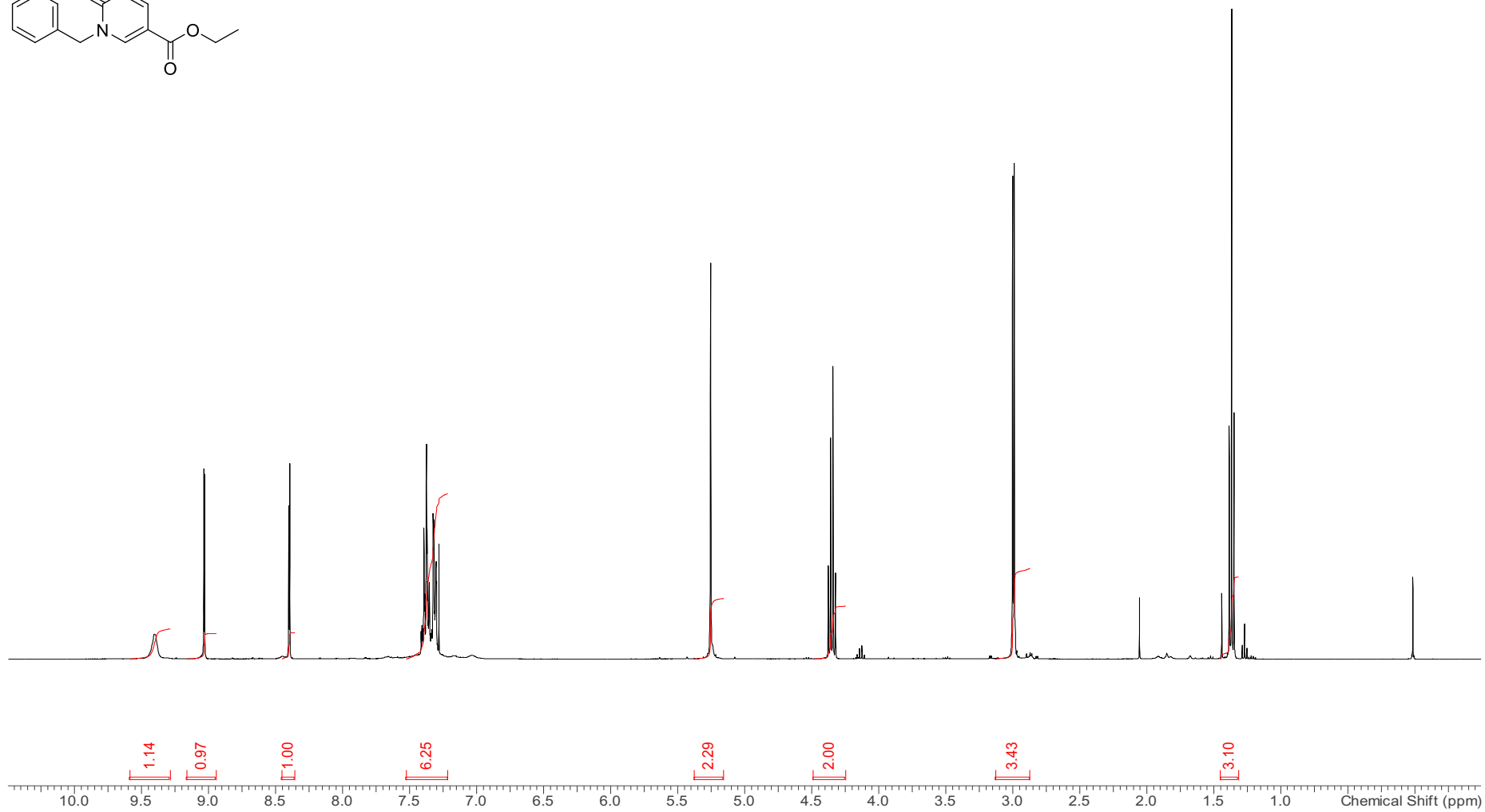
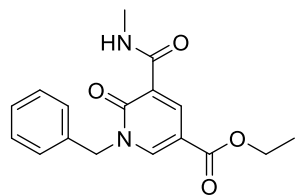
^1H NMR for 1-benzyl-5-bromo-2-oxo-1,2-dihydropyridine-3-carboxylic acid: 303 K, 400 MHz, CDCl_3



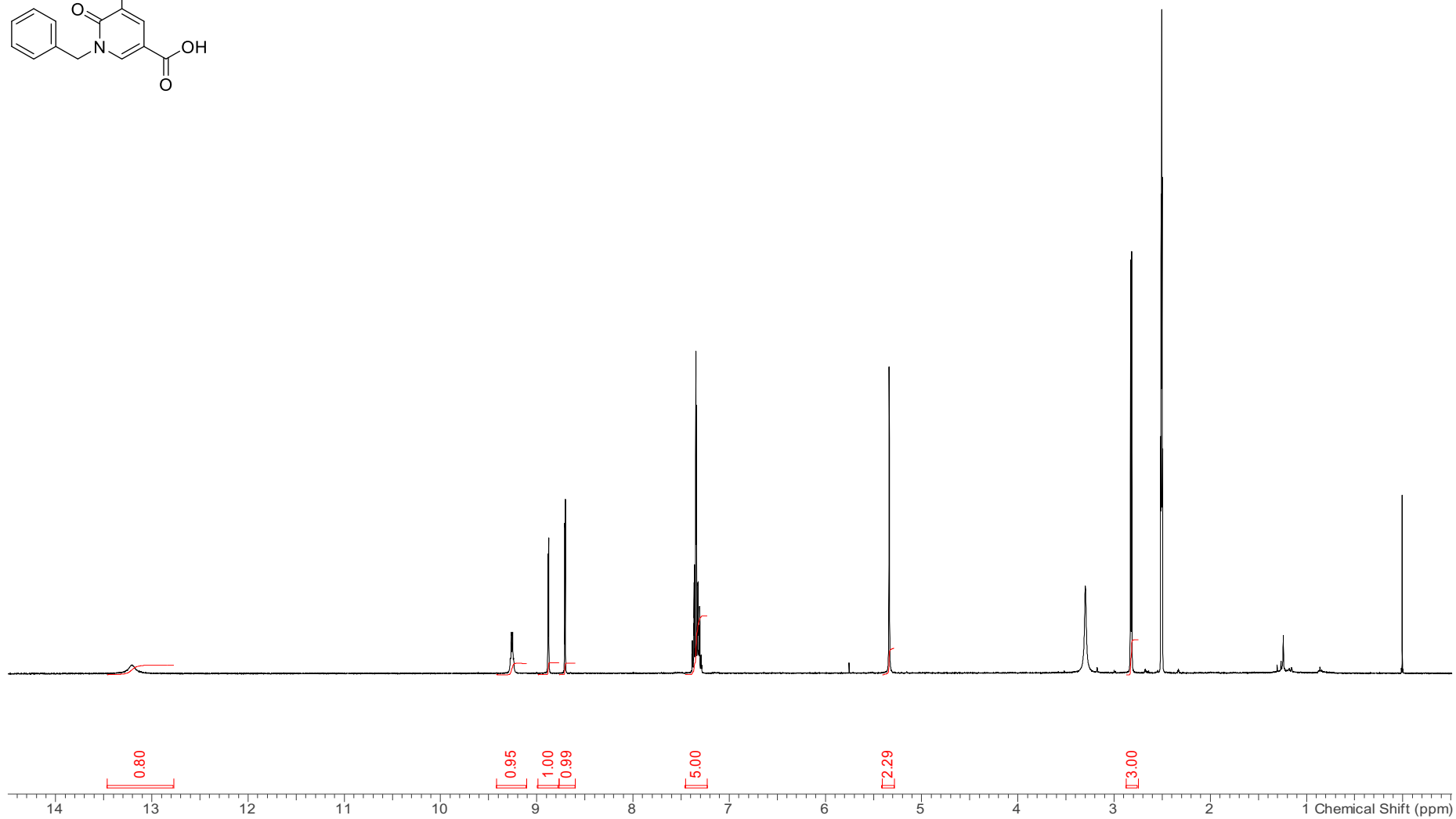
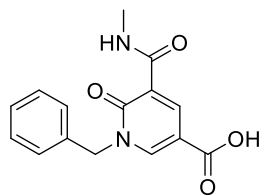
^1H NMR for **32**: 303 K, 400 MHz, CDCl_3



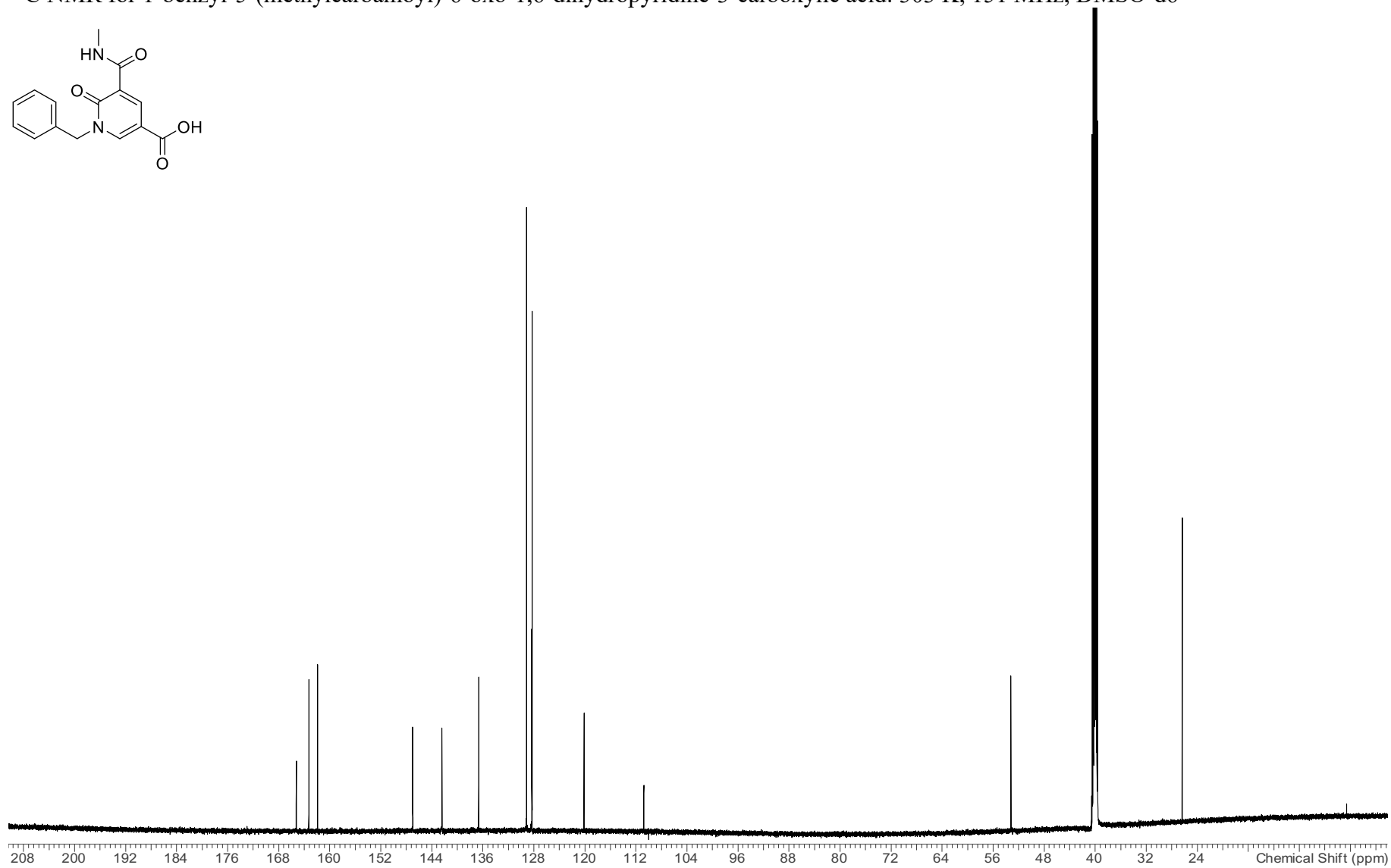
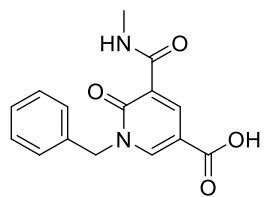
^1H NMR for **33**: 303 K, 400 MHz, CDCl_3



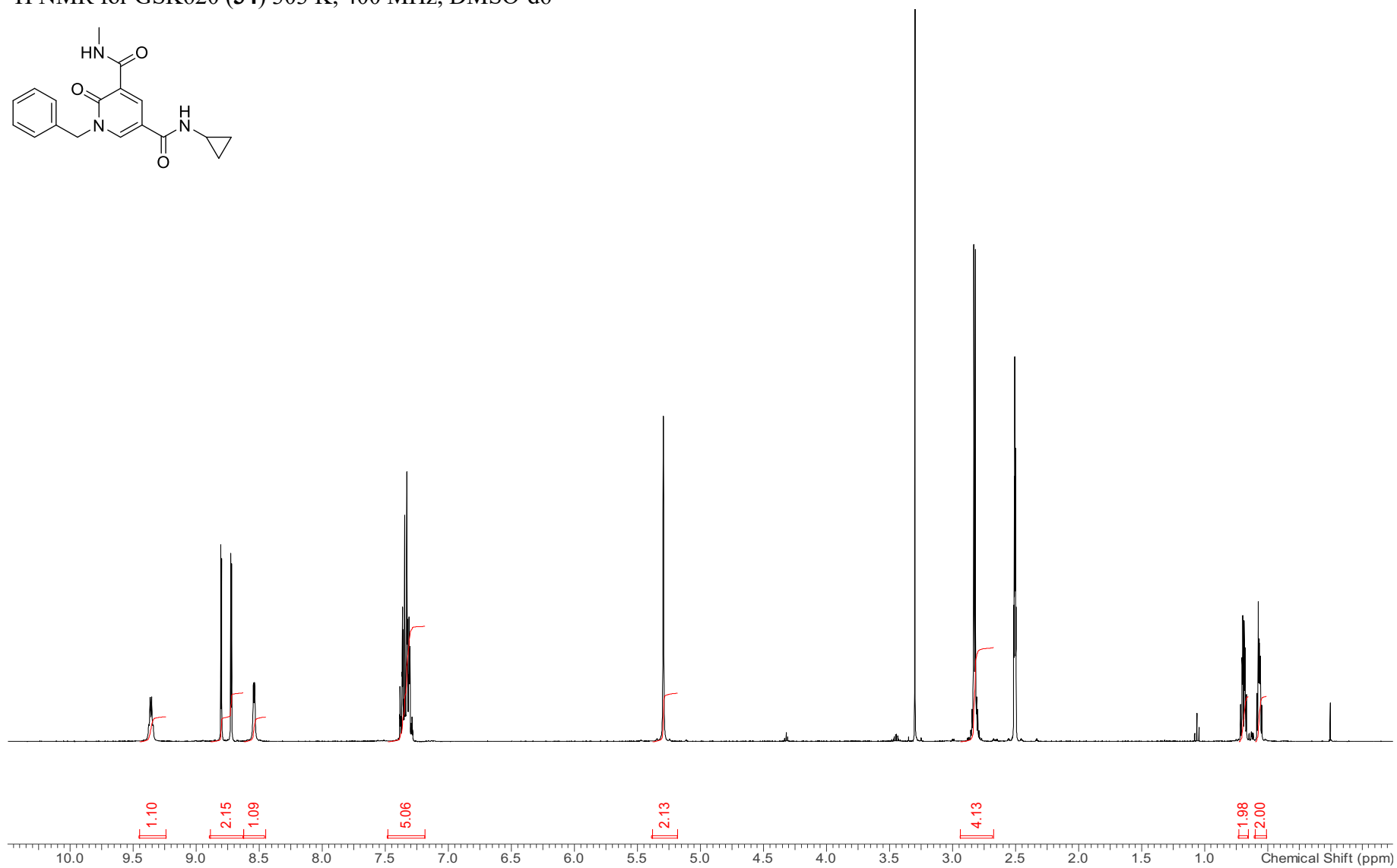
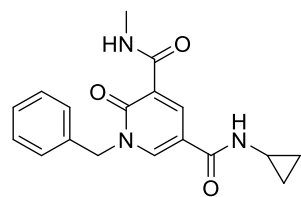
^1H NMR for 1-benzyl-5-(methylcarbamoyl)-6-oxo-1,6-dihydropyridine-3-carboxylic acid: 303 K, 400 MHz, DMSO- d_6



¹³C NMR for 1-benzyl-5-(methylcarbamoyl)-6-oxo-1,6-dihydropyridine-3-carboxylic acid: 303 K, 151 MHz, DMSO-d₆



^1H NMR for GSK620 (**34**) 303 K, 400 MHz, DMSO-d₆



^{13}C NMR for GSK620 (**34**), 303 K, 151 MHz, DMSO- d_6

